ELECTROCHEMICAL SUPERCAPACITORS

NANOCOMPOSITE ELECTRODES FOR ELECTROCHEMICAL SUPERCAPACITORS

By

Gideon Moses Jacob, B. Tech.

A Thesis

Submitted to the School of Graduate Studies

in Partial Fulfillment of the Requirements

For the Degree

Master of Applied Science

McMaster University

© Copyright by Gideon Moses Jacob, 2009

MASTER OF APPLIED SCIENCE (2009) McMaster University

(Materials Engineering) Hamilton, Ontario

TITLE: Nanocomposite electrodes for electrochemical supercapacitors

AUTHOR: Gideon Moses Jacob, B.Tech., (Central Electrochemical Research Institute, India)

SUPERVISOR: Dr. Igor Zhitomirsky

NUMBER OF PAGES: XIV, 109

ABSTRACT

The electrochemical supercapacitors (ESs) are an emerging technology that promises to play an important role in meeting the demands of electronic devices and systems both now and in the future. A notable improvement in performance has been achieved through recent advances in understanding charge storage mechanisms and the development of advanced nanostructured materials. Nanostructured manganese oxides in various forms have been found to be promising electrode materials for ES.

Cathodic electrodeposition method has been developed for the fabrication of nanostructured manganese dioxide films. Manganese oxide films were obtained by galvanostatic, pulse and reverse pulse electrodeposition from $KMnO_4$ solutions. The diffusion-controlled deposition mechanism is based on the reduction of anionic MnO_4^- at the cathode surface. It was shown that film porosity is beneficial for the charge transfer during deposition, crack prevention in thick films and electrolyte diffusion in fabricated ES electrodes. The microstructure, chemical properties and charge storage properties of films prepared by different deposition methods are investigated and compared.

Novel chemical precipitation methods have been developed to produce manganese dioxide and Ag-doped manganese dioxide nanoparticles. Composite electrodes for ES were fabricated by impregnation of slurries of the manganese dioxide nanoparticles and carbon black into porous nickel foam current collectors. The microstructure and chemical properties of the powders were characterized. The capacitive behaviour of the composite electrodes was studied.

ACKNOWLEDGEMENT

First, I would like to praise the Lord for all the good things in my life.

I would like to express my sincere gratitude to my supervisor Dr. Igor Zhitomirsky for offering me the opportunity to work on this project and for his continuous support and guidance throughout this research work. His patience and willingness to always provide extra help are greatly appreciated.

Many thanks to all members of Dr. Zhitomirsky's team, Xing Pang, Janice Wei, Marco Cheong, Jun Li, Feng Sun, Travis Casagrande, Chao Shi, Rong Ma, Yaohui Wang, Koming Wu and Yingying Li for their kind help and friendship.

Finally and foremost, my special thanks to my parents and brother for their love and support.

TABLE OF CONTENTS

LIST OF FIGURES

1. INTRODUCTION

Energy consumption or production that relies on the combustion of fossil fuels is forecast to have a severe future impact on world economics and ecology. Electrochemical energy production is under serious consideration as an alternative energy and power source. Electrochemical energy storage and conversion systems include batteries, fuel cells and ESs. Although the energy storage and conversion mechanisms are different, there are electrochemical similarities of these three systems. Common features are that the energy providing process take place at the electrode/electrolyte interface and that electron and ion transport are separated[1].

ESs are currently, widely investigated due to their interesting characteristics in terms of power and energy densities. Supercapacitors have much larger power densities than batteries and fuel cells, and larger energy densities than conventional capacitors. Supercapacitors are becoming attractive energy storage systems particularly for applications involving high power requirements. For example, hybrid systems consisting of batteries/fuel cells and supercapacitors are being investigated for electric vehicle propulsion. In such hybrid systems, the supercapacitors can provide the peak power during acceleration and therefore the battery/fuel cell can be optimized primarily for higher energy density and better cycle life without the requirement of high power density. Supercapacitors are also attractive for other applications such as power sources for camera flash equipment, lasers, pulsed light generators and backup power sources for computer memory.

Many charge-storage mechanisms have been proposed for ES, most notably double-layer capacitance and pseudocapacitance. The large specific capacitance (SC) of supercapacitors is the result of one or a combination of these charge-storage mechanisms. Double-layer capacitance arises from the separation of charge at the interface between a solid electrode and an electrolyte[2, 3], whereas pseudocapacitance arises from fast, reversible Faradaic reactions occurring at or near a solid electrode surface over an appropriate range of potential[4, 5]. The most widely used active electrode materials are carbon, conducting polymers and metal oxides.

Many transition-metal oxides have been shown to be excellent electrode materials for supercapacitors. Recently, a hydrous form of ruthenium oxide, RuO_2, in aqueous H_2SO_4 has been found to possess very high SC (720 F g^{-1}), which is associated with pseudocapacitance[5]. Although the RuO_2 system gives very high SC, it has the inherent disadvantage of being expensive. Less expensive oxides of iron, vanadium, nickel and cobalt have been tested in aqueous electrolytes, but none has been investigated as much as manganese dioxide, MnO_2. The utility of MnO_2 in batteries has long been recognized and well established, its potential application as an electrode material for supercapacitor is being extensively studied. The natural abundance of MnO_2 coupled with its environmental compatibility makes it a very promising electrode material for various energy-storage technologies and, in particular, supercapacitors.

2. LITERATURE REVIEW

2.1 Historical Background

The concept of charge storage in the electrical double layer at the interface is known since the late 1800s, but the first electrical device using double-layer charge storage was patented by H.I. Becker[6] of General Electric in 1957, using porous carbon electrodes in an aqueous electrolyte. After General Electric, in 1966 Standard Oil Company of Ohio (SOHIO) Corporation[7] built a device with higher energy density by utilizing the double-layer capacitance of high area- carbon in a non aqueous electrolyte. The term supercapacitor was coined by Nippon Electric Company (NEC) in 1978, after their first commercial double-layer capacitor developed under the license of SOHIO. In the same year Panasonic started to manufacture its double-layer capacitor under the name "Goldcap". The major differences between the Panasonic and NEC products were that NEC used an aqueous electrolyte in a pasted electrode with bipolar cell construction, while Panasonic used a nonaqueous electrolyte in a non-pasted electrode with cell construction. In early days these double-layer capacitors were developed primarily to replace the unreliable coin cell batteries used in memory back-up applications. In late 1980s ELNA developed its double-layer capacitor Dyncap using organic electrolyte. Between 1975 and 1980, Conway utilized a different principle called pseudocapacitance and carried out extensive fundamental and development work on the ruthenium oxide type of electrochemical capacitor. Pseudocapacitance arises due to some electrosorption

processes and redox reactions at surfaces of oxide materials, e.g, RuO_2, MnO_2, IrO_2, Co_3O_4. The whole field has burgeoned since 1990 and is very active in fundamental and R&D directions. In the present days several other companies like Maxwell Technologies, ESMA, CAP-XX, NCC, NessCap have invested in the development of supercapacitors.

2.2 Applications of Supercapacitor

In earlier days because of their limited energy and power density, supercapacitors were initially used for low-power, low energy applications such as for memory backup. Recently, intensive research has been done to increase their energy and power density; as a result, supercapacitors offer new solutions for many applications.

The idea of using ES for electric vehicle application is much appealing because of high energy efficiency, high power density of such devices and ability to recuperate energy lost during braking. Fuel cells and batteries are promising energy storage devices for electric vehicles because of their high energy density, but they do not meet the high power requirement needed for acceleration and hill climbing. Hence by using a combined power source the peak power requirement can be met by the supercapacitors. As supercapacitors have fast charge rate, the regenerative braking is possible. It was found that by applying regenerative braking the fuel consumption was reduced by 15%[8]. Also supercapacitors can be used to crank the internal combustion engines thereby can reduce the power load of batteries and hence increase their lifetime. Significant interest has been generated in high power supercapacitors for railway and subway type applications.

Supercapacitors can also be used to provide the energy needed by power quality systems that ensure reliable and disturbance-free power distribution. Supercapacitors will supply the energy needed to inject power into the distribution line and thus compensate for any voltage fluctuations. Similarly in wind power applications, an energy storage system is required to have a large power capacity to absorb power surges during wind gusts, and also a large energy capacity for deep wind fluctuations lasting for minutes or longer. A battery-supercapacitor hybrid energy storage system[9] will take advantages of both technologies and provide high power and energy capacities thereby increasing the overall efficiency of the storage system.

The largest part of the supercapacitors sold nowadays is used in consumer electronic products, where they mainly serve as backup sources for memories, microcomputers, system boards, and clocks. In these applications there is a primary power source which normally supplies the load. In case of power outages due to disconnection or turn-off of the primary source, contact problems due to vibration or shocks, or a drop of the system voltage due to switching in of other heavy loads, supercapacitors can supply the critical power. Supercapacitors development is also underway to reduce cell size and cost. These two issues, particularly the latter, are considered critical to the continued migration of supercapacitors into new applications. As cost per Farad drops over time, applications of supercapacitors will tend to expand.

2.3 Principles of Energy Storage

2.3.1 Background

Conventional capacitors consist of two conducting electrodes separated by an insulating dielectric material. When a voltage is applied to a capacitor, opposite charges accumulate on the surfaces of each electrode. The charges are kept separate by the dielectric, thus producing an electric field that allows the capacitor to store energy. This is illustrated in Figure 2-1. For a conventional capacitor, capacitance C, is directly proportional to the surface area A, of each electrode and inversely proportional to the distance D, between the electrodes as expressed by the following equation:

$$C = \frac{\varepsilon_0 \varepsilon_r A}{D} \tag{2-1}$$

where, ε_0 is the dielectric constant (or permittivity) of free space and ε_r is the dielectric constant of the insulating material between the electrodes.

In ES the electrical energy is stored in an electrochemical double layer (Helmholtz Layer) formed at the electrode/electrolyte interface. Positive and negative ionic charges within the electrolyte accumulate at the surface of the solid electrode and compensate for the electronic charge at the electrode surface. The thickness of the double layer depends on the concentration of the electrolyte and on the size of the ions and is in the order of 5–10 Å, for concentrated electrolytes. This is illustrated in Figure 2-2.

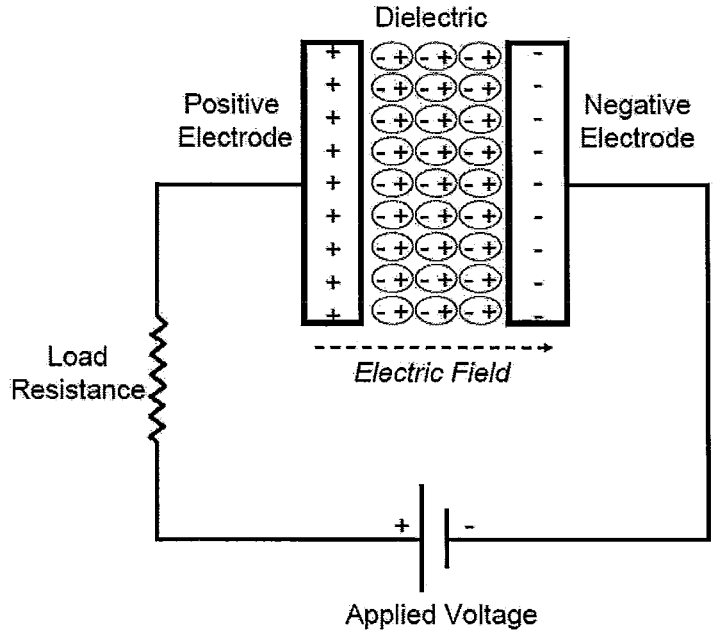

Figure 2-1 Schematic of a conventional capacitor[10]

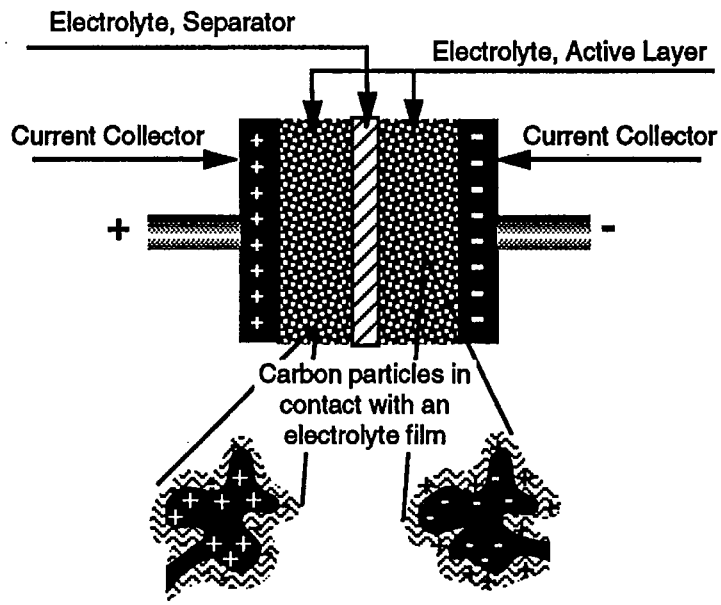

Figure 2-2 Schematic of an ES[11]

The two main attributes of any energy storage devices are its energy density and power density. Energy density describes the amount of energy that can be stored while power density describes how fast the stored energy can be delivered. The maximum energy stored E and maximum usable power P for a capacitor is calculated by:

$$E = \frac{CV^2}{2} \tag{2-2}$$

$$P = \frac{V^2}{4R} \tag{2-3}$$

where V is the voltage, C is the capacitance and R is the equivalent series resistance (ESR). An ideal energy storage system must have a high energy and power density and from the above equation it should have high capacitance, large voltage window and low ESR.

Figure 2-3 shows a Ragone plot of different energy storage devices. This graph presents the power densities of various energy storage devices, along the vertical axis, versus their energy densities, along the horizontal axis. Electrochemical capacitors currently fill the gap between batteries and conventional solid state and electrolytic capacitors. Despite greater capacitances than conventional capacitors, ESs have yet to match the energy densities of mid to high-end batteries. In the recent years due to extensive research of new electrode materials, improved understanding of ion behaviour and the design of new hybrid systems combining Faradic and capacitive electrodes have increased the performance of ESs.

Based on the charge storage mechanism ES can be classified in to three types. The first type is electrochemical double layer capacitors (EDLCs); it uses high surface

area carbon based active materials. The second type is known as pseudo-capacitors or redox supercapacitors; it uses transition metal oxides as well as conducting polymers as active materials. The last type is hybrid capacitors which combines the capacitive and pseudo-capacitive electrode and hence exhibit better performance.

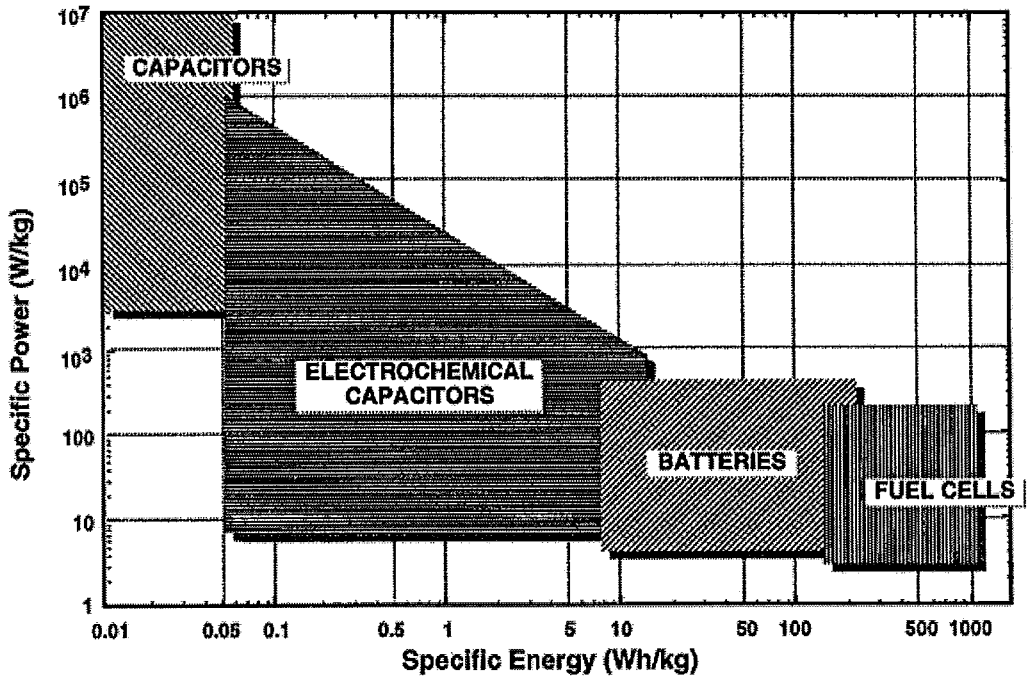

Figure 2-3 Ragone plot[11]

2.3.2 Electrochemical double layer capacitors

When an electronic conductor is brought in contact with a solid or liquid ionic-conductor, a charge accumulation is achieved electrostatically on either side of the

interface, leading to the development of an electrical double-layer. No charge transfer takes place across the interface and the current observed during this process is essentially a displacement current due to the arrangement of charges. Therefore, this process is non-Faradaic in nature[12]. An Electrochemical double layer capacitor (EDLC) has two electrodes immersed in an electrolyte with a separator between the electrodes. The electrodes are fabricated from high surface area, porous material having pores of diameter in the nanometer range. EDLCs utilize the double layer to store charge electrostatically, and there is no charge transfer between electrode and electrolyte. These double-layers, coupled with an increase in surface area and a decrease in the distance between electrodes, allow EDLCs to achieve higher energy densities than conventional capacitors[11, 13, 14].

The double layer capacitance of each electrode is calculated according to the Equation 2-1. The thickness of the double layer is very small (fraction of nm in liquid electrolytes), hence the charged electrode/electrolyte interface have a high specific capacitance of 15-30 $\mu F\ cm^{-2}$. With electrodes having large surface area (> 1000 $m^2\ g^{-1}$) carbon powders, felts, and aerogels, capacitances as large as ~ 150 – 300 $F\ g^{-1}$ can be achieved, which is far superior then conventional capacitor. Further, as there is no transfer of charge between electrolyte and electrode, there are no chemical or composition changes associated with non-Faradaic processes. Hence EDLCs exhibit a very high degree of reversibility in repetitive charge–discharge cycling with stable performance characteristics and have demonstrated cycle lives in excess of 500,000

cycles[15]. Carbon and its various other forms are widely used as electrodes for EDLC with studies focused on increasing the surface area and reducing the matrix resistivity[15]. A number of carbon manufacturers are now targeting supercapacitors as a market for their products.

2.3.3 Pseudo-capacitors

Pseudo-capacitors or redox supercapacitors, utilize the fast and reversible surface reactions for charge storage. The capacitance exhibited by such systems is called pseudo-capacitance. Pseudo-capacitance can arises due to three types of electrochemical processes[14], such as surface adsorption of ions from the electrolyte, redox reactions involving ions from the electrolyte, and the doping and undoping of active conducting polymer material in the electrode. The first two processes are primarily surface mechanisms and are hence highly dependent on the surface area of the electrode material. The third process involving the conducting polymer material is more of a bulk process and the specific capacitance of the material is much less dependent on its surface area, although relatively high surface area with micropores is required to distribute the ions to and from the electrodes in a cell. In all cases, the electrodes must have high electronic conductivity to distribute and collect the electron current. These Faradaic electrochemical processes involve the passage of charge across the double layer, similar to battery charging or discharging. The charges transferred in these reactions are voltage dependent. The capacitance can be calculated using the following equation:

$$C = \frac{Q_{tot}}{V_{tot}} \quad (2\text{-}4)$$

where the Q_{tot} and V_{tot} are the total charge and voltage change for a charge or discharge of the electrode. Transition metal oxides [16] as well as electronically conducting polymers [17], have been extensively studied in the past decades as electrodes for pseudo-capacitors. The Faradaic processes may allow pseudo-capacitors to achieve greater capacitances and energy densities than EDLCs and hence in recent days significant interest is shown in this system.

2.3.4 Hybrid systems

Hybrid capacitors attempt to exploit the relative advantages and mitigate the relative disadvantages of EDLCs and pseudocapacitors to obtain better performance characteristics[10]. Hybrid capacitors utilizes both Faradaic and non-Faradaic processes to store charge, hence they achieve energy and power densities greater than EDLCs without sacrificing cycling stability and affordability that have limited the success of pseudocapacitors. Based on their electrode configuration they are classified as composite, asymmetric and battery- type electrodes[10].

Composite electrodes integrate carbon-based materials with either conducting polymer or metal oxide materials and incorporate both physical and chemical charge storage mechanisms together in a single electrode. The carbon-based materials facilitate a capacitive double-layer of charge and also provide a high-surface-area backbone that increases the contact between the deposited pseudocapacitive materials and electrolyte.

The pseudocapacitive materials are able to further increase the capacitance of the composite electrode through Faradaic reactions[18, 19]. Asymmetric hybrids combine Faradaic and non-Faradaic processes by coupling an EDLC electrode with a pseudocapacitor electrode. In particular, the coupling of an activated carbon negative electrode with a conducting polymer positive electrode has received a great deal of attention[20, 21]. Like asymmetric hybrids, battery-type hybrids couple two different electrodes; however, battery-type hybrids are unique in coupling a supercapacitor electrode with a battery electrode. This specialized configuration reflects the demand for higher energy supercapacitors and higher power batteries, combining the energy characteristics of batteries with the power, cycle life, and recharging times of supercapacitors. Research has focused primarily on using nickel hydroxide, lead dioxide, and LTO ($Li_4Ti_5O_{12}$) as one electrode and activated carbon as the other[22-24].

2.4 Electrode Materials

The enormous progress in ES technology, resulting in electrode materials with higher and higher specific capacitance values, has led to an extension of their application range to the battery market. Selection of electrode materials plays a crucial role in determining the electrical properties of a supercapacitor. ESs can be classified based on charge storage mechanism as well as electrode materials. EDLCs utilize high surface area carbon-based active materials, while pseudo-capacitors utilize transition metal oxides and conducting polymers as active materials.

2.4.1 Carbon materials

Carbon materials are widely used for supercapacitor applications because of their unique combination of chemical and physical properties, namely; high conductivity, high surface-area, good corrosion resistance, high temperature stability, controlled pore structure, processability and compatibility in composite materials, and relatively low cost[15]. The different forms of carbon materials that are widely used as electrodes for ES are activated carbons, carbon aerogels, carbon fibres and carbon nanotubes.

Activated carbons

The process of increasing the surface-area (porosity) of carbonaceous material by thermal or chemical treatment is referred to as 'activation' and the resulting broad group of materials is referred to as activated carbons. As activated carbon is less expensive and possesses a higher surface area than other carbon based materials, it is widely used as electrode material in EDLCs. It utilizes a complex porous structure[25] composed of micropores (diameter < 2 nm), mesopores (diameter from 2 – 50 nm), and macropores (diameter > 50 nm) to achieve their high surface area. Usually, the capacitance values of activated carbons range from 100 to 200 F g^{-1} in aqueous medium, and from 50 to 150 F g^{-1} in organic medium. Although capacitance is directly proportional to surface area, empirical evidence suggests that, not all of the high surface area contributes to the capacitance of the device. Electrolyte ions that are larger than smaller micropores cannot diffuse into them, hence preventing some pores from contributing to charge storage[15].

The influence of capacitance on pore size distribution of activated carbon electrodes is a major area of research in the design of EDLCs.

Carbon aerogels

Carbon aerogels are highly porous materials prepared by the pyrolysis of organic aerogels. They are usually synthesized by the poly-condensation of resorcinol and formaldehyde, via a sol–gel process, and subsequent pyrolysis[26]. The aerogel solid matrix is composed of interconnected colloidal like carbon particles or polymeric chains. After pyrolysis, the resulting carbon aerogels have good electrically conductivity, high surface area (400 – 1000 $m^2 g^{-1}$), uniform pore size (mostly between 2 – 50 nm) and high density. They can also be produced as monoliths, composites, thin films, powders or micro-spheres. Further the surface area of aerogels can be substantially increased by activation. Different activation methods have been investigated, like thermal activation, electrochemical activation and chemical vapor impregnation in order to enhance the capacitive performance of the carbonaceous structure [15, 26, 27].

Carbon fibres

Commercially carbon fibres are usually produced from thermosetting organic materials such as cellulose, phenolic resins, polyacrylonitrile and pitch-based materials. The carbon fibres are prepared by the extrusion of precursor material through a die or spinnerets and then drawing of extrudant into a thin fibre. The raw fibre can be activated

in a controlled oxidising environment. The quality of carbon fibre depends on precursor and the manufacturing process. Activated carbon fibres have a typical diameter of ~10 μm and predominant micropores. The pores are largely situated at the surface of the fibre and hence provide good accessibility to active sites. As high adsorption capacities and a high adsorption rates are attainable, activated carbon fibres is a very attractive electrode for EDLCs. Even though activated carbon fibre and cloths have low electrical resistance along the fibre axis, the contact resistance between the individual fibres is high. The products of activated carbon fibre are generally more expensive then products of powder carbon [15].

Carbon nanotubes

Carbon nanotubes (CNTs) are of great interest in variety of applications from the fundamental research to applied perspectives. Recent research trend shows that there is an increasing interest in using CNTs as electrode materials for EDLCs [10, 15, 25]. CNTs can be grown directly onto the current collectors, subjected to heat-treatment, or cast into colloidal suspension thin films, with an open and accessible network of mesopores. The mesopores are interconnected allowing a continuous charge distribution and easy diffusion of ions. Hence, CNTs achieve capacitance comparable to those of activated carbon even though they have moderate surface area and have lower ESR than activated carbon. The high cost of production limits its application, but it can be used as conductive agent, in conjugation with other active materials for fabricating electrodes.

2.4.2 Metal oxides

Metal oxides present an attractive alternative as an electrode material because of high specific capacitance at low resistance, possibly to construct high energy, high power supercapacitors. Pseudo-capacitances arise due to fast, reversible redox reaction at the surface of active materials. RuO_2, NiO, Co_3O_4 and MnO_2 have been extensively studied as electrodes for pseudo-capacitors and are discussed below. Some of the other metal oxides are IrO_2, Fe_3O_4, TiO_2, SnO_2, V_2O_5 and MoO_3.

Ruthenium Oxide

Using RuO_2 as an electrode material for ES has many advantages. RuO_2 has a high capacitance which is about ten times higher than that of carbon based electrodes. The resistivity of RuO_2 is in the order of 10^{-5} Ω cm which is about two orders of magnitude lower than that of carbon[28]. As the ESR of RuO_2 is lower than that of other electrode materials, they are able to achieve higher energy and power densities than similar carbon based electrodes. The capacitance of ruthenium oxide in acidic solution is achieved by fast, reversible electron transfer together with an electro-adsorption of protons on the surface of active materials as described by [16]:

$$RuO_2 + xH^+ + xe^- \leftrightarrow RuO_{2-x}(OH)_x \qquad (2\text{-}5)$$

The specific capacitance of the hydrous RuO_2 in aqueous electrolyte (sulphuric acid) was about 750 F g^{-1}, which is much higher than anhydrous ruthenium oxide[14]. RuO_2 exhibit an ideal capacitive behaviour, which is evident from the mirror like cyclic voltammetry

response. Because of these properties, RuO_2 becomes an attractive material for ES. However, ruthenium oxide is an expensive material; it requires the use of strong acidic electrolyte such as sulphuric acid. Thus, a major area of research is the development of fabrication methods and composite materials to reduce the cost of active material, without reducing the performance.

Nickel Oxide

Nickel oxide is also a potential candidate as an electrode material for ES. Liu et al. were the first to develop porous nickel oxide[29] based electrodes for ES. They prepared porous NiO_x films by sol-gel techniques and were able to obtain a SC of 200 to 256 F g^{-1}. Later Srinivasan et al. developed an electrochemical precipitation technique[30] which was relatively inexpensive and highly controllable then sol gel techniques. Nickel oxide is stable in basic solutions and the charge storage mechanism has been reported to be based on the OH^- adsorption and desorption reaction as described by[30, 31]:

$$NiO + OH^- \leftrightarrow NiOOH + e^- \quad (2\text{-}6)$$

The disadvantages of using nickel oxide as electrode materials for ES stems from the facts that this material has relatively low capacitance and small voltage window. Even though nickel oxide films exhibit capacitive behavior, the current-potential response is potential dependent in contrast to the potential-independent current response of an ideal capacitor.

Cobalt Oxide

Cobalt oxide is a battery electrode material that has been studied for supercapacitor applications. There are three forms of cobalt oxide; cobaltous oxide (CoO), cobaltic oxide (Co_2O_3) and cobalt cobaltite (Co_3O_4). The most widely studied oxide for ES application is the spinel Co_3O_4[32]. The charge storage mechanism was suggested to be[33]:

$$Co_3O_4 + H_2O + OH^- \leftrightarrow 3CoOOH + e^- \quad (2\text{-}7)$$

Cobalt oxide based electrodes have lower capacitance valve of 164 F g^{-1}. Cobalt oxide is one among the few materials that operate in negative potential range[34, 35] (-0.4 to 0.4 V), hence they can be coupled with other positive electrodes (ruthenium oxide , manganese oxide or nickel oxide) to form a hybrid system.

Manganese oxide

Manganese oxides, in various crystalline and amorphous forms, have been used as electrode materials for batteries starting from the initial work of Leclanche in the 1860s, which ultimately formed the basis for the Zn/MnO_2 alkaline cell. The analysis of literature indicates that manganese dioxides are important materials for lithium batteries[36], alkaline Zn/MnO_2 cells[37], catalysts[38] and sensors[39]. Significant interest has been generated in the application of nanostructured manganese dioxide for the fabrication of ES[16, 40-45]. The use of manganese oxides for electrochemical energy storage has continued to expand to new applications, most recently to the field of ES. In 1999, Lee et

al[46] proposed manganese oxide as an electrode material for ES. Manganese oxides are considered as promising electrode materials due to the low cost of raw materials, the fact that manganese is environmentally friendlier than other transition metal oxide systems and because of its excellent electrochemical properties. The electrochemical performance of MnO_2 is determined by many variables, including the particle size and its crystal structure (or lack thereof), which are, in turn, determined by the synthesis methods and post synthesis heat treatments used to produce the oxide [43].

The capacitance of manganese dioxide is believed to be predominantly due to pseudocapacitance as a result of redox processes. The charge storage mechanism of manganese dioxide is based on surface adsorption of electrolyte cations C^+ (K^+, Na^+) as well as proton incorporation according to the reaction:

$$MnO_2 + xC^+ + yH^+ + (x+y)e^- \leftrightarrow MnOOC_xH_y \quad (2\text{-}8)$$

Figure 2-4 compares the cyclic voltammetric responses of different less expensive oxides. The figure show that manganese oxides exhibit an ideal box shaped voltammogram. Its rectangular shape is characteristic of the fast and reversible surface redox reactions mechanism for charge storage according to:

$$I = C \frac{dV}{dt} \quad (2\text{-}9)$$

where I is the current, (dV/dt) is the potential scan rate and C is the capacitance. Assuming a constant value for C, for a given scan rate the current I is constant.

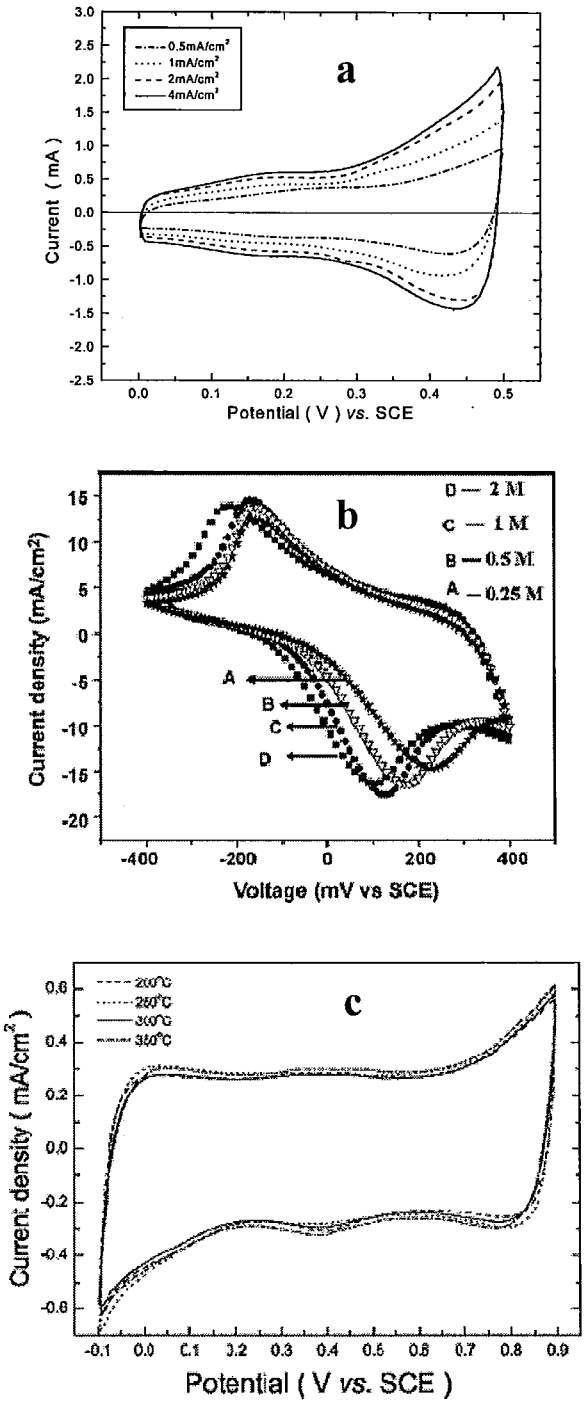

Figure 2-4 Cyclic voltammogram of (a) nickel oxide[31] (b) cobalt oxide[34] and (c) manganese oxide[42].

Many studies have been focused on the fabrication of manganese dioxide films[44, 47-50]. The values of SC reported in the literature[51, 52] are usually in the range between 100 and 250 F g^{-1}. These values are far from the theoretical SC of ~ 1370 F g^{-1} and reported experimental SC of ~700 F g^{-1} for very thin films[53, 54]. However, the SC values are much higher than NiO and Co_3O_4. Also the operating voltage window of manganese oxides is 1 V which is broader than nickel oxides and cobalt oxides. As energy density is proportional to the square of the voltage window, manganese oxides exhibit better energy density. The low cost and environmental friendly manganese oxide exhibits ideal capacitive behaviour, large voltage window and high capacitance, hence it has been chosen as the electrode material for this investigation.

2.4.3 Conducting Polymers

Electronically conducting polymers (ECP) are regarded as promising electrode materials for ES for two main reasons: (i) they provide high specific capacitance, as not only surface, but also bulk material is involved in charge storage mechanism (ii) they have high conductivity in the charged state, hence devices with low ESR are feasible. In addition, their plastic properties readily enable their manufacture as thin film, and their cost is lower than that of other electrode materials[55].

The storage in ECP is due to Faradaic process which takes place at the electrode materials. When oxidation occurs, (also referred to as 'doping'), ions are transferred to the polymer backbone. When reduction occurs ('dedoping') the ions are released back into the solution (Figure 2-5). Charging in conducting polymer film takes place

throughout the bulk volume of the film, and not just on the surface as is the case with carbon, hence they achieve high levels of specific capacitance[17]. The mechanical stress on conducting polymers during reduction-oxidation reactions limits the stability of these pseudocapacitors through many charge-discharge cycles. This reduced cycling stability has hindered the development of conducting polymer pseudocapacitors.

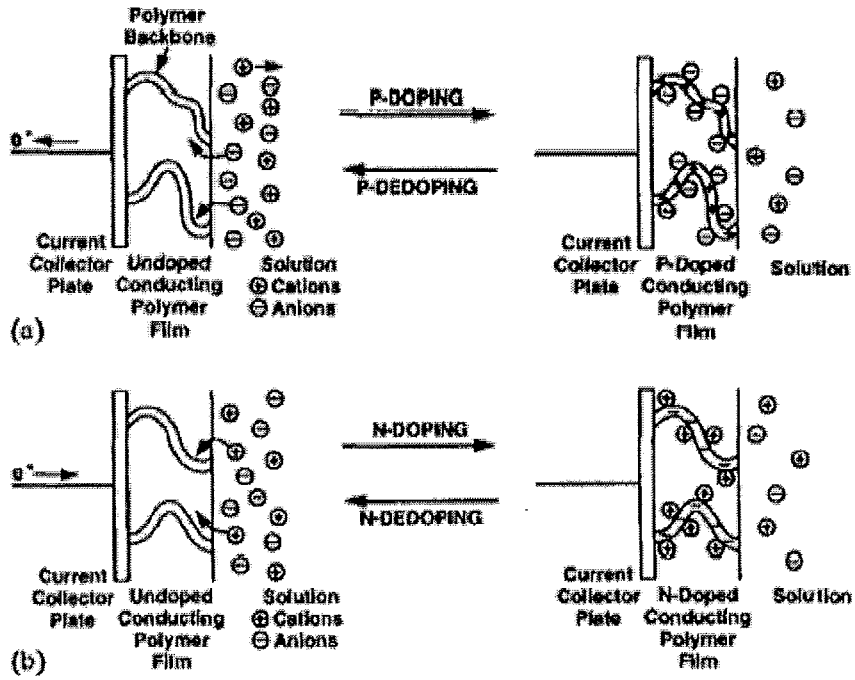

Figure 2-5 Charge storage mechanism of ECP[56].

2.5 Design of Supercapacitors

The construction of an ES is much similar to that of a battery in that it consists of two active layers with a separator between them wetted with an electrolyte as indicated in Figure 2-6. The maximum current density and power density of ES are limited by the ESR, which comprises the ionic and electrical resistances. The ionic resistance depends on the ionic conductivity of the electrolyte, the porosity of the electrode, the porosity of the separator and the thickness of the electrode and separator[57]. The ionic resistance of the ES is also strongly dependent on size of the ions from the electrolyte that diffuse into and out of the pores of the electrode particles. This is usually not a problem for an aqueous electrolyte, such as KOH, Na_2SO_4 or H_2SO_4, but is almost always a problem using organic electrolytes based on propylene carbonate or acetonitrile.

The pore size requirements for organic electrolytes (15–20 Å) are also greater than that of aqueous electrolytes (5–10 Å) [14]. Organic electrolytes are the most commonly used in commercial devices, due to their higher dissociation voltage (2-2.5 V). The resistivity of organic electrolytes is relatively high, however, limiting cell power. Aqueous electrolytes have a lower dissociation voltage, typically 1 V, but the resistivity of aqueous electrolytes are much lower (1–2 Ω cm) than that of organic electrolytes (20–60 Ω cm).

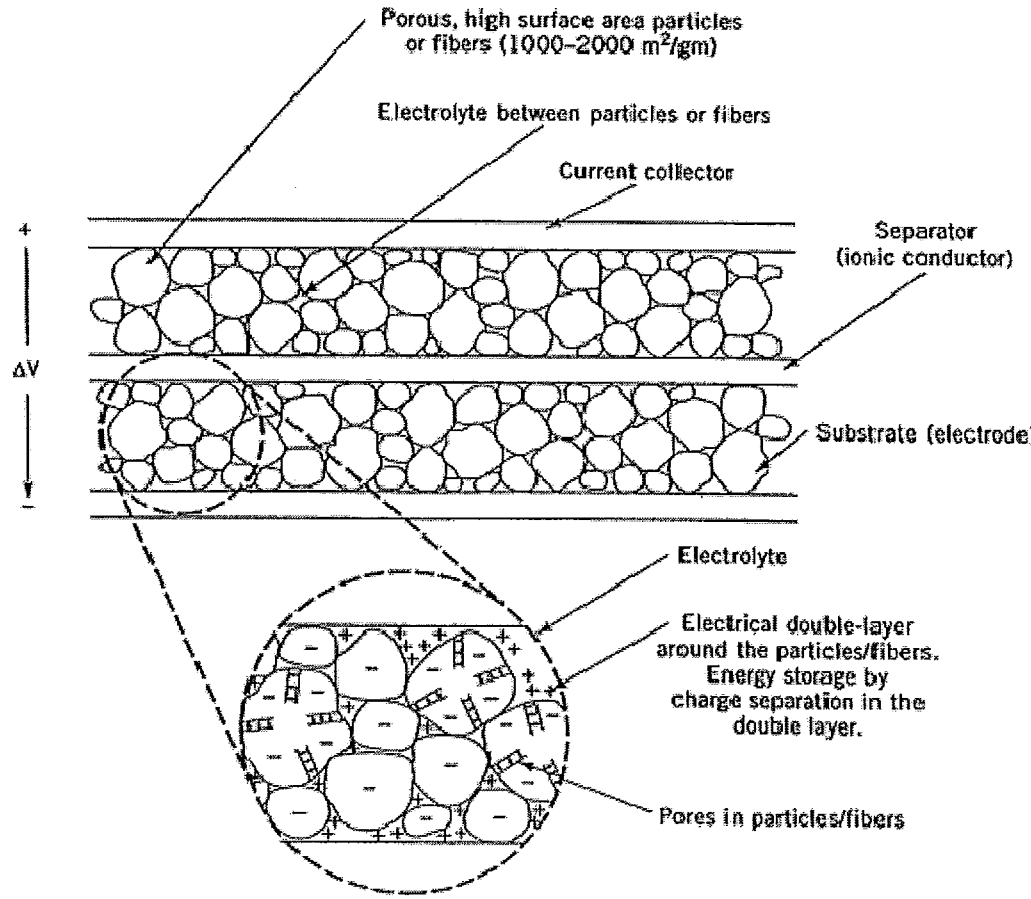

Figure 2-6 Electrochemical Supercapacitor[14]

A porous nanostructured electrode material with high surface area is essential for obtaining high capacitance in a supercapacitor. The porous electrode is often described by a truncated RC-transmission line (Figure 2-7). The equivalent circuit of the pore of a porous electrode is approximated by a line of *R* and *C* elements representing the electrolyte resistance and the respective elemental double layer capacitance at a particular depth of the pore[11].

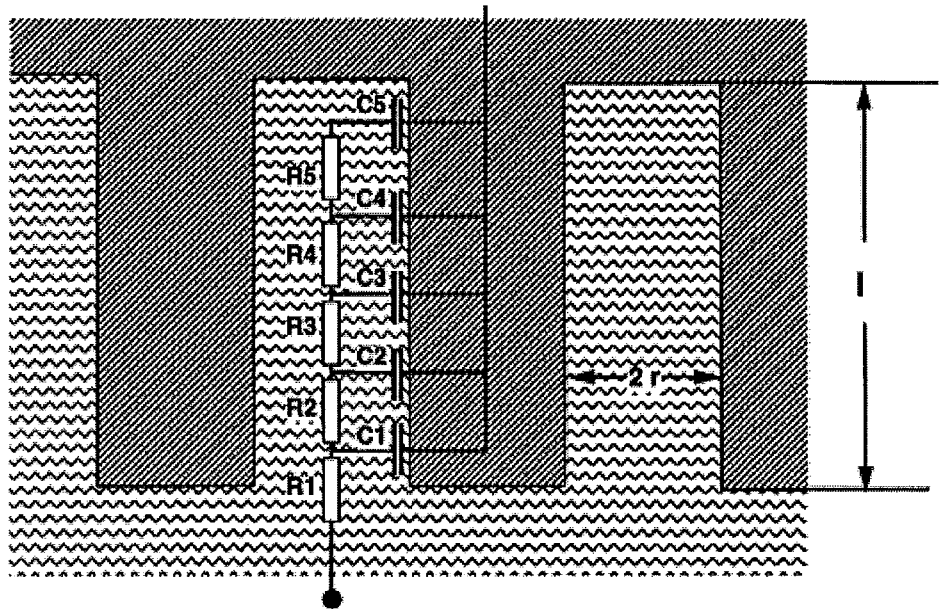

Figure 2-7 Equivalent circuit representation of the distributed resistance and capacitance with in a pore[11].

At low scan rates, the electrolyte ions penetrate deep in-to the pores utilising maximum active material, but at high scan rates due to the diffusion limitation in pores, the current flows predominantly along R1 to C1 and almost no current flow in to the deep. As scan rates are increased the electrolyte penetration in to the pores is poor and less surface area is utilised when compared to low scan rates, hence capacitance decreases as scan rate increases. Significant research has been directed to optimize the pore size to reduce the ionic resistance and obtain high power density.

The electrical resistance is mainly due to the electrode material including the bulk resistance and the contact resistance between particles, the contact between the current collector and the electrode, the contact between the current collector to the neighbouring

current collector of the same polarity for a multi-cell capacitor, and the contact between the current collector and the end metal plate[57]. Contact resistance between the particles and contact resistance between the current collector and the electrode is the two major sources of electrical resistance.

The contact resistance between the particles can be reduced by mixing the active materials with conducting agents (carbon black, carbon nanotubes, activated carbon) and by utilising conducting binder. Carbon black has high conductivity and it is cheap when compared to carbon nanotubes, but its capacitance is poor. Activated carbon has better capacitance but its conductivity is inferior to carbon black[15]. Hence there is a trade off in selecting a suitable conducting agents based upon the application.

Only a few particles at the interface of the electrode side are directly in contact with the current collector side; therefore, the interface is a bottleneck for the current flow, and causes a high electrical resistance. Surface treatments and conducting coating[58,59] on current collector have already been shown to decrease ohmic drops at the electrode/current collector interface. The design of nanostructured current collectors with an increased contact area is another way to control the interface between current collector and electrode.

When two capacitors (C_1, C_2) with different capacitance value ($C_1 < C_2$) are connected in series (Figure 2-8), the total capacitance will be lesser then the lowest capacitance according to the equation:

$$1/C_T = 1/C_1 + 1/C_2 \qquad (2\text{-}10)$$

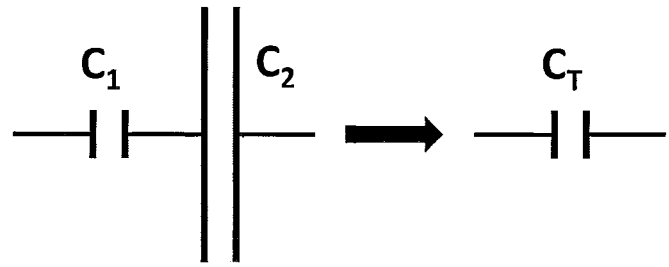

Figure 2-8 Capacitors in series

Hence, for high total capacitance, the capacitance of the electrode material and the capacitance of the conducting coating on current collector must be high.

2.6 Electrode Fabrication

Recently, MnO_2 electrode materials for supercapacitor application have been prepared by various synthetic methods, such as the sol-gel[53, 58, 60] and solution-based chemical routes[46, 61-63], electrostatic spray deposition (ESD)[42], sputtering followed by electrochemical oxidation[45] and electrochemical deposition[41, 50, 64-66]. Thin films of manganese oxide are used to produce thin electrodes and to modify the interface between current collector and electrodes material, while composite electrodes are fabricated to produce bulk electrodes.

2.6.1 Thin film electrodes

Sol-gel derived manganese oxide thin films are formed by either dip-coating or drop coating[53]. For the dip-coating process, a thin-film coating was formed on clean substrate by dipping the foil in to the sol and withdrawing it at a controlled speed. For the

drop-coating process, sols are dropped directly onto a horizontal substrate, forming a small circular spot, and then left to dry in air. Thin sol-gel derived manganese oxide films (~4 μg cm^{-2}) exhibited specific capacitance of 700 F g^{-1} [53]. Films of different thicknesses can be prepared by repeating the dip-coating or drop-coating process until desired thickness is reached. The sol-gel techniques are relatively complicated and introduction of binders in to the coating matrix were found to have certain unfavourable effects on electrochemical properties and conductivity of the electroactive materials[67].

The ESD technique was developed by Schoonman et al.[68] and has subsequently been applied to the preparation of transition-metal oxide films for various applications, such as electrodes for rechargeable lithium-ion batteries, ESs, organic solar cells, catalysts, solid oxide fuel cells, and gas sensors. In ESD technique thin film are deposited by utilizing electrohydrodynamic forces to spray the precursor on to the heated substrate. The major advantages of the ESD technique in the synthesis of metal oxide films are simple set-up, inexpensive and non-toxic precursors, high deposition efficiency and easy control of the surface morphology of the deposited layers. The specific capacitance of porous manganese oxide thin films prepared by ESD technique[42] decreased from 330 to 150 F g^{-1} as the mass of the oxide was increased from 18 to 116 μg cm^{-2}. Pseudocapacitive manganese oxide films have also been synthesized by anodic oxidation of metallic manganese films deposited by sputtering[45]. Electrochemical oxidation converts the metal film into a porous, dendritic structure which displays significant pseudocapacitance.

Electrochemical method of fabricating thin films can offer the advantages of low temperature processing, high purity, high uniformity, high reproducibility, controlled deposition rate and controlled microstructure[69]. Significant interest has been generated in the application of electrodeposition techniques to fabricate manganese oxide based ES electrodes. Previous investigations were focused on anodic deposition of manganese oxide[41, 44, 49, 64-66, 70]. In this work manganese oxide films were prepared by cathodic electrodeposition technique. As we have utilized electrodeposition technique to fabricate nanostructured films, a brief outline of the technique is given below.

2.6.1.1 Electrodeposition

Electrolytic deposition (ELD) and electrophoretic deposition (EPD) are the two electrodeposition methods. ELD leads to thin films from solutions of metal salts by production of colloidal particles in electrode reactions. EPD is achieved by motion of charged particles dispersed in a liquid towards an electrode under an applied electric field. The electrode reactions in ELD and electrophorectic motion of charged particles in EPD result in accumulation of ceramic particles and formation of films at the electrode[71,72].The deposition mechanism of the two techniques is illustrated in Figure 2-9.

EPD is an important tool for the preparation of thick films, while ELD enables the formation of nanostructured thin ceramic films (Figure 2-10). To modify the current collector/active material interface we need a highly porous, nanostructured thin film which has high conductivity and high capacitance. As ELD enables us to achieve these desired properties ELD techniques was chosen and is discussed below.

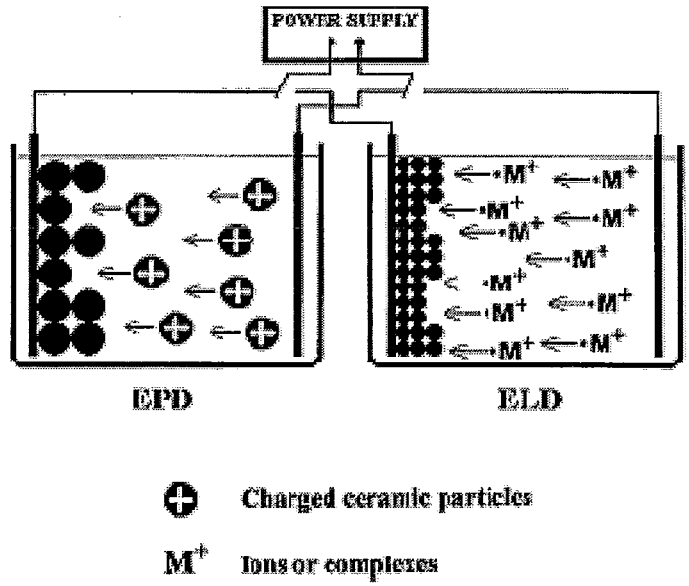

Figure 2-9 Schematic of cathodic EPD and ELD[73].

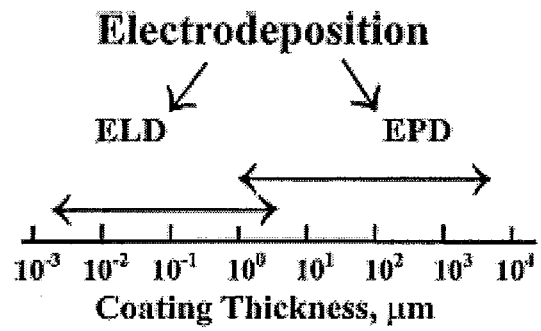

Figure 2-10 Thickness of films deposited using ELD and EPD[73].

2.6.1.2 Electrolytic deposition

There are several features which distinguishes electrosynthesis from other thin film fabrication methods[74]:

(i) Electrochemical synthesis takes place close to the electrode within the electric double layer, which has a very high potential gradient of 10^5 V cm^{-1}. Under these conditions, the reactions often lead to products which cannot be obtained in a chemical synthesis.

(ii) The product is deposited on the electrode in the form of a thin film or a coating. Further, a solid-liquid interface facilitates the growth of conformal coatings on substrates of any shape, especially if a suitably shaped counter electrode is employed to provide uniform field.

(iii) Electrochemical synthesis is a low-temperature technique limited by the boiling point of the electrolyte. This can be raised by using molten salt electrolytes.

(iv) Kinetic control can be exercised by controlling the current passed through the cell, while thermodynamic control can be exercised by choosing the applied cell potential.

(v) An electrochemical synthesis is an oxidation or a reduction reaction. By fine-tuning the applied cell potential, the oxidizing or reducing power can be continuously varied and suitably selected.

(vi) The film composition can be controlled by varying the bath composition.

(vii) The experiments are simple to perform and the instruments are inexpensive and readily available.

In a typical ELD process, the deposition is achieved by passing an electric current between two or more electrodes immersed in an electrolyte. The two important parameters that determine the course of the reaction are (i) the deposition current and (ii) the cell potential. Of the two, anyone can be controlled as a function of time during the reaction. In a galvanostatic synthesis, a delicate control can be exercised over the rate of the reaction leading to deposits with good adhesion and a controlled morphology, while a potentiostatic synthesis, yield a pure single phase product corresponding to the applied potential[74]. ELD can be achieved by anodic deposition and cathodic deposition techniques.

2.6.1.2.1 Anodic deposition

In this technique, a metal ion in a lower oxidation state is oxidized to a higher oxidation state anodically. The pH of the electrolyte is chosen in such a way that the lower oxidation state is stable while the higher oxidation state readily undergoes hydrolysis to yield the metal oxide or hydroxide [69, 74] according to the following equations:

$$M^{z+} \rightarrow M^{(z+\Delta)+} + \Delta e^{-} \quad (2\text{-}11)$$

$$M^{(z+\Delta)+} + (z+\Delta)\ OH^{-} \rightarrow M(OH)_{z+\Delta} \rightarrow MO_{(z+\Delta)/2} + (z+\Delta)/2\ H_2O \quad (2\text{-}12)$$

Manganese oxide films can be prepared by anodic oxidation of Mn^{2+} ions. Different precursors such as $MnSO_4.5H_2O$, $Mn(CH_3COO)_2$, $MnCl_2.4H_2O$ and $Mn(NO_3)_2.4H_2O$[50] were utilised to synthesis MnO_2 films anodically. The anodic deposition variables such as current density, pH, composition and temperature of plating bath were found to be the

key factors influencing the specific capacitance on manganese oxide[47, 70]. However this technique will cause anodic oxidation and dissolution of high surface area current collector. Hence it is necessary to develop cathodic technique instead of anodic deposition.

2.6.1.2.2 Cathodic deposition

In this method, cathodic reactions are used to generate OH-groups and increase the pH at the electrode. Metal ions or complexes which are stable in the bulk of solutions at low pH are hydrolysed by electrogenerated base at the electrode surface to form cathodic deposit[69, 71]. Cathodic electrodepositon of manganese oxides enables deposition of active materials on the metallic current collectors of high surface area. The problem related to the anodic oxidation and dissolution of metallic collectors can be prevented. Also, it enables co-deposition of various inorganic materials and modification of electrode composition.

Recently, manganese oxide films were obtained by polymer assisted cathodic electrosynthesis from $MnCl_2$ solutions in a mixed ethanol-water solvent. The obtained films were heat treated to 300 ℃ which resulted in burning out of polymer, partial oxidation of Mn^{2+} species and the formation of crystalline Mn_3O_4 phase. Electrochemical cycling resulted in further oxidation of Mn speices to form electrochemically active MnO_x films, which exhibited the peusdocapacitive behaviour[75]. In this work manganese oxide films have been deposited by cathodic reduction of Mn^{7+} species using $KMnO_4$

solutions. This approach offers the advantages of polymer-free aqueous processing and room temperature reduction of Mn^{7+} species using aqueous solutions.

2.6.2 Composite electrodes

A complicating factor in the application of manganese dioxide for supercapacitor is low electronic and ionic conductivity of this material. It is important to note that the manufacturing of efficient supercapacitor requires higher materials loadings using light weight current collectors. Many successful efforts have been made in the area of the fabrication of composite materials, where higher electronic conductivity has been achieved by the use of conductive additives[76-79]. The SC of 72 F g^{-1} in the 0.1 M K_2SO_4 electrolyte was reported for composite manganese dioxide – acetylene black electrodes[76] with material loading in the range of 10-40 mg cm^{-2}.

The improvement in performance of composite electrodes can be achieved using porous current collectors. Porous nickel foams are used in industry as advanced current collectors for nickel-cadmium, nickel-metal hydride, nickel-zinc and lithium ion batteries[80-84]. In the batteries, nickel foams contain active material within their light weight web, which provides structural strength, improved electrolyte access to the active material, high electronic conductivity and reduced contact resistance. Composite electrodes are produced by pasting slurry of active material into porous nickel foam, followed by impregnation, drying and calendering. The high porosity and large pore size of nickel foams allow for easy impregnation of the active material slurry into the porous

current collectors. However, the increase in foam porosity resulted in reduced electronic conductivity but this problem has been addressed by the use of conductive additives[80].

The goal of this investigation was the fabrication of nanostructured composite manganese dioxide electrodes for ES using nickel foam current collectors. Manganese dioxide nanoparticles prepared by a chemical precipitation method and carbon black conductive additives were used for the impregnation of nickel foams and the formation of porous electrodes.

3. OBJECTIVES

The objective of this work is to develop advanced manganese dioxide based electrodes for supercapacitors.

- Materials: Synthesis of nanostructured manganese dioxide coatings and manganese dioxide nanoparticles from solutions of $KMnO_4$.
- Processing Techniques: The development of cathodic electrodeposition of manganese dioxide from $KMnO_4$ solutions. The development of novel chemical precipitation methods to produce manganese dioxide and Ag-doped manganese dioxide powders.
- Fabrication: The development of fabrication techniques to obtain nanostructured coatings by cathodic electrodeposition. Fabrication of manganese dioxide-carbon black and Ag-doped manganese dioxide-carbon black composite electrodes using advanced current collectors.
- Characterisation: Investigate the influence of deposition kinetics, microstructure, composition, deposition and co-deposition conditions on electrochemical properties of the films. Investigate the influence of calendaring conditions, electrode porosity, electrode and electrolyte composition and doping on the electrochemical properties of the composite electrodes.

4. EXPERIMENTAL PROCEDURES

4.1 Cathodic Electrodepositon of MnO_2 films

Electrodeposition was performed from the 0.01 - 0.15 M $KMnO_4$ (Aldrich) aqueous solutions. The electrochemical cell for deposition included a stainless steel substrate and two platinum counter-electrodes. The deposits were obtained on stainless steel foils (50×50×0.1 mm) substrates. Deposit weight was studied by weighing the substrates before and after deposition followed by drying at room temperature for 24 hours.

The deposition process has been monitored using a quartz crystal microbalance (QCM 922, Princeton Applied Research) controlled by a computer using a WinEchem software. The QCM measures the frequency change associated with the increase in deposit weight during deposition. The relationship between frequency change (ΔF) and mass change (Δm) is described by the Sauerbrey's equation[85]:

$$-\Delta F = \frac{2F_0^2}{A\sqrt{\rho_q \mu_q}} \times \Delta m \qquad (4\text{-}1)$$

where, F_0 is the parent frequency of QCM (9 MHz), A is the area of gold electrode (0.2 cm^2), ρ_q is the density of the quartz (2.65 g cm^{-3}) and μ_q is the shear modulus of quartz (2.95×10^{11} dyne cm^{-2}).

4.2 Composite Electrodes

4.2.1 Preparation of MnO_2 powders using isopropanol as a reducing agent

Manganese oxide powders were prepared by a chemical reduction method. Precipitation was achieved by addition of 5 – 50 ml of isopropanol to 100 mL of aqueous 0.2 M $KMnO_4$ (Aldrich) solution. Stirring was continued during 1 hour after precipitation. The precipitate obtained was filtered and washed repeatedly in water and dried under ambient temperature for 72 hours.

4.2.2 Preparation of MnO_2 powders using potassium borohydride (KBH_4) as a reducing agent

KBH_4, $KMnO_4$ and $AgNO_3$ were purchased from Aldrich. Manganese dioxide was prepared by a chemical reduction method using aqueous solutions[61, 62]. Precipitation was performed by slow addition of 10 mL of 0.25 M KBH_4 to 50 mL of 0.1 M $KMnO_4$ solution.

The pH of the KBH_4 solution was adjusted to pH 11 using KOH. The initial pH needs to be maintained high in order to prevent the rapid loss of hydrogen before the reduction reaction, as the hydrolysis of borohydrides is facilitated by acidic conditions[61] as shown below:

$$BH_4^- + 2H_2O \rightarrow BO_2^- + 4H_2 \quad (4\text{-}2)$$

HNO_3 was added to $KMnO_4$ solutions during the reduction reaction in order to maintain constant pH of 3 or 6. Acidic conditions (pH $\leq$ 3) tend to stabilize predominantly Mn^{4+}, nearly neutral conditions (pH ~6) can stabilize Mn^{3+}. The potassium content that can be incorporated into manganese oxide powders increases with increasing pH.

KBH_4 has been also utilized as a reducing agent for the precipitation of Ag and composite manganese dioxide-Ag powders. Precipitation was performed at a constant pH 3 by slow addition of 10 mL of 0.25 M KBH_4 to 50 mL of 0.01 M $AgNO_3$ solution or to mixed 0.1 M $KMnO_4$ and 0.005-0.1 M $AgNO_3$ solutions. Stirring was continued during 1 h after precipitation. The precipitate obtained was filtered and washed repeatedly in water and dried under ambient temperature for 72 hours.

4.2.3 Fabrication of composite electrodes

The slurry was prepared by mixing the MnO_2 powders with carbon black (average particle size 15 nm, CABOT) and polyvinyl butyral (PVB) binder. The slurry was then impregnated in to the porous INCOFOAM® current collectors followed by drying and calendering to desired thickness[80]. INCOFOAM® current collectors with a volumetric porosity of 95% were made by Vale Inco using carbonyl technology[81]. The total mass of manganese dioxide and carbon black in the composite electrodes was 50-55 mg cm^{-2}. A schematic representation of the fabrication process is shown in Figure 4-1.

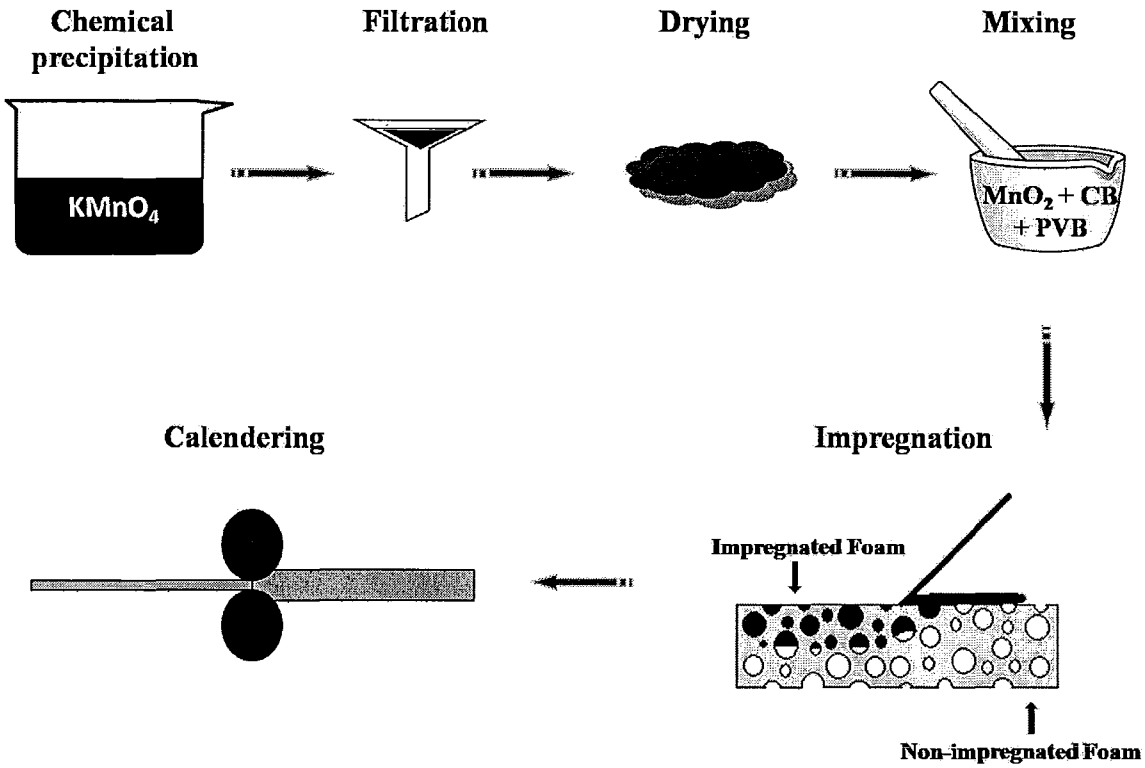

Figure 4-1 Fabrication of composite electrodes.

4.3 Materials Characterization

The phase content of the deposits and powders was determined by XRD with a diffractometer (Nicolet I2) using monochromatic Cu Kα radiation at a scanning speed of 0.5° min^{-1}. TGA and DTA studies were carried out in air between room temperature and 1000°C at a heating rate of 5°C min^{-1} using a thermoanalyzer (Netzsch STA-409). The microstructure of the coatings deposited on stainless steel substrates and the powders was investigated using a JEOL JSM-7000F scanning electron microscope (SEM) equipped

with Energy Dispersive Spectroscopy (EDS) and a JEOL 2010F transmission electron microscope (TEM).

4.4 Electrochemical Characterization

Electrochemical characterization of the deposited films and fabricated composite electrodes was studied using a potentiostat (PARSTAT 2273, Princeton Applied Research) controlled by a PowerSuite electrochemical software. A standard three-electrode cell contained a working electrode, a platinum gauze counter electrode and a standard calomel reference electrode (SCE). The surface area of the working electrodes was 1 cm^2. Testing was performed in the 0.1 – 0.5 M Na_2SO_4 aqueous solution, degassed with purified nitrogen gas.

Cyclic voltammetry (CV) measures charge-response with regard to a changing voltage, and is therefore a means of evaluating capacitance. In CV analysis, a series of changing voltages at a constant sweep rate (dV/dt) are applied and the current response is recorded. An ideal capacitor with no resistance would display a rectangular shape. CV studies were performed within a potential range of 0 – 1.0 V vs. SCE at scan rates of 2 – 100 mV s^{-1}. The SC was calculated using half the integrated area of the CV curve to obtain the charge (Q), and subsequently dividing the charge by the mass of the film (m) and the width of the potential window (ΔV):

$$C=Q/m\Delta V \tag{4-3}$$

Faster sweep rates correspond to charging and discharging at higher power levels. Multiple plots obtained at increasing sweep rates are therefore often displayed on the same graph to demonstrate the impact of power levels on the charging characteristics. From such plots it is evident that capacitance decreases at higher frequencies. Charge/discharge behavior was examined by chronopotentiometry. The galvanostatic charge/discharge cycling was performed between 0 and 0.1 V vs. SCE at different current densities.

Electrochemical impedance spectroscopy is a method to measure complex impedance of electrochemical cells. Figure 4-2 shows the equivalent circuits for a pseudocapacitance and involves the following circuit elements: the double-layer capacitance C_{dl}, a Faradaic reaction resistance R_F, a pseudocapacitance C_p, and the resistance of electrolyte R_S. At low frequency, the real part of the impedance approximately equals to the sum of R_F and R_S while at high frequency, the real part of the impedance equals to R_S. The complex impedance $Z^*=Z'-iZ''$ for the fabricated electrodes was investigated in the frequency range of 0.1 Hz-100 kHz at voltage of 10 mV.

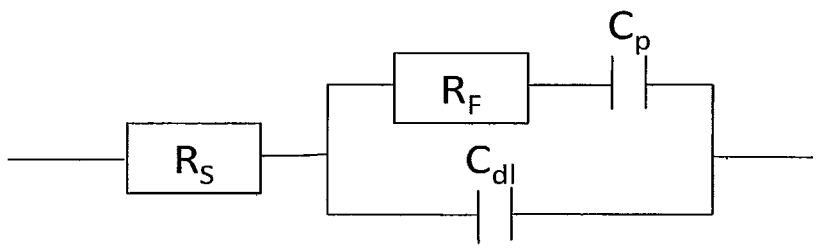

Figure 4-2 Equivalent circuit of a supercapacitor[13].

5. RESULTS AND DISCUSSION

5.1 Cathodic Electrodeposition of MnO_2 Films

Cathodic deposits were obtained from 0.01 M – 0.15 M $KMnO_4$ solutions. The deposition mechanism can be attributed to the diffusion and cathodic reduction of anionic MnO_4^- species. The reduction of MnO_4^- species and precipitation of MnO_2 are in agreement with the Pourbaix diagram for Mn[86]. However, only limited information is available in the literature related to the complex chemistry of the reduction of MnO_4^- species. The kinetic pathway of reducing Mn^{7+} to Mn^{4+} depends on the electrode potential, current density, pH, concentration of MnO_4^- species and deposition conditions. In neutral aqueous solution MnO_4^- species can be reduced to MnO_2 according to the following equation [86]:

$$MnO_4^- + 2H_2O + 3e^- \rightarrow MnO_2 + 4OH^- \quad (5\text{-}1)$$

5.1.1 Influence of current density

The results presented in Figure 5-1 shows deposition yield obtained at galvanostatic conditions from 0.02 M $KMnO_4$ solution. The deposit mass increased with increasing deposition time at a constant current density. The increase in current density resulted in higher deposition yield. Deposition yield obtained at a current density of 1 and 2 mA cm^{-2} resulted in a linear increase in deposit mass with increasing deposition time, which indicates a possibility of easy control of the film thickness. However, at a

current density of 3 mA cm^{-2}, time dependent deposition rate was observed. It should be noted that the deposition yield is influenced by diffusion, electromigration, kinetics of electrochemical reactions and other factors.

The increase in current density and electric field in the solution resulted in higher rate of cathodic reactions and enhanced electromigration of anionic MnO_4^- species. This can result in time-dependent concentration gradient at the cathode surface and time dependent deposition rate at the initial stage of the deposition process.

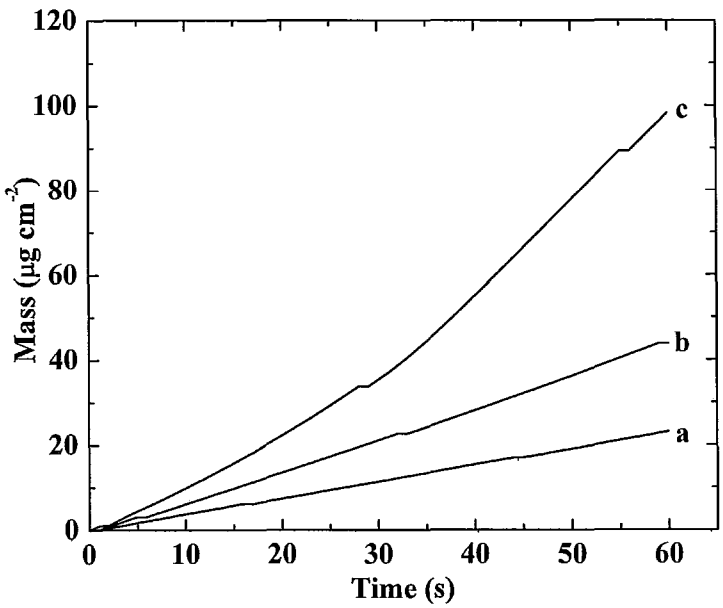

Figure 5-1 Deposit mass vs. deposition time for deposits obtained from 0.02 M $KMnO_4$ solutions at current densities of (a) 1 mA cm^{-2} (b) 2 mA cm^{-2} (c) 3 mA cm^{-2}.

5.1.2 Influence of concentration

The results presented in Figure 5-2 indicate that the deposition rate decreased with increasing $KMnO_4$ concentration at a constant current density of 2 mA cm^{-2}. It is suggested that electrosynthesis of MnO_2 is governed by diffusion-electromigration kinetics in the $KMnO_4$ solutions. When a negatively charged MnO_4^- ion is reduced cathodically, it has to approach the cathode by diffusion against an adverse potential gradient. In concentrated solutions, the interactions between ions can result in enhanced friction effect.

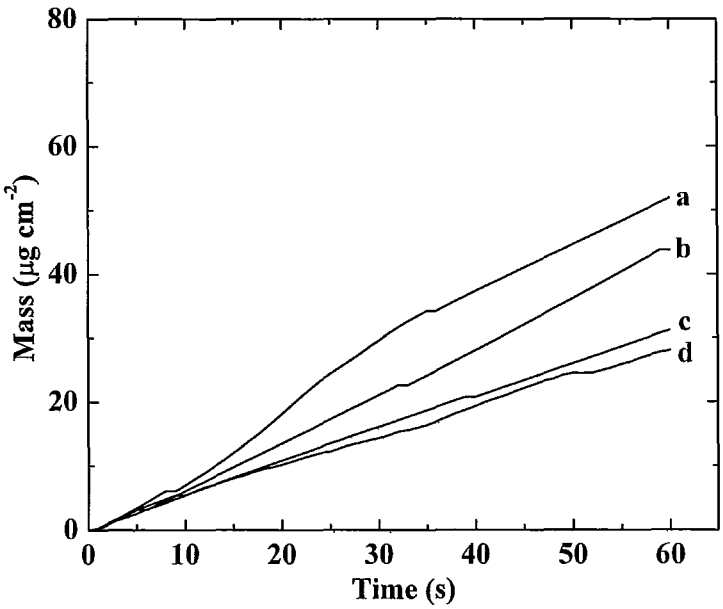

Figure 5-2 Deposit mass vs. deposition time for deposits prepared from (a) 0.01 M, (b) 0.02 M, (c) 0.1 M, (d) 0.15 M $KMnO_4$ solutions at a current density of 2 mA cm^{-2}.

It is important to note, that the decrease in diffusion coefficient with increasing solution concentration has been observed in many electrochemical and non-electrochemical processes and discussed quite extensively in the literature[87, 88]. In our experiments, the enhanced friction effect in concentrated solutions can be expected as a result of the adverse potential gradient and interactions of ions moving in cathodic direction due to the diffusion with ions moving in anodic direction due to the electromigration.

Figure 5-3 compares microstructures of the deposits prepared at different experimental conditions. The deposits prepared from the 0.02 M $KMnO_4$ solutions without stirring were crack-free (Figure 5-3a). SEM image at higher magnification (Figure 5-3b) shows a porous microstructure with typical pore size of about 100-200 nm. The surface structure is composed of nanowhiskers with typical length of ~100 nm. It is important to note, that electrical conductivity of manganese dioxide is low, therefore film porosity is beneficial for charge transfer during electrosynthesis. The stirring of the 0.02 M $KMnO_4$ solutions resulted in a "cracked-mud" morphology, which consisted of dense islands (Figure 5-3c, d).

The films prepared from the 0.1 - 0.15 M $KMnO_4$ solutions without stirring showed a similar morphology (Figure 5-3e, f). The increase in the $KMnO_4$ concentration from 0.02 M to 0.1 - 0.15 M or stirring of the 0.02 M solutions resulted in reduced concentration gradient at the cathode surface. The MnO_4^- depletion during deposition from the 0.02 M $KMnO_4$ solutions without stirring provided higher MnO_4^- concentration

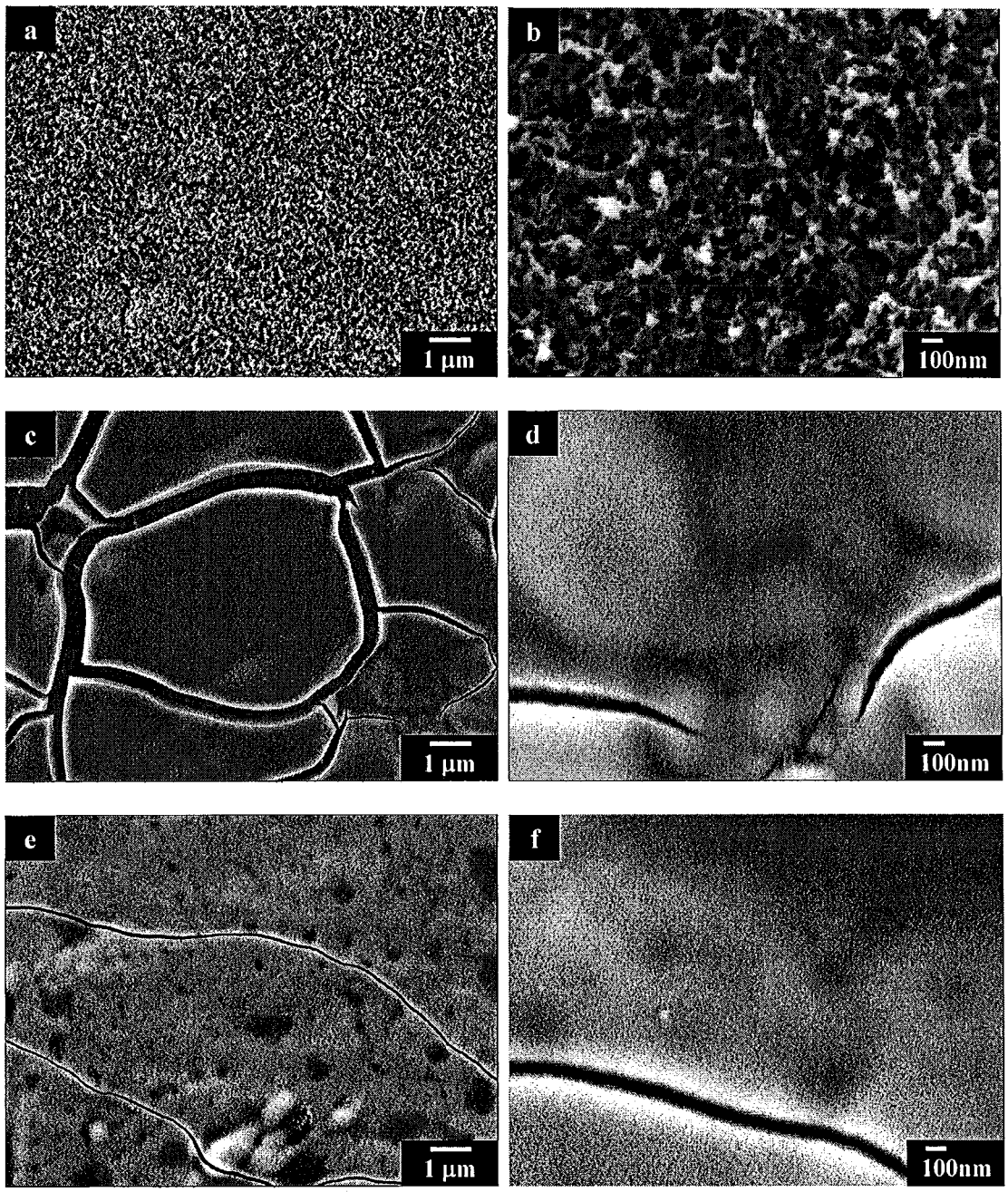

Figure 5-3 SEM images for deposit prepared at a constant current density of 2 mA cm^{-2} from (a, b) 0.02 M (c, d) 0.02 M stirring at 180 rpm and (e, f) 0.1 M $KMnO_4$ solutions .

gradient at the electrode surface, resulting in enhanced diffusion of MnO_4^- ions towards the cathode and higher MnO_2 deposition rate (Figure 5-1). The higher deposition rate can result in porous films. It is suggested that the porous microstructure of MnO_2 films prepared from the 0.02 M $KMnO_4$ solutions without stirring promoted the charge transfer during electrosynthesis. Moreover, the porous microstructure is beneficial for crack prevention. It is well known that crack propagation can be prevented in porous materials by the crack-tip blunting mechanism [89, 90]. Our results indicate that porous films with thickness of 1-2 μm can be produced by electrodeposition from the 0.02 M $KMnO_4$ solutions.

5.1.3 Influence of deposition conditions

The porosity of MnO_2 films is an important requirement for supercapacitors, batteries, catalysts and other applications. Therefore, it is necessary to investigate the influence of other processing conditions on the deposition mechanism and microstructure of MnO_2 films.

Pulse deposition has been further utilized for the deposition of MnO_2 films. In the pulse electrodeposition experiments, a series of pulses of constant current density was separated by periods of zero current. The deposition was performed from the 0.02 M $KMnO_4$ solutions with "on" time 20 s, "off" time 10 s. The current density was 2 mA cm^{-2} and total cathodic current duration was 2 min.

The deposit mass versus time dependence shown in Figure 5-4 indicates mass gain during the "on" time, when the current was applied. The sample mass remained constant during the "off' time, corresponding to zero current.

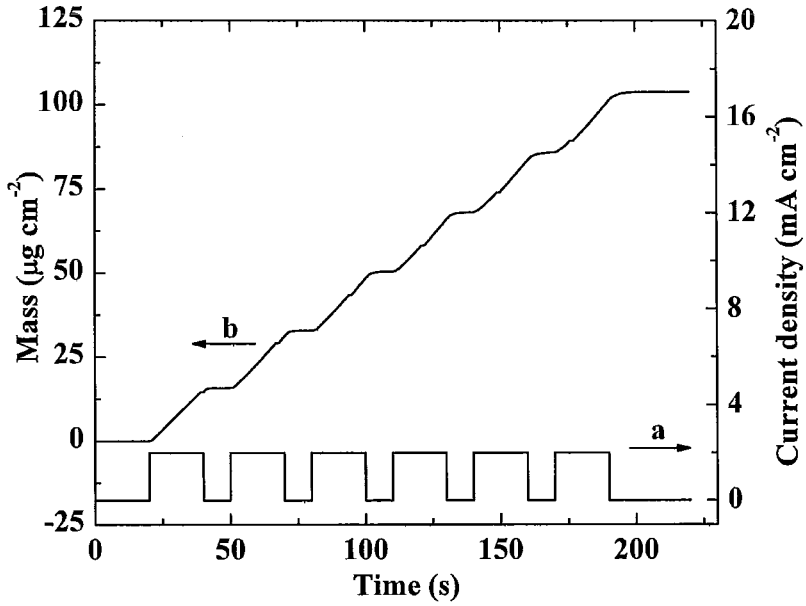

Figure 5-4 (a) Current density and (b) deposit mass vs. deposition time for deposits prepared from 0.02 M $KMnO_4$ solutions using pulse deposition.

SEM investigations revealed relatively dense microstructure of the deposited films, which exhibited cracks (Figure 5-5). This is in contrast with the results obtained at the galvanostatic regime using the solutions of the same concentration and at the same current density. The microstructure of the films prepared using pulse deposition from 0.02 M $KMnO_4$ solutions was similar to that for films of the same mass prepared from the 0.1 M $KMnO_4$ solutions. It is suggested that MnO_4^- concentration at the electrode

surface decreased during the "on" time due to reaction (5-1) and increased during the "off" time due to diffusion, which resulted in reduced concentration gradient at the cathode surface. It is suggested that MnO_4^- depletion at the electrode surface is an important factor controlling the microstructure of the films.

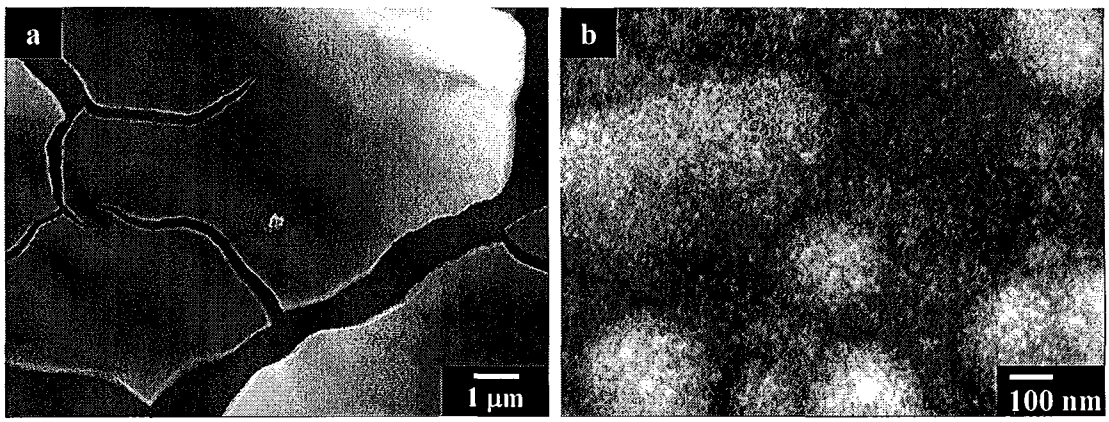

Figure 5-5 SEM images at different magnifications of the deposits prepared using pulse deposition from 0.02 M $KMnO_4$ solutions, "on" time 20 s, "off" time 10 s. The current density was 2 mA cm^{-2} and total cathodic current duration was 2 min.

Deposition was also performed in a reverse pulse regime. In this approach, films were deposited at a constant cathodic current density of 1-2 mA cm^{-2} during 2-5 min, than current of 0.5-2 mA cm^{-2} of opposite polarity and duration of 0.5-1 min was applied. Figure 5-6 shows mass change during the film deposition in the reverse pulse regime. The QCM data shows mass gain corresponding to the cathodic current and a small mass reduction when a current of opposite polarity was applied.

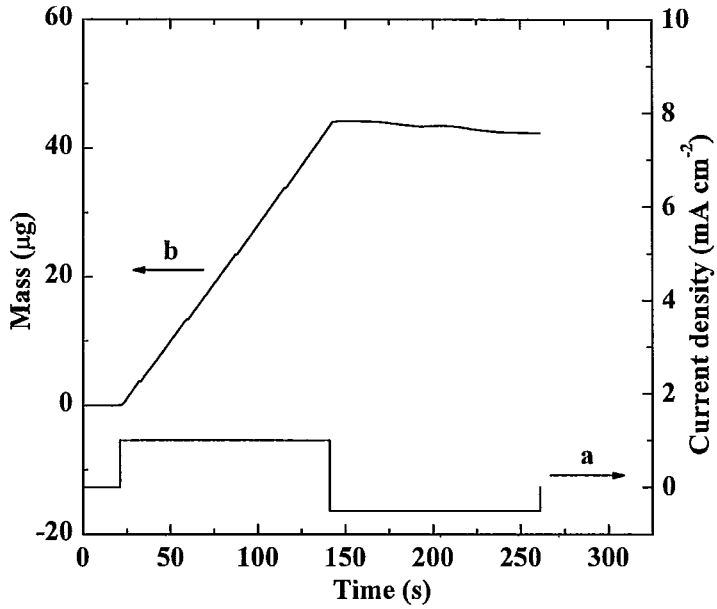

Figure 5-6 (a) Current density and (b) deposit mass vs. deposition time for deposits prepared from 0.02 M $KMnO_4$ solutions in the reverse pulse regime.

Figure 5-7 shows typical microstructure of a film prepared in the reverse pulse regime. SEM images at different magnifications show that the films are crack free and exhibit porosity. In contrast, the application of one additional cathodic pulse resulted in reduced porosity. Such films exhibited cracks and consisted of nearly spherical particles (Figure 5-8).

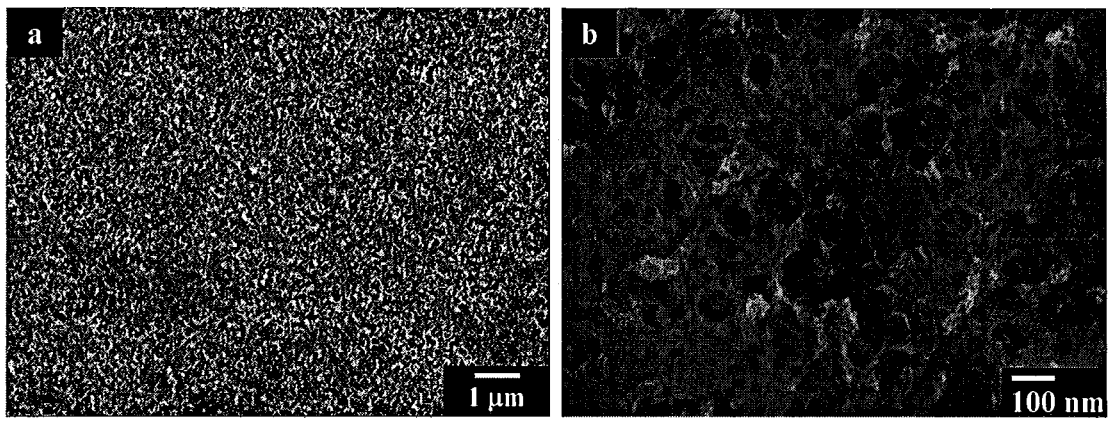

Figure 5-7 SEM images at different magnifications of the deposit prepared from the 0.02 M $KMnO_4$ solutions in the reverse pulse regime at a cathodic current density of 2 mA cm^{-2} during 2 min, and anodic current density of 2 mA cm^{-2} during 1 min.

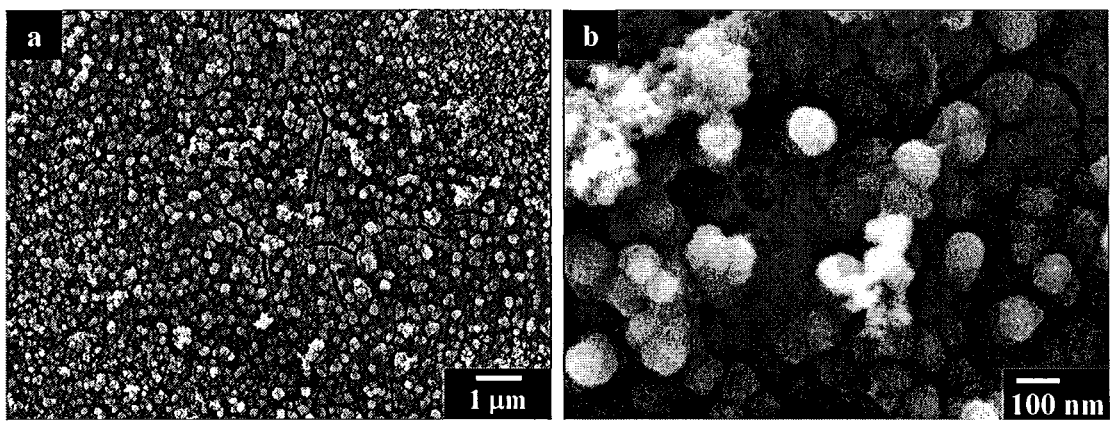

Figure 5-8 SEM images at different magnifications of the deposit prepared from the 0.02 M $KMnO_4$ solutions in the reverse pulse regime followed by a cathodic pulse of 2 mA cm^{-2} during 1 min.

Porosity is of great importance for the performance of supercapacitor electrodes. The charge-discharge mechanism involves adsorption-desorption of ions. Therefore efficient ion transport from solution to the active material in pores is necessary in order to achieve a high SC. Moreover, the transport of ions in the pores is essential in order to reduce the electrical resistance of the electrodes. The results described above indicate that porous and crack free films can be obtained at galvanostatic conditions from 0.02 M $KMnO_4$ solutions without stirring and using reverse pulse regime. Such films were further investigated for the application in electrodes of electrochemical supercapacitors. Porous crack-free films, prepared from the 0.02 M $KMnO_4$ solutions at the galvanostatic conditions and in the reverse pulse regime were studied by EDS, XRD, TGA and DTA.

EDS analyses showed that the K/Mn ration in the galvanostatic films prepared at a current density of 2 mA cm^{-2} and duration of 2-5 min was 0.28 ± 0.01. The K/Mn ratio for the films(Figure 5-9), prepared at the reverse pulse regime at the same cathodic current and 2 mA cm^{-2} anodic current density during 1 min, was found to be 0.21 ± 0.01. Therefore, the reduction in film mass during the anodic current can be partially attributed to the removal of positively charged K^+ ions from the films and higher Mn content in the films. However, the reduction in film mass during the anodic current can also be attributed to dissolution of Mn species.

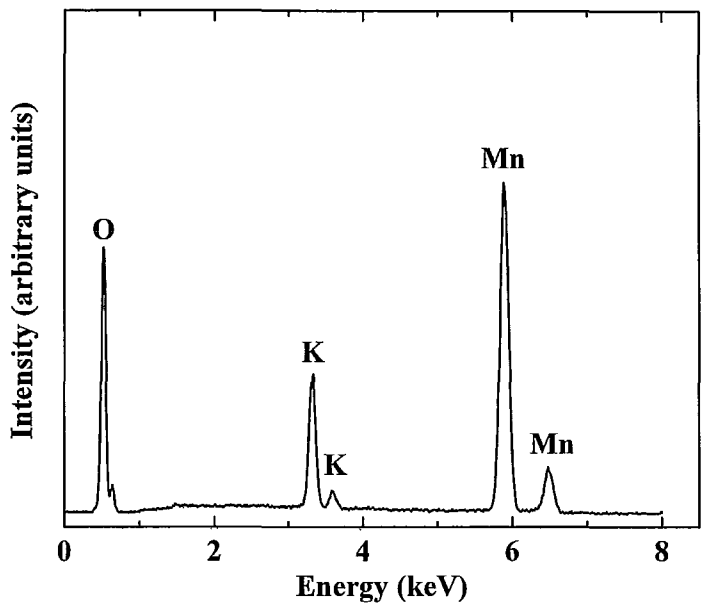

Figure 5-9 EDS data for deposit prepared using reverse pulse deposition at a cathodic current density of 2 mA cm^{-2} and anodic current density of 2 mA cm^{-2}.

X-ray studies showed crystallinity of the films prepared at the galvanostatic and reverse pulse conditions (Figure 5-10). The X-ray diffraction patterns are similar, however the films prepared in the reverse pulse regime exhibited broader peaks of lower intensity. The peak broadening can be attributed to the small particle size and poor crystallinity of the deposits. The X-ray diffraction patterns can be attributed to rancieite (JCPDS file 22-0718) or birnessite (JCPDS file 87-1497) structures. However, it is difficult to distinguish between the rancieite and birnessite phases owing to the peak broadening. The rancieite and birnessite phases have near MnO_2 composition, which can be described by the formula $K_xMnO_{2+y}(H_2O)_z$.

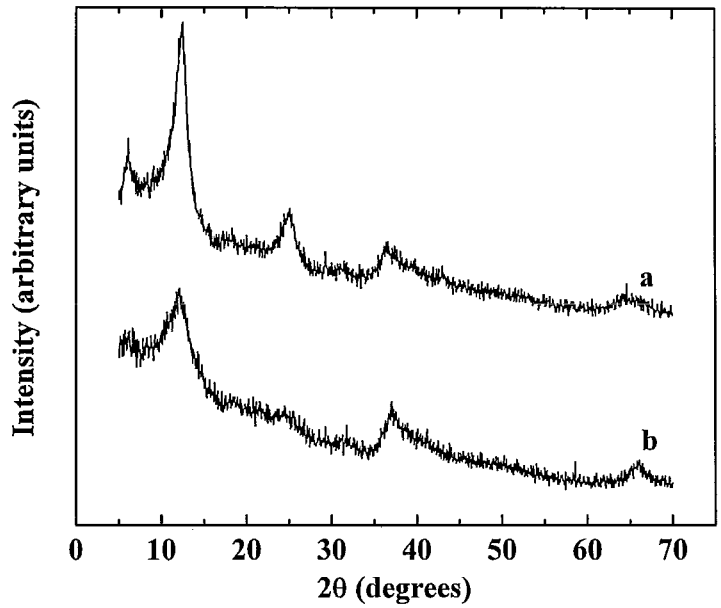

Figure 5-10 XRD data for the deposits prepared from the 0.02 M $KMnO_4$ solutions (a) galvanostatically and (b) using reverse pulse deposition at a cathodic current density of 2 mA cm^{-2} and anodic current density of 2 mA cm^{-2}.

Figure 5-11 compares TGA and DTA data for films deposited using galvanostatic and reverse pulse conditions. The TGA data show a sharp reduction in sample weight below ~ 200 °C and higher weight loss for the reverse pulse films. The weight loss in the temperature range of 20- 400°C and broad DTA endotherms around ~100 °C can be attributed to dehydration. The weight gain of 0.3 wt% observed in the TGA data for the reverse pulse films and corresponding exotherm in DTA data can be attributed to oxidation[91]. The weight loss at ~ 900 °C in TGA data and corresponding DTA endotherms can be attributed to reduction and formation of Mn_3O_4 phase[91]. The total

weight loss at 1000 °C was found to be 19.1 and 23.6 wt% for the galvanostatic and reverse pulse films, respectively.

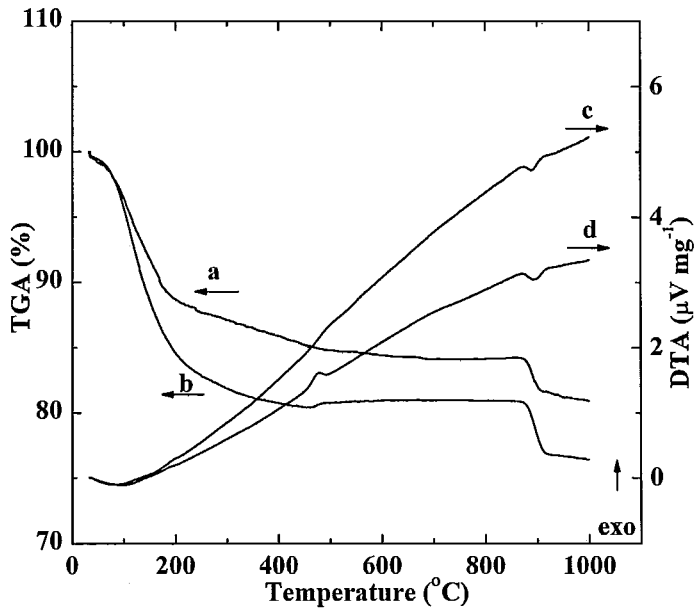

Figure 5-11 (a, b) TGA and (c, d) DTA data for (a, c) galvanostatic deposits and (b, d) reverse pulse deposits prepared from 0.02 M $KMnO_4$ solutions at a cathodic current density of 2 mA cm^{-2} and anodic current density of 2 mA cm^{-2}.

Figure 5-12 compares Nyquist impedance spectra for the samples prepared at different deposition conditions. Impedance testing was carried out in the frequency range of 100 mHz-100 kHz. The high frequency value of the real part of complex impedance has been used for the estimation of the ESR of the electrodes. The ESR of electrodes was found to be 0.22 and 0.16 Ohm for films deposited under galvanostatic and reverse pulse regime conditions, respectively.

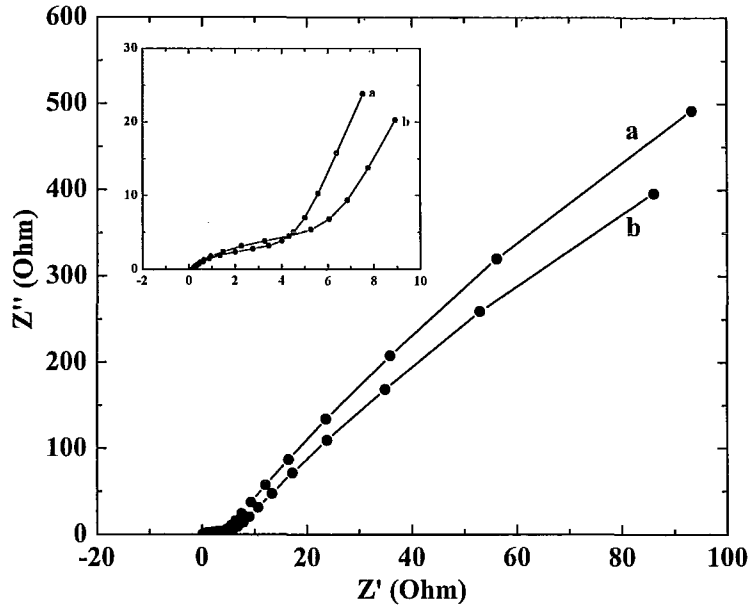

Figure 5-12 Nyquist plots for deposits prepared (a) galvanostatically (b) using reverse pulse deposition. The insert shows the high frequency range of the curves.

The capacitive behavior of the films was investigated in the potential range of 0-1.0 V versus SCE. Figure 5-13 shows CVs in the 0.1 M Na_2SO_4 solutions. Within the potential range of 0 - 1.0 V versus SCE, the manganese oxide electrodes exhibited capacitive-like current-potential responses, indicated by the box shape of the CVs. Figure 5-14 compares the CV for films obtained from revere pulse regime and films obtained galvanostatically.

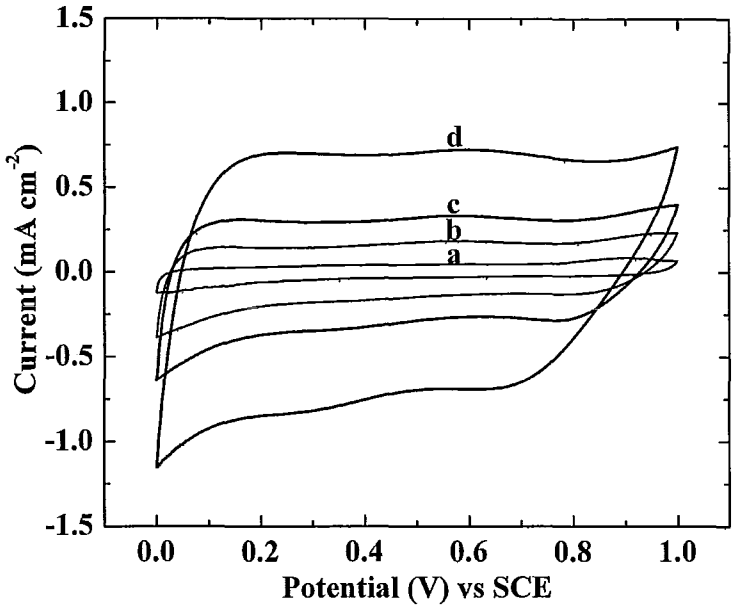

Figure 5-13 CVs in the 0.1 M Na_2SO_4 solution at a scan rate of (a) 2 (b) 10 (c) 20 (d) 50 mV s^{-1} for the 80 μg cm^{-2} deposit prepared using reverse pulse deposition

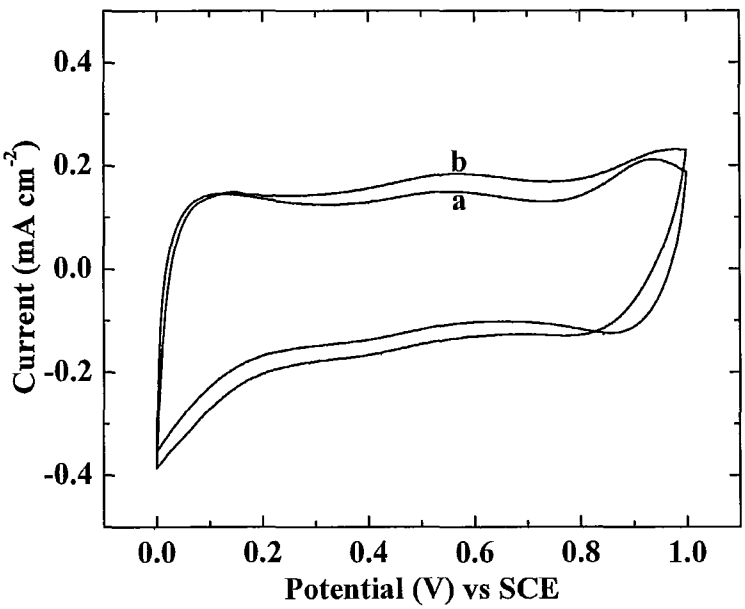

Figure 5-14 CV at a scan rate of 5 mV s^{-1} for deposits prepared (a) galvanostatically and (b) reverse pulse deposition from 0.02 M $KMnO_4$ solutions.

The films prepared using reverse pulse deposition showed higher SC compared to the SC of galvanostatic films (Figure 5-15). The highest SC of 279 F g^{-1} was obtained at a scan rate of 2 mV s^{-1} for the reverse pulse films. The galvanostatic film of the same mass exhibited a SC of 188 F g^{-1} at the same scan rate. The higher SC of the reverse films can be attributed to larger CV area, lower K content and higher porosity.

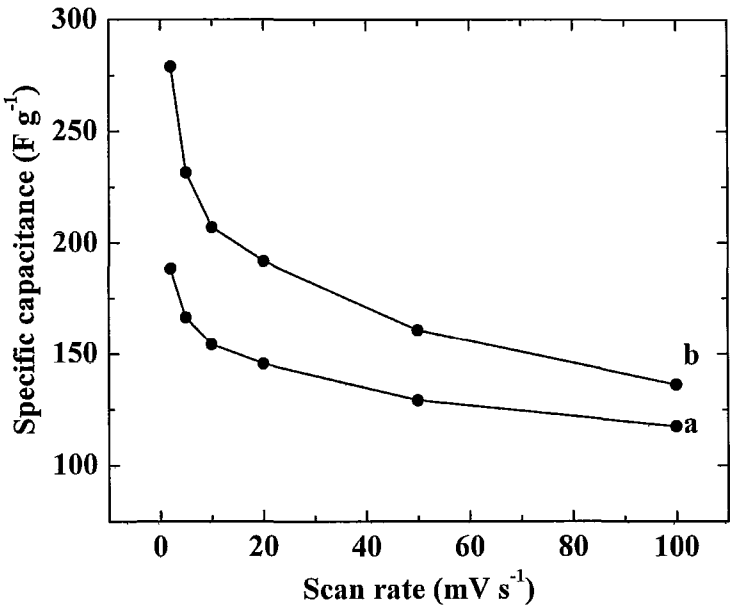

Figure 5-15 SC vs. scan rate for the 80 µg cm^{-2} deposits prepared (a) galvanostatically and (b) reverse pulse deposition from 0.02 M $KMnO_4$ solutions.

However, the SC decreased with increasing scan rate. Similar reduction in SC was observed in other investigations and was attributed to low electronic and ionic conductivity of the MnO_2 electrodes[44, 92]. At slow scan rates the ions can penetrate the pores and interact with the inner surface of the active material. The reduction in SC with

increasing scan rate highlights the importance of the ionic diffusion in the porous electrode. At high scan rates, diffusion limitations reduce the accessibility of Na^+ ions and protons to the inner surface of manganese oxide electrodes. It is suggested that at high scan rates some pores and voids remain inaccessible. As a result the reduction in charge storage properties was observed.

5.1.4 Influence of Molybdenum

Recent investigation demonstrated that MnO_2-MoO_2 mixed oxide films exhibited a pseudocapacitive behaviour with higher specific capacitance and better reversibility compared to that of pure MnO_2 films[93]. MnO_2-MoO_2 mixed oxide films were deposited anodically from $MnSO_4$ and Na_2MoO_4 solutions. The mechanism behind the anodic deposition of molybdenum is not clear, as Mo ions in the solution are in their maximum oxidation sate of 6+ and cannot be oxidised further. Further, anodic deposition method will involve anodic oxidation and dissolution of the high surface metallic current collectors which limits its extensive applications.

Alternatively, we have already developed a cathodic electrosynthesis method based on the diffusion-controlled mechanism, which involved diffusion and cathodic reduction of anionic MnO_4^- (Mn^{7+}) species. Hence, it is more desirable to employ this technique to cathodically reduce anionic MnO_4^- (Mn^{7+}) and MoO_4^{2-} (Mo^{6+}) species to obtain MnO_2-MoO_2 mixed oxide films.

Cathodic deposits were obtained galvanostatically at a current density of 2 mA cm^{-2} from 0.02 M $KMnO_4$ solutions containing 0.002 – 0.01 M K_2MoO_4 solutions. Figure

5-16 shows that SC increases as amount of Mo in solution increases and reaches a maximum at 30 molar % and then decreases. But the EDS analysis indicated that Mo was not included in the deposit.

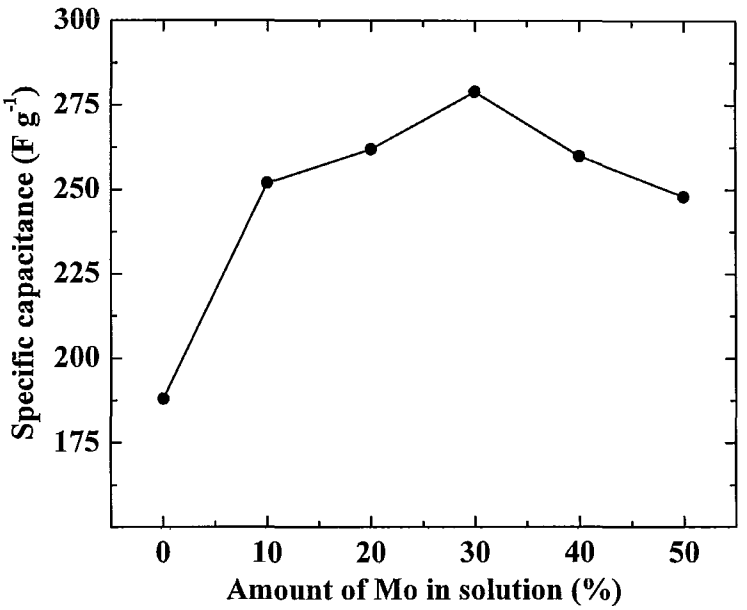

Figure 5-16 SC vs. amount of K_2MoO_4 in $KMnO_4$ solutions in molar %.

Thin uniform films of MoO_2 oxides were obtained from 0.002 – 0.01 M K_2MoO_4 solutions at a pH $\leq$ 2. However, the cathodic deposits obtained from the 0.02 M $KMnO_4$ solutions containing 0.002 – 0.01 M K_2MoO_4 solutions at a pH 2 were not uniform. EDS analysis of the MnO_2-MoO_2 mixed oxide films deposited at pH 2 showed Mo/Mn ratio of 0.13. Films obtained at pH $\geq$ 2 was uniform, but Mo was not included in the deposit. As soon as pH is reduced to 2 Mo was included in the deposit but the quality of the

coatings are very poor. Current density and concentration of the solution did not influence the codepostion of Mo.

Figure 5-17 shows the SEM images of deposit prepared from 0.02 M $KMnO_4$ solutions containing 30 molar % K_2MoO_4. The morphology is more porous and completely different from that obtained without K_2MoO_4 (Figure 5-3a,b). The difference in microstructure, can explain the higher SC observed for deposit obtained in the presence of Mo (Figure 5-18), then without Mo (Figure 5-15a). Figure 5-19 shows CVs of films obtained from solution containing 30 molar % K_2MoO_4 in the 0.1 M Na_2SO_4 solutions.

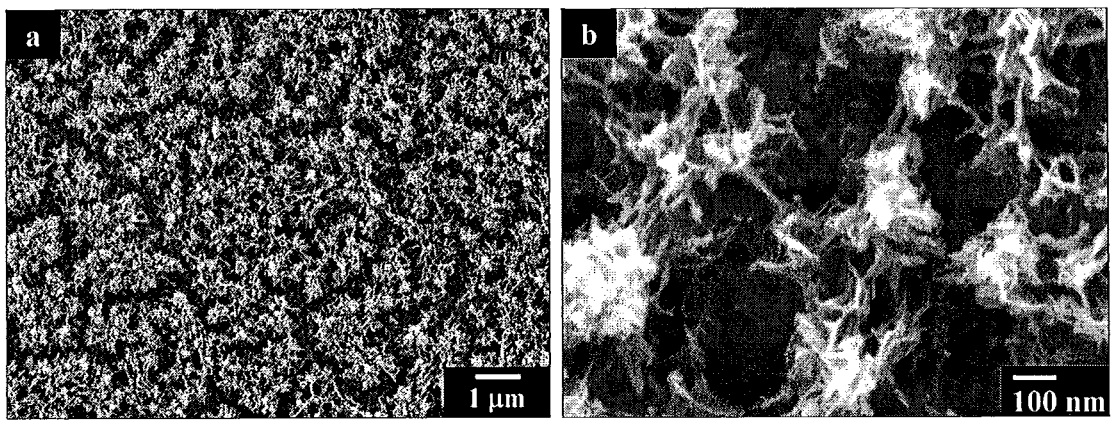

Figure 5-17 SEM images with different magnifications for deposit prepared at a constant current density of 2 mA cm^{-2} from $KMnO_4$ solutions containing 30 molar % of K_2MoO_4.

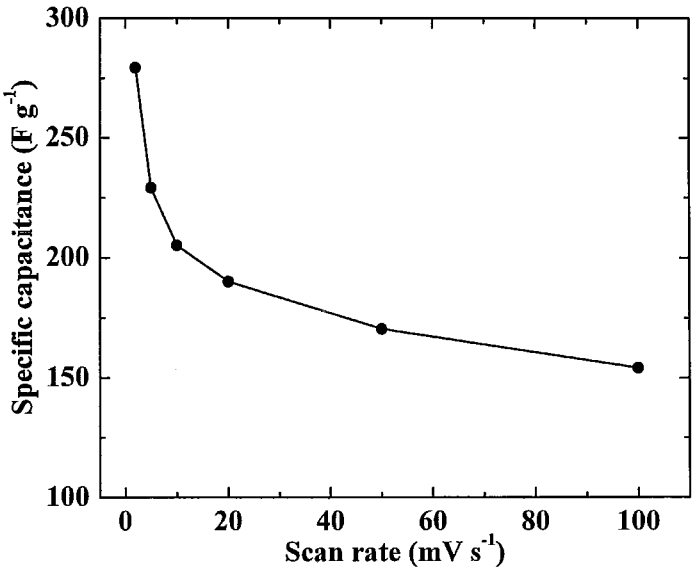

Figure 5-18 SC vs. scan rate for deposit prepared from $KMnO_4$ solutions containing 30 molar % of K_2MoO_4.

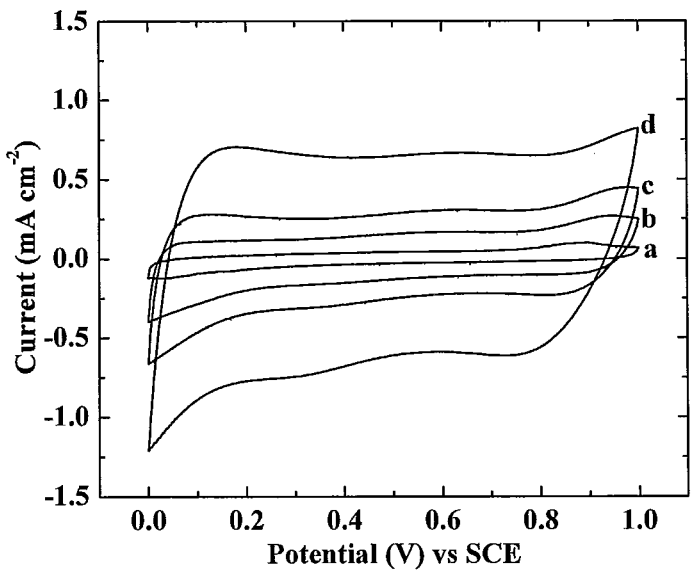

Figure 5-19 CVs in the 0.1 M Na_2SO_4 solution at a scan rate of (a) 2 (b) 10 (c) 20 (d) 50 mV s^{-1} for the 80 μg cm^{-2} deposit prepared from $KMnO_4$ solutions containing 30 molar % of K_2MoO_4.

Obtained results indicate that cathodic electrosynthesis can be utilized for the fabrication of manganese dioxide electrodes for electrochemical supercapacitors. However, further optimization of the deposition parameters is necessary in order to optimize the microstructure and properties of the electrode materials.

5.2 Composite Electrodes

Manganese dioxide nanoparticles prepared by chemical precipitation method and carbon black conductive additives were mixed with PVB binder and impregnated in to INCOFOAM® to form a composite electrode. The influence of electrode and electrolyte composition, electrode microstructure, processing conditions and Ag-doping on the capacitive behavior has been investigated.

5.2.1 Composite electrodes fabricated from MnO_2 powders prepared using isopropanol as a reducing agent

Previous investigations showed that MnO_2 can be obtained by reduction of permanganate ions by ethanol[94, 95]. The results of our investigation indicate that isopropanol can be used as a reducing agent. It was found that the rate of the reduction reaction is much faster when isopropanol is used as a reducing agent instead of ethanol. Also manganese dioxide powders prepared from isopropanol were much finer and easier to process, when compared to powders prepared from ethanol. The reduction reaction with isopropanol occurs according to the following reaction:

$$2MnO_4^- + 3(CH_3)_2CH\text{-}OH + 2H^+ \rightarrow 2MnO_2 + 3(CH_3)_2CO + 4H_2O \quad (5\text{-}2)$$

Manganese oxide powders were prepared by chemically reducing 0.2 M $KMnO_4$ solution with isopropanol. Different amounts of isopropanol (5, 25, 50 ml) were used to reduce $KMnO_4$, but there was no significant variation in chemical and electrochemical properties. Hence, MnO_2 powders prepared using 25 ml isopropanol were further investigated. XRD studies of as-prepared manganese dioxide powders showed broad peaks of low intensity (Figure 5-20). The peak broadening can be attributed to the small particle size and poor crystallinity of the prepared material. Heat treatment at 300 °C resulted in increasing intensity of the peaks. The X-ray diffraction peaks can be attributed to birnessite (JCPDS file 80-1098) structure.

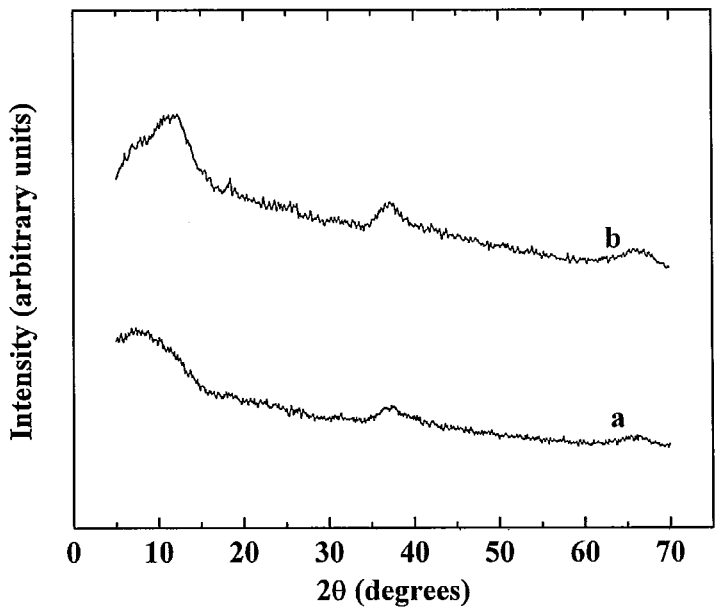

Figure 5-20 XRD pattern of manganese dioxide powder: (a) as-prepared and (b) heat treated at 300°C during 1 h.

According to the literature[96, 97], the birnessite phase has near-MnO_2 stoichiometry. The birnessite formula is generally expressed as $A_xMnO_{2+y}(H_2O)_z$, where A represents an alkali metal cation. The average oxidation state of Mn usually falls between 3.6 and 3.8, which represents a predominance of Mn^{4+} with minor amount of Mn^{3+} and Mn^{2+}. Birnessite has a two-dimensional layered structure that consists of edge shared MnO_6 octahedra with cations and water molecules occupying the interlayer regions. Thermal dehydration usually results in the formation of dehydrated form of birnessite with reduced interlayer distance[96, 97].

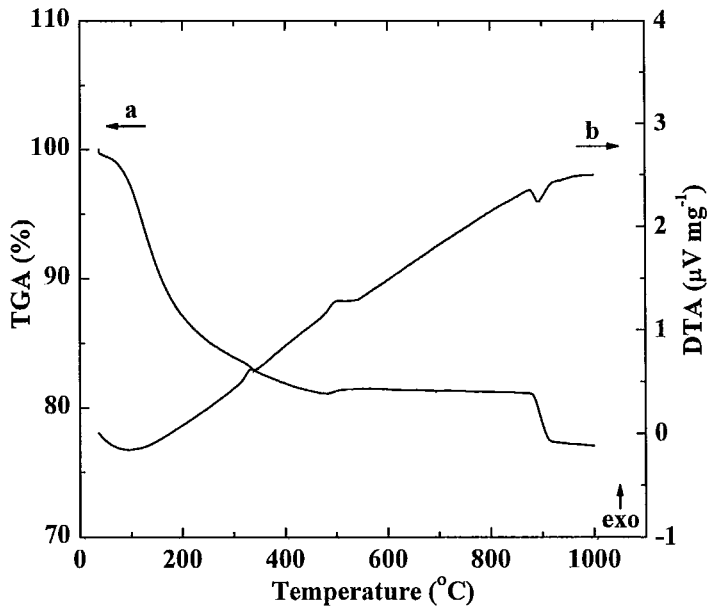

Figure 5-21 (a) TGA and (b) DTA data for as-prepared manganese dioxide powder.

TGA studies (Figure 5-21) revealed weight loss of 18.1 wt.% below 400 °C. This weight loss and endotherm at ~ 100 °C in the corresponding DTA data can be attributed

to dehydration. The weight gain of 0.38 wt.% in the range of 484-546 °C and corresponding exotherm can be attributed to oxidation[91]. Additional weight loss of 3.7 wt.% observed in the TGA and corresponding endotherm in DTA in the temperature range of 873-917 °C can be attributed to reduction and formation of Mn_3O_4 phase[91]. The total weight loss at 1000 °C was found to be 22.9 wt.%.

TEM investigations showed that as-prepared powders contained nearly spherical particles with particles size of about 50 nm (Figure 5-22). EDS analysis showed that obtained powders included K with a K/Mn atomic ratio of 0.28 ± 0.01. As-prepared manganese dioxide powders were used for the fabrication of electrodes for ES. The slurry containing manganese dioxide, carbon black and binder was impregnated into the INCOFOAM® (Figure 5-23a) followed by drying and calendering to desired thickness.

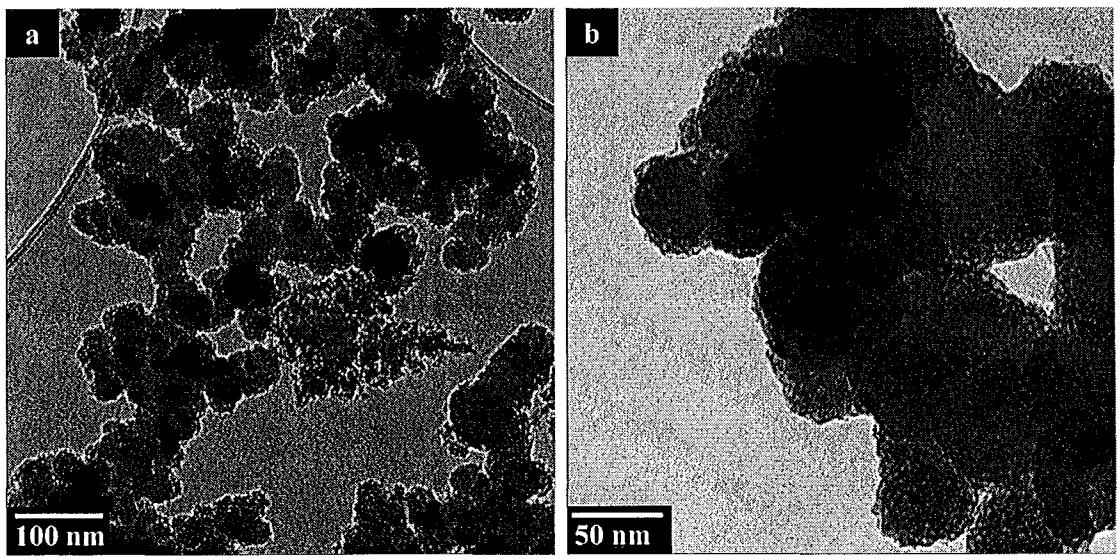

Figure 5-22 TEM image of as-prepared manganese dioxide powder at different magnifications.

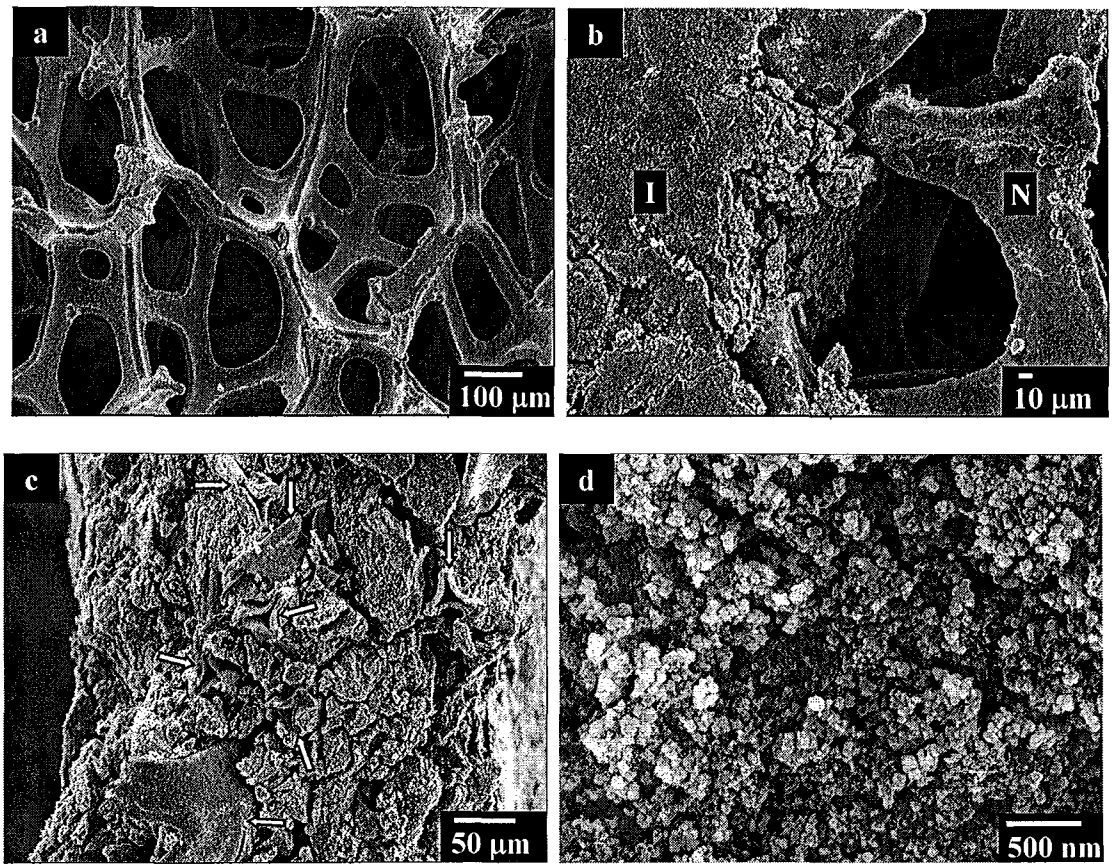

Figure 5-23 SEM image of (a) INCOFOAM® (b) impregnated (I) and non-impregnated (N) area of the INCOFOAM® after pressing, (c) cross section of impregnated and pressed INCOFOAM® with arrows showing the INCOFOAM® and (d) surface of impregnated and pressed INCOFOAM® at high magnification.

The SEM images of impregnated and non-impregnated areas of the electrode (Figure 5-23b) and cross section of impregnated area (Figure 5-23c) indicated that active material filled the voids in the nickel foam. The SEM image of the surface of the impregnated area at high magnification showed that electrode material consists of

manganese dioxide and carbon black nanoparticles and exhibits porosity with pore size of 0-300 nm (Figure 5-23d). Such porosity is beneficial for the electrolyte access to the active material.

5.2.1.1 Influence of compression ratio of the pressed electrodes

Compression ratio, D, is the ratio between final thickness and initial thickness of the impregnated nickel foam. From Figure 5-24 it can be seen that SC decreases as D increases. This is due to the fact that as D increases, the particle-particle contact resistance increases. A similar observation has been observed in the literature[57]. Even though 0.1 D gives higher SC, the probability of damaging the electrodes is high when the Ni foam is heavily loaded. Hence a D of 0.2 was chosen for our further investigations.

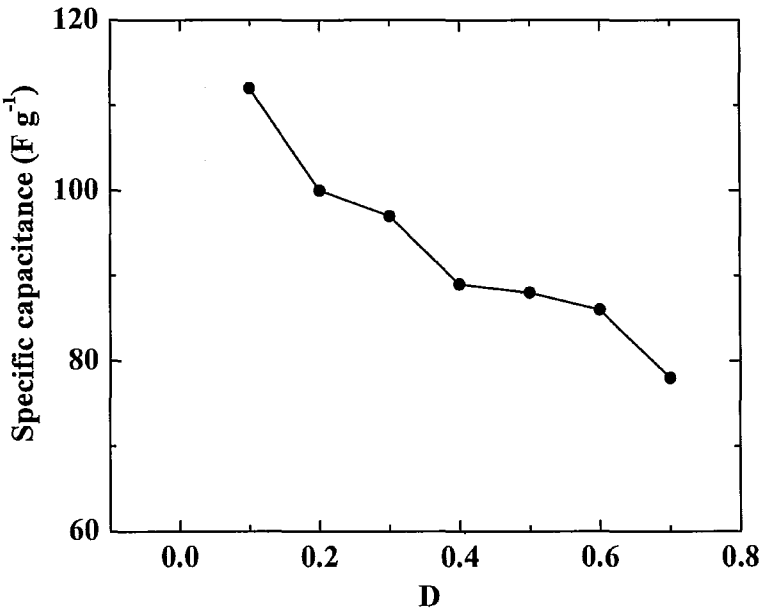

Figure 5-24 SC vs. D for the composite electrode containing 20 wt. % carbon black.

5.2.1.2 Influence of electrode composition

Figure 5-25 shows the influence of active material composition on the capacitive behavior of the electrodes. For manganese dioxide electrodes prepared without carbon black additives, the relatively small area of the CV indicated poor capacitive behavior. The SC at a scan rate of 10 mV s^{-1} in the 0.1 M Na_2SO_4 electrolyte of such electrodes was only 2 F g^{-1}. It should be noted that thin manganese dioxide films with low materials loading showed a box shape CV and high SC in the same electrolyte[42, 47, 49, 53]. The difference in capacitive behavior can be attributed to different material loadings and insulating properties of the manganese dioxide.

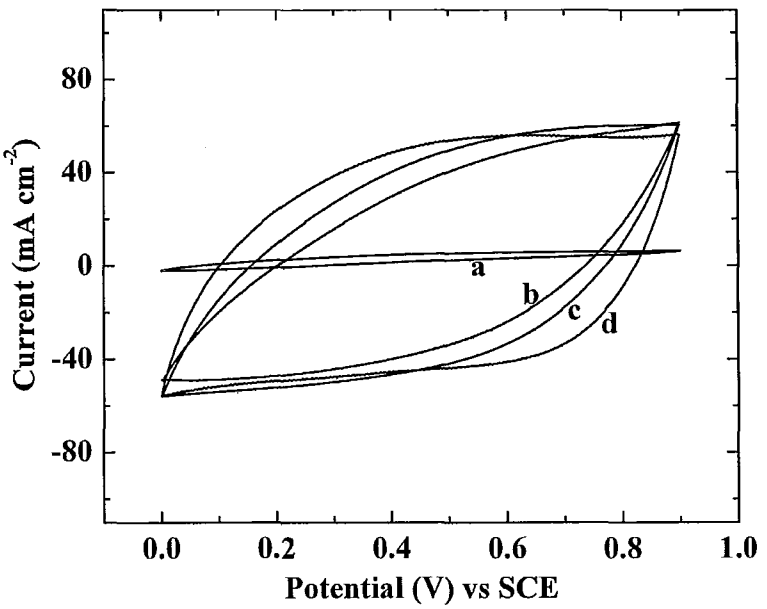

Figure 5-25 CVs for composite electrodes containing (a) 0 (b) 10 (c) 20 (d) 30 wt.% of carbon black at 10 mV s^{-1} scan rate in 0.1 M Na_2SO_4 solutions.

This result indicated that the conductivity of the Ni foam is insufficient at materials loading of 55 mg cm^{-2} used in this work. The additional conducting network, provided by carbon black, improved the capacitive behavior of the composite electrodes. The electrodes containing 10 wt. % carbon black showed higher SC (Figure 5-26) at lower scan rates. This is because at lower scan rates ions can penetrate the pores and interact with the inner surface of the active material and utilise the maximum active material available. As electrodes containing 10 wt. % carbon black has more active material they exhibit high SC. The electrodes containing 30 wt. % carbon black showed higher SC at higher scan rates, as conductivity of the electrode, provided by carbon black plays an important role in the capacitive behaviour.

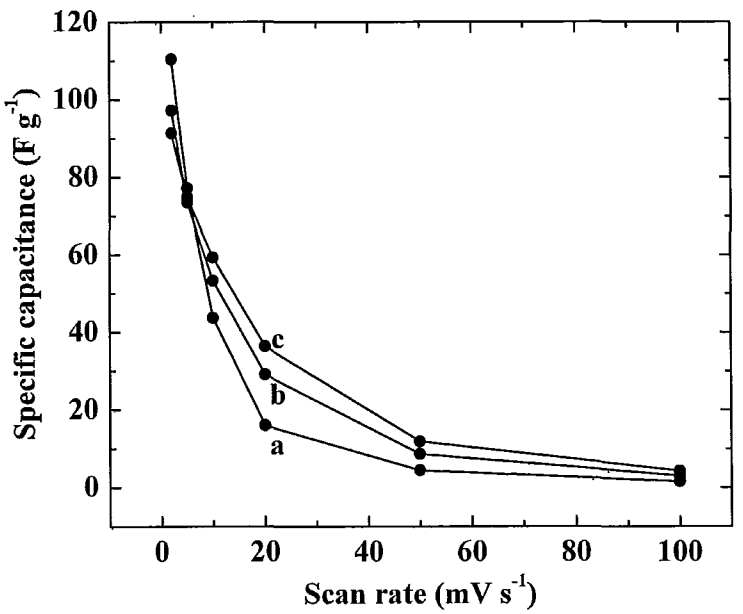

Figure 5-26 SC vs. scan rate for composite electrodes containing (a) 10 (b) 20 (c) 30 wt.% of carbon black in 0.1 M Na_2SO_4 solutions.

The optimum electrode composition is 80 wt.% active material and 20 wt.% of carbon black. Figure 5-27 shows CVs at different scan rates for electrode containing 20 wt.% of carbon black.

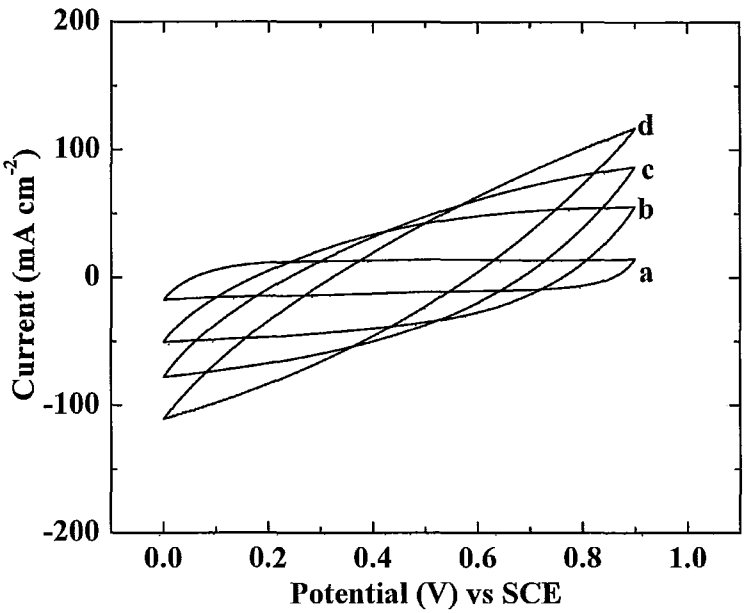

Figure 5-27 CVs for composite electrodes containing 20 wt.% of carbon black at a scan rate of (a) 2 (b) 10 (c) 20 (d) 50 mV s^{-1} in the 0.1 M Na_2SO_4 solutions.

5.2.1.3 Influence of electrolyte concentration

Electrochemical testing in the 0.1-0.5 M Na_2SO_4 solutions revealed capacitive behavior of the composite electrodes. However, the shapes of CVs obtained in the 0.1 M Na_2SO_4 electrolyte (Figure 5-27) deviated significantly from the ideal box shape and indicated relatively high electrode resistance. Further improvement in the capacitive behavior of the composite electrodes was achieved by the increase in the electrolyte

concentration. The comparison of the CVs obtained at the scan rate of 5 mV s^{-1} in the 0.1 and 0.5 M Na_2SO_4 solutions showed a smaller area of the CV obtained in the 0.1 M Na_2SO_4 solutions (Figure 5-28).

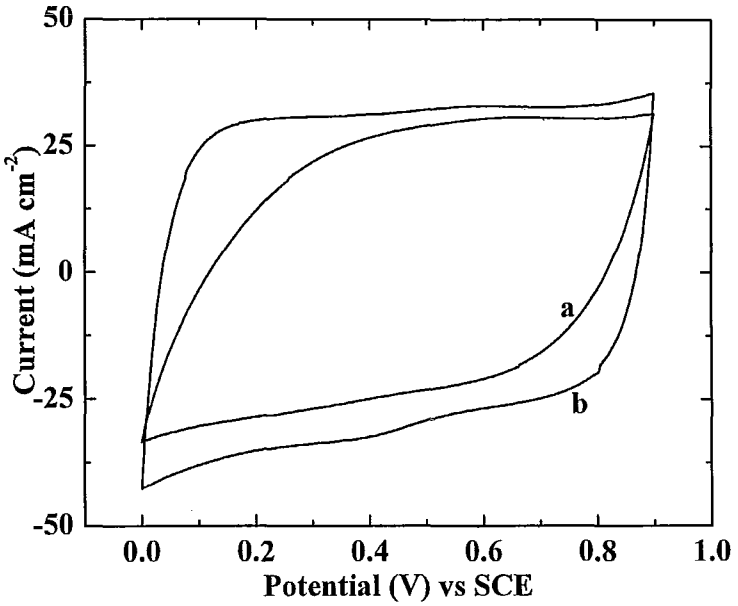

Figure 5-28 CVs for composite electrodes containing 20 wt.% of carbon black at 5 mV s^{-1} scan rate in (a) 0.1 M and (b) 0.5 M Na_2SO_4 solutions.

The difference can be attributed to the lower conductivity of the 0.1 M Na_2SO_4 solutions and diffusion limitations in pores of the composite electrodes[11, 98]. This result is in a good agreement with the experimental data shown in (Figure 5-29). Higher SC was obtained in the 0.5 M Na_2SO_4 solutions compared to the 0.1 M Na_2SO_4 solutions for the samples of the same mass and composition.

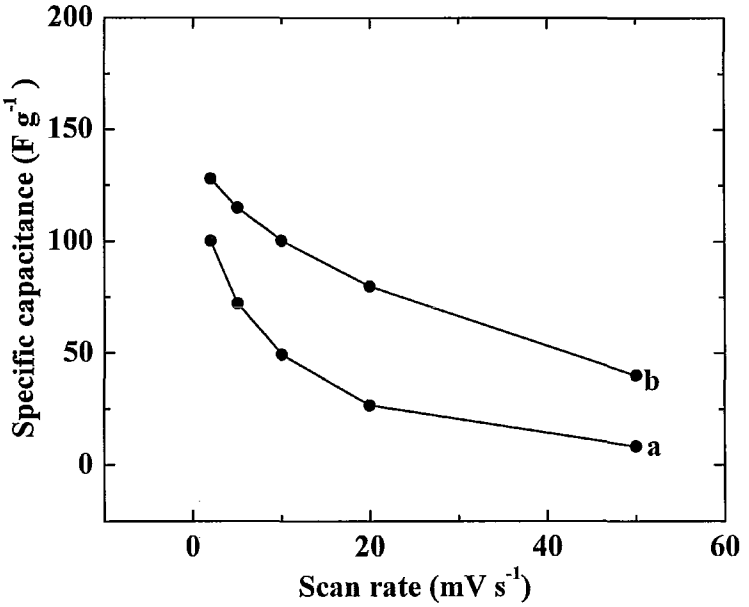

Figure 5-29 SC vs. scan rate for the composite electrode containing 20 wt.% of carbon black in (a) 0.1 M and (b) 0.5 M Na_2SO_4 solutions.

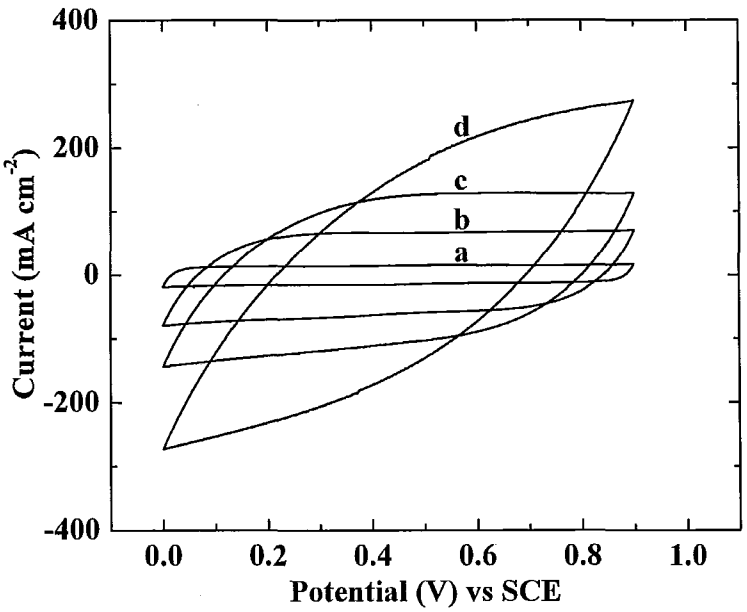

Figure 5-30 CVs in the 0.5 M Na_2SO_4 solution at a scan rate of (a) 2 (b) 10 (c) 20 (d) 50 mV s^{-1} for the composite electrode containing 20 wt.% of carbon black.

The highest SC of 128 Fg^{-1} was obtained from a box shape CV at a scan rate of 2 mV s^{-1} in 0.5 M Na_2SO_4 solutions. The SC decreased with increasing scan rate for electrodes of fixed composition. The decrease in SC with increasing scan rate can be attributed to the diffusion limitations in pores. Figure 5-30 shows the CVs at different scan rates in 0.5 M Na_2SO_4 solutions.

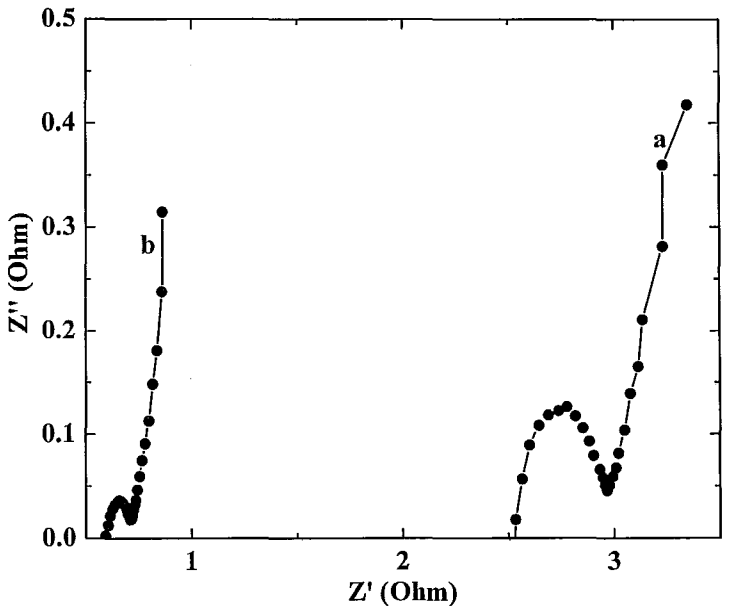

Figure 5-31 Nyquist plots of the complex impedance for composite electrode containing 20 wt.% of carbon black in (a) 0.1 M and (b) 0.5 M Na_2SO_4 solutions.

The improved capacitive behaviour in the 0.5 M Na_2SO_4 solutions is in a good agreement with the impedance spectroscopy data. Figure 5-31 shows complex impedance of the electrode in the frequency range of 100 mHz-10 kHz. The high frequency value of the real part of complex impedance has been used for the estimation of the ESR of the

electrodes. The ESR of electrodes with area of 1 cm^2 was found to be 2.5 and 0.6 Ohm in the 0.1 M and 0.5 M Na_2SO_4 solutions, respectively. Therefore, further testing was performed in the 0.5 M Na_2SO_4 solutions. It is suggested that the further optimization of electrode composition and microstructure will result in reduced resistance and improved capacitive behavior.

Figure 5-32 shows charge – discharge behaviour of the composite electrode at different current densities. The discharge curve is nearly linear, however initial voltage drop was observed, which can be attributed to electrode resistance. Obtained electrodes showed good cycling behaviour with no loss in SC obtained from the CV data during 1000 cycles (Figure 5-33).

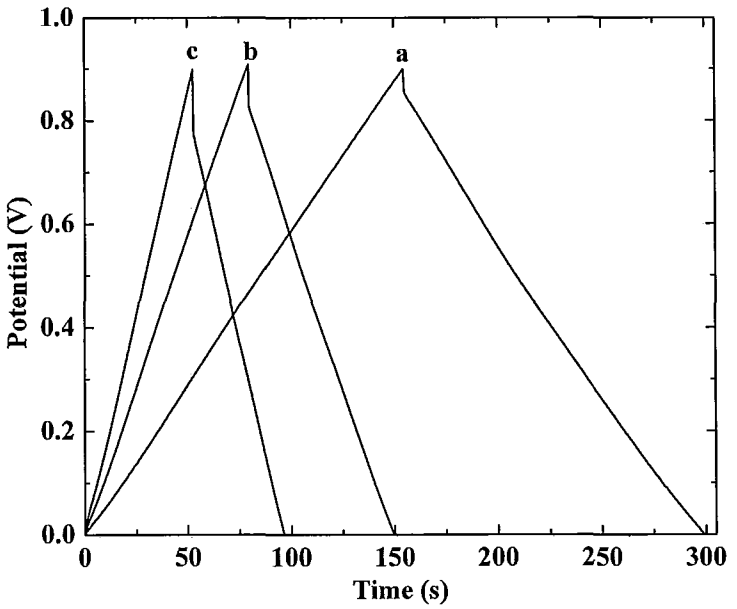

Figure 5-32 Charge-discharge behavior for the composite sample containing 20 wt.% of carbon black at current densities of (a) 40 (b) 80 and (c) 120 mA cm^{-2}.

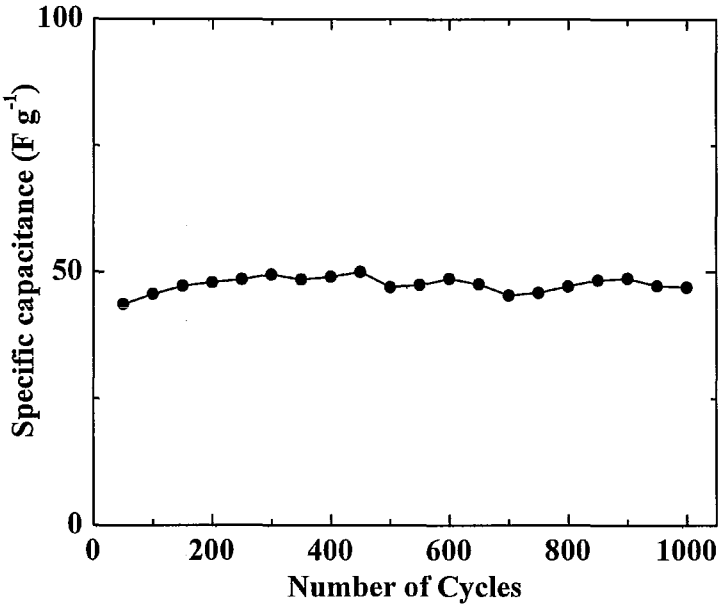

Figure 5-33 Cycling stability for the composite electrode containing 20 wt.% of carbon black at 50 mV s^{-1} scan rate in 0.5 M Na_2SO_4 solutions.

5.2.2 Composite electrodes fabricated from MnO_2 powders prepared using KBH_4 as a reducing agent.

KBH_4 has been utilized as a reducing agent for the precipitation of manganese dioxide powders. A general chemical reaction for the formation of the reduction products is as follows[61]:

$$KMnO_4 + KBH_4 + (1 - x - \delta)\, H_2O \rightarrow KBO_2 + K_xMnO_{2-\delta} + (1 - x)\, KOH + (2.5 - 0.5x - \delta)\, H_2 \quad (5\text{-}2)$$

The influence of pH, processing conditions, Ag-doping and electrode composition on the capacitive behavior has been investigated.

5.2.2.1 Influence of pH

SEM studies of the powders (Figure 5-34), prepared from the 0.1 M $KMnO_4$ solutions at pH 3 and pH 6, showed that the powders contained nanoparticles of irregular shape and nanofibers. Some nanofibers formed bundles, containing several nanofibers. The samples prepared at pH 6 showed much larger content of fibrous particles.

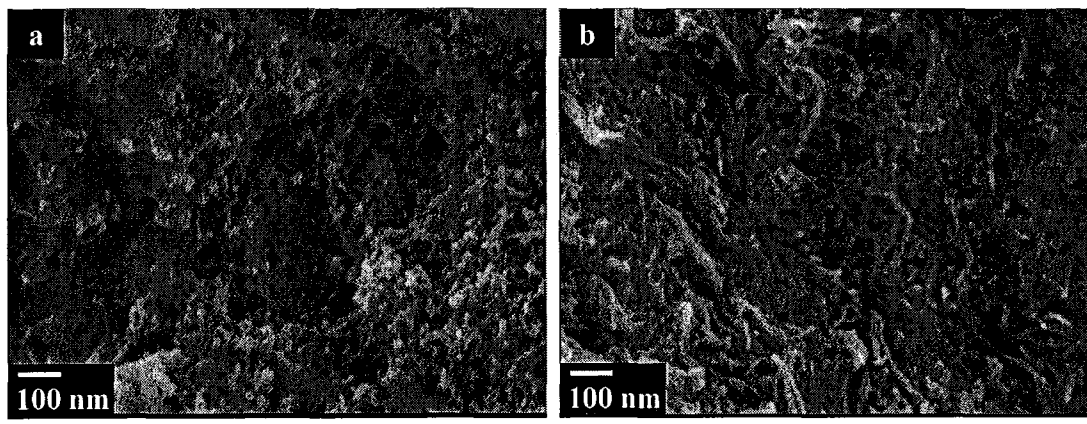

Figure 5-34 SEM images of powders prepared from 0.1 M $KMnO_4$ solutions at (a) pH 3 and (b) pH 6.

TEM studies (Figure 5-35) showed that powders prepared at pH 3 contained nanoparticles with particle size of 5-10 nm and nanofibers with diameter of ~5 nm and length of 0.1-0.5 μm. It was found that the nanofibers are not individual crystals, but are

composed of small nanoparticles with a diameter less than 5 nm. The powders prepared at pH 6 showed significant agglomeration and larger particle size. Moreover, the powders contained large amount of bundles of individual fibrous particles. Figure 5-35 shows typical image of individual nanofibers prepared at pH 6. The agglomeration of individual particles and larger content of fibers, which formed bundles, is in agreement with the lower surface area reported for the powders prepared at pH 6[62].

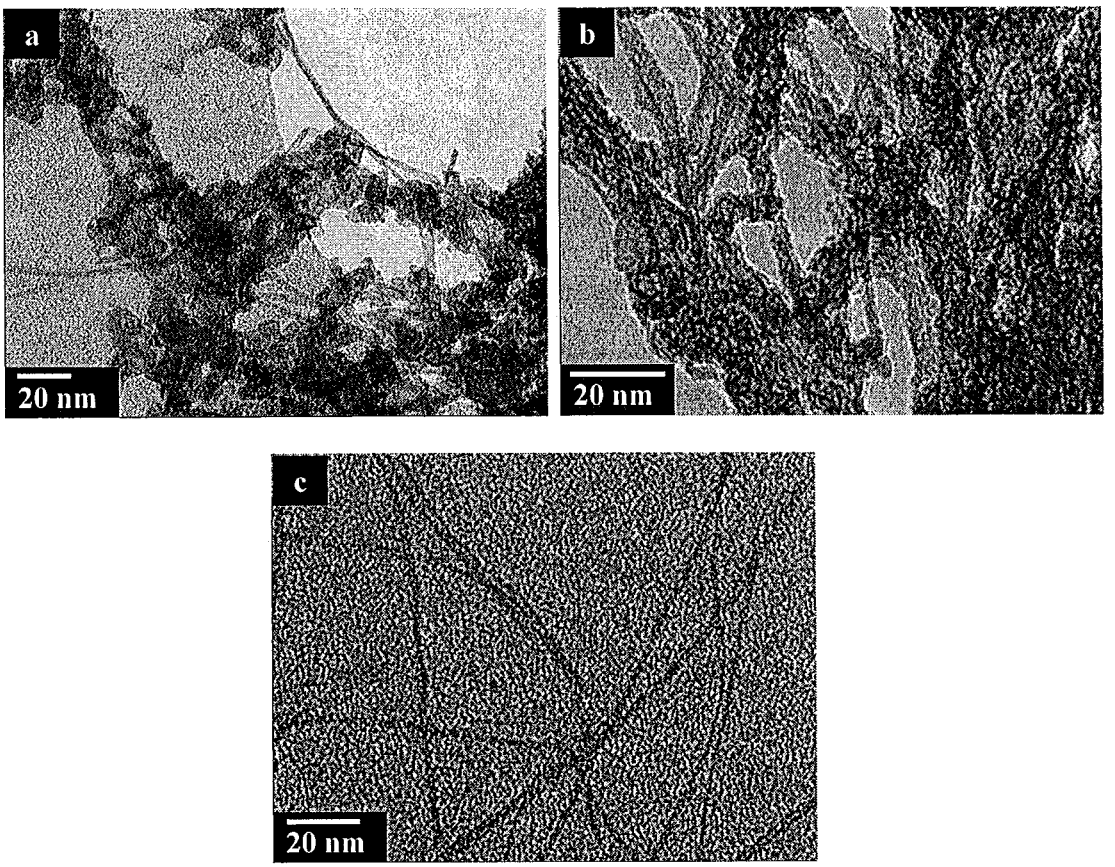

Figure 5-35 TEM images of powders prepared from 0.1 M $KMnO_4$ solutions at (a) pH 3 and (b,c) pH 6.

Figure 5-36 shows X-ray diffraction patterns of powders prepared at different pH 3 and pH 6. The X-ray diffraction patterns of the powders showed very small peaks of manganese dioxide. The peaks are very broad and indicate small crystallite size. The X-ray diffraction peaks can be attributed to birnessite (JCPDS file 87-1497) structure. Obtained results are in agreement with literature data for powders prepared at similar conditions[61].

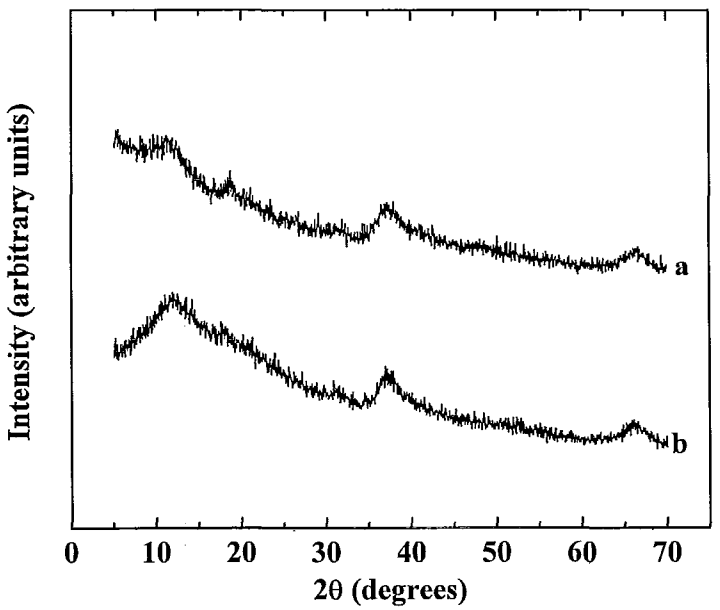

Figure 5-36 XRD patterns of powders prepared from 0.1 M $KMnO_4$ solutions at (a) pH 3 and (b) pH 6.

EDS analysis showed that the powders precipitated from the 0.1 M $KMnO_4$ solutions at pH 3 and 6 contained K with the K/Mn atomic ratio of 0.09 and 0.2 respectively. TGA studies (Figure 5-37) of the powders showed weight loss mainly

below 200 °C related to dehydration. The corresponding broad endotherms were observed at ~120 °C in the DTA data. Small exotherms at ~200 °C can be attributed to crystallization of an amorphous phase. The weight loss at higher temperatures and small exotherm at ~480 °C can be related to the reduction of manganese dioxide and formation of other manganese oxide phases[75,47]. The total weight loss at 800 °C was found to be 24.2 wt% and 20.0 wt%, for the samples precipitated at pH 3 and 6, respectively.

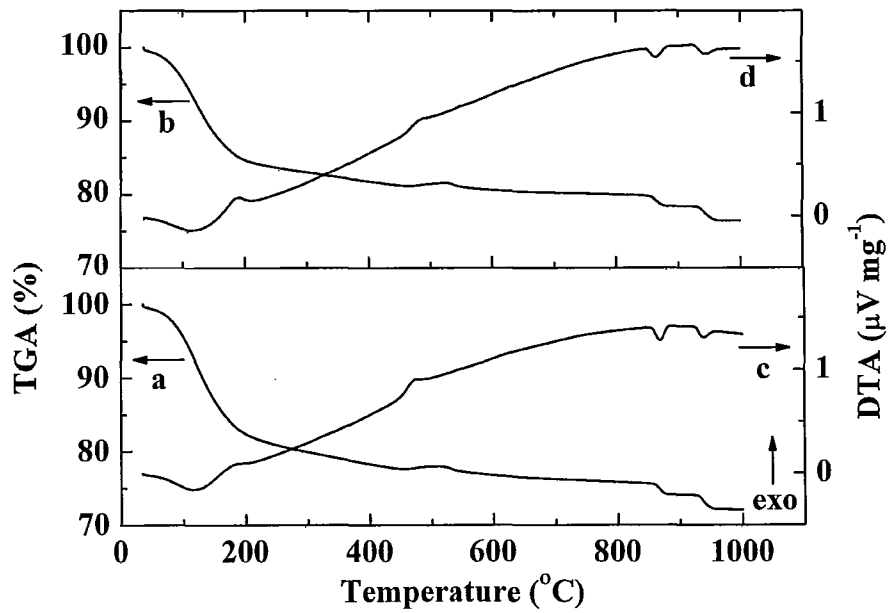

Figure 5-37 (a,b) TGA and (c,d) DTA data for powders prepared from 0.1 M $KMnO_4$ solutions at (a,c) pH 3 and (b,d) pH 6.

The precipitated powders were washed with water, dried, mixed with carbon black then binder was added to make slurry and impregnated in to the nickel foam to fabricate a composite electrode. The capacitive behavior of the composite electrodes was

studied using cyclic voltammetry. Figure 5-38 shows typical CVs in the 0.5 M Na_2SO_4 electrolyte solutions in the potential range of 0-0.9 V vs. SCE. The composite electrodes exhibited capacitive-like current-potential response. It is clear that there are no redox peaks in the range between 0 and 0.9 V. The composite electrodes, containing manganese dioxide powders precipitated at pH 6, showed significantly lower capacitance as indicated by lower area of corresponding CV plotted in Figure 5-38.

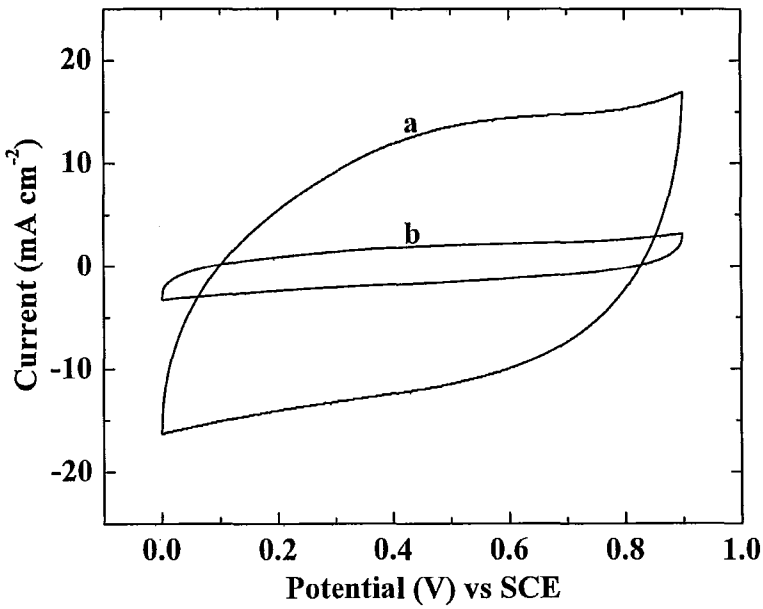

Figure 5-38 CVs at a scan rate of 2 mV s^{-1} for composite electrodes containing manganese dioxide prepared at (a) pH 3 and (b) pH 6.

The composite electrodes containing manganese dioxide prepared at pH 3 and pH 6 with 20 wt.% carbon black showed a SC of 82 F g^{-1} and 15 F g^{-1}, respectively, at a scan

rate of 2 mV s^{-1} in the 0.5 M Na_2SO_4 solution. The SCs calculated from CVs obtained at different scan rates are shown in Figure 5-39.

The different capacitive behavior of the composite materials can be attributed to the difference in particle morphology. Turning again to the electron microscopy data presented in Figure 5-35, it is suggested that the formation of fibrous particles and agglomeration of the individual fibers can result in reduced surface area, which in turn, can result in lower SC. It is also suggested that lower content of fibrous particles in powders prepared at pH 3 can facilitate mixing of the particles with carbon black and impregnation of nickel foam.

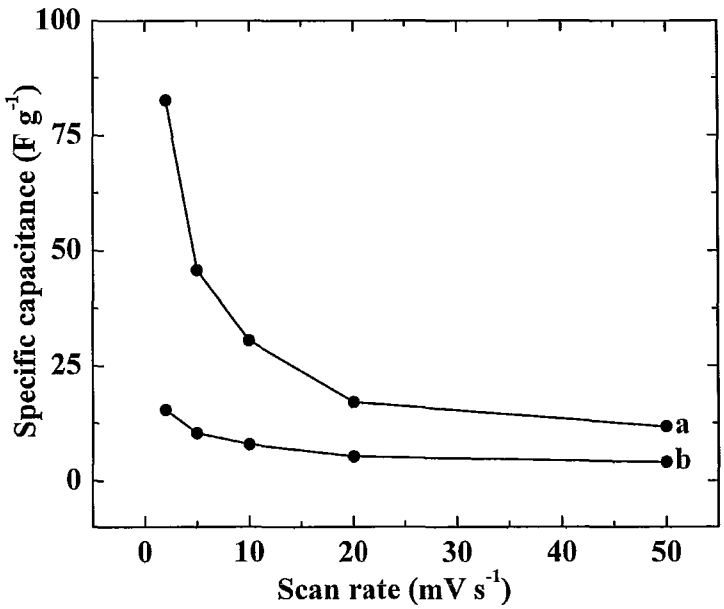

Figure 5-39 SC vs. scan rate for composite electrodes containing manganese dioxide prepared at (a) pH 3 and (b) pH 6.

5.2.2.2 Influence of processing conditions

The fabrication of efficient electrodes with high SC requires good mixing of the components and uniform distribution of a conductive phase in the matrix of manganese dioxide. Two methods were used for mixing of manganese dioxide powders with carbon black. In the method A, the precipitated powders were washed with water, dried and mixed with carbon black. In the method B, carbon black was added to the suspension of precipitated manganese dioxide and the mixture was stirred during 1 h, washed with water and dried. The powders prepared using methods A and B were used for the preparation of slurries and impregnation of current collectors.

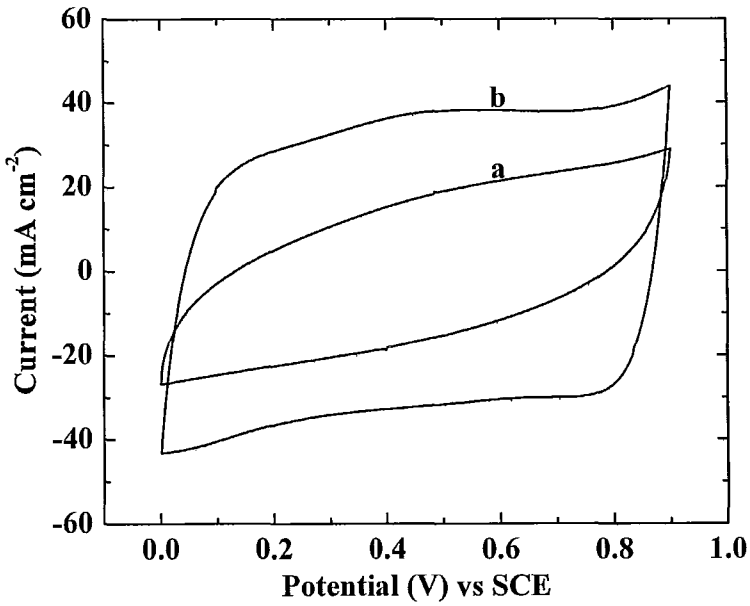

Figure 5-40 CVs at a scan rate of 5 mV s^{-1} for composite electrodes containing manganese dioxide prepared at pH 3 and mixed with 20 wt% of carbon black using methods (a) A and (b) B.

Figure 5-40 shows that the shape of the CV obtained using powder precipitated at pH 3 and mixed with carbon black by method A, deviates significantly form ideal box shape. In contrast, the composite electrode prepared by method B showed improved shape of the voltage window and higher SC. Further, electrode prepared by method B exhibited larger CV area then electrode prepared by method A and hence a better SC. CVs at different scan rates for electrodes prepared by method B is shown in the Figure 5-41. The SCs calculated from CVs obtained at different scan rates are shown in Figure 5-42. Significantly higher SCs were obtained for composites prepared using method B, compared to method A. The difference can be attributed to better mixing of the individual components, which can provide improved conductivity of the composite material.

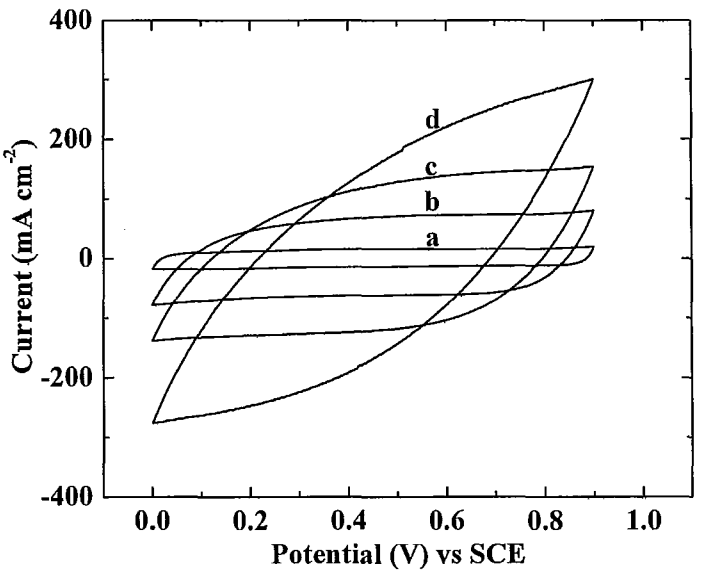

Figure 5-41 CVs at a scan rate of (a) 2 (b) 10 (c) 20 (d) 50 mV s^{-1} for electrodes containing manganese dioxide prepared at pH 3 and mixed with 20 wt% of carbon black using methods B.

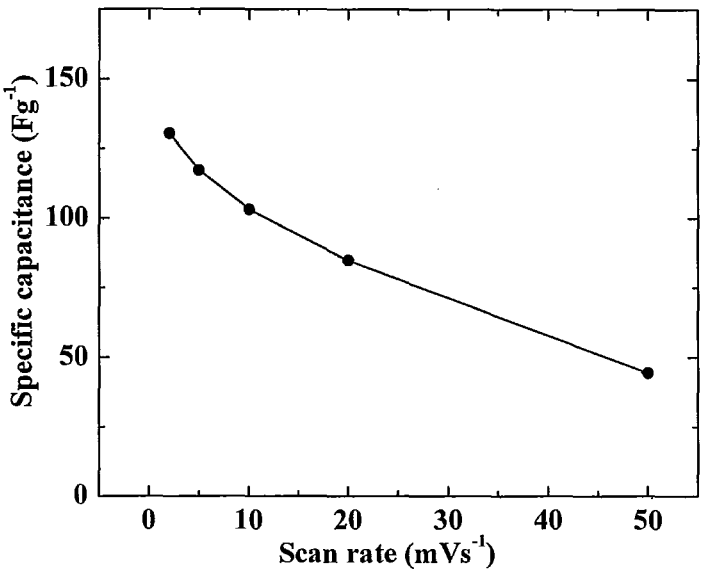

Figure 5-42 SC vs. scan rate for composite electrodes containing manganese dioxide prepared at pH 3 and mixed with 20 wt.% of carbon black using methods B.

The improved capacitive behavior of the electrodes prepared by method B is in a good agreement with the impedance spectroscopy data (Figure 5-43). The electrodes prepared by method B showed lower ESR compared to electrodes prepared by method A. The ESR of the electrodes prepared by method A and B were 0.27 Ohm and 0.16 Ohm respectively. This reduction in resistance is due to better mixing of the active material and the conducting agent.

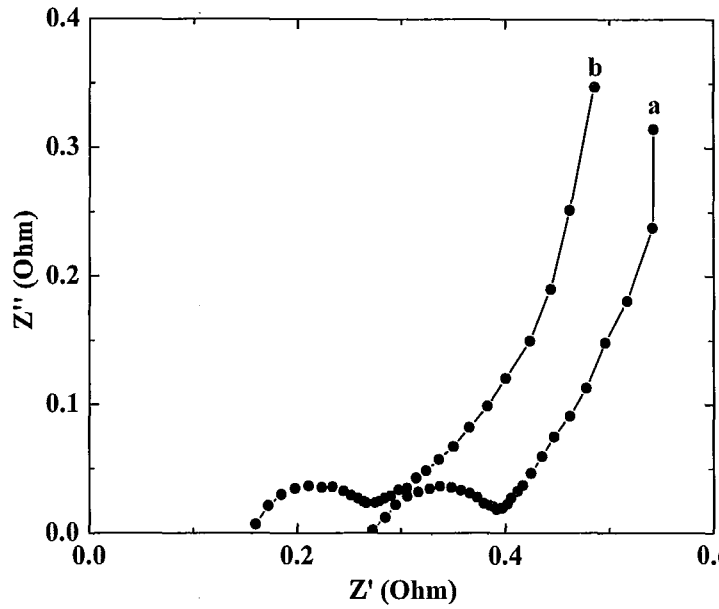

Figure 5-43 Nyquist plots of the impedance for the composite electrodes containing manganese dioxide prepared at pH 3 and mixed with 20 wt% of carbon black using method (a) A and (b) B.

5.2.2.3 Influence of doping

Recent studies showed that conductivity of lithium manganese dioxide can be increased significantly using 1-8 wt% Ag additives[99]. The resistivity of the film was found to decrease with the increase of Ag content. The use of Ag-doped lithium manganese dioxide enabled improved performance of batteries. Similar increase in the electronic conductivity of Ag-doped RuO_2 was also reported[100]. The investigation of Ag-doped RuO_2 for application in ES showed much higher SC compared to the SC of

undoped RuO_2. Therefore, it would be important to prepare and investigate Ag – doped MnO_2 for application in ES. The SC of the composite materials can be improved using Ag additives.

The results of our investigation showed that Ag particles can be precipitated from the $AgNO_3$ solutions at pH 3 using KBH_4 as a reducing agent. Obtained precipitate showed X-ray diffraction peaks (Figure 5-44a) of Ag corresponding to the JCPDS file 4-783. KBH_4 has been further used for co-precipitation of manganese dioxide and Ag from mixed $KMnO_4$ and $AgNO_3$ solutions. X-ray diffraction pattern of the samples showed small peaks of manganese dioxide and Ag (Figure 5-44b).

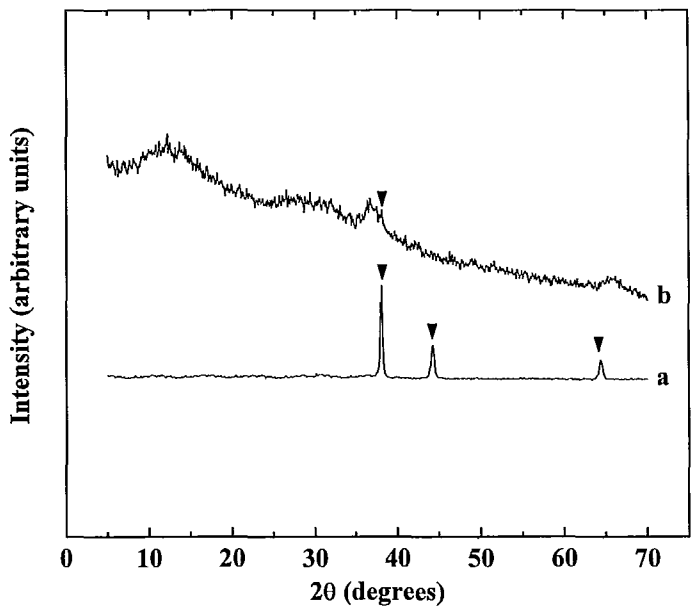

Figure 5-44 XRD patterns of powders prepared (a) 0.01 M $AgNO_3$ solution at pH 3 (b) mixed 0.1 M $KMnO_4$ and 0.1 M $AgNO_3$ solution at pH 3 (arrows shows the peaks of Ag).

EDS analysis of the powders precipitated at pH 3 from the 0.1 M $KMnO_4$ solutions containing 0.005, 0.01, 0.020 and 0.1 M $AgNO_3$ showed Ag/Mn atomic ratio of 0.04, 0.07, 0.15 and 0.29, respectively. However, as the concentration of $AgNO_3$ was increased above 0.01 M, Ag started to precipitate as second phase resulting in non-homogeneous dispersion of silver in the powder. As a result of this inhomogenity, SC dropped as Ag/Mn ratio in the powder increased above 0.07. The higher silver content resulted in lower electrochemically active manganese dioxide and lower SC. Figure 5-45 shows that SC increased as Ag/Mn atomic ratio increases and reaches a maximum at 0.07 and then decreases. Hence the optimum Ag/Mn atomic ratio was found to be 0.07.

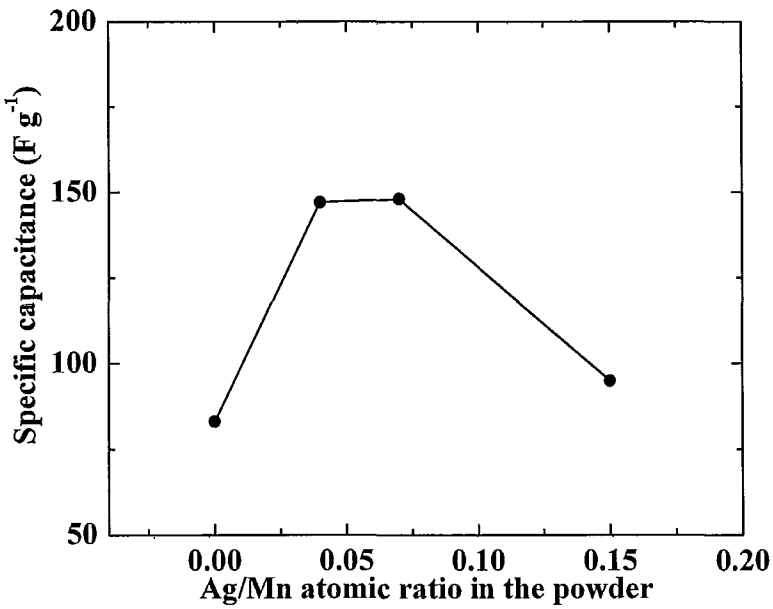

Figure 5-45 SC vs. Ag/Mn atomic ratio in the Ag-doped manganese dioxide powder.

Figure 5-46 compares CVs for the manganese dioxide powder without Ag and powder containing Ag with Ag/Mn atomic ratio of 0.07, mixed with carbon black using method A. The results indicate that Ag additive can improve the capacitive behaviour of the composite material, as indicated by the improved shape of CV and higher SC. The highest SC of 150 F g^{-1} was obtained at a scan rate of 2 mV s^{-1}. The SCs calculated from CVs obtained at different scan rates for electrodes prepared from Ag-doped manganese oxide is shown in Figure 5-47.

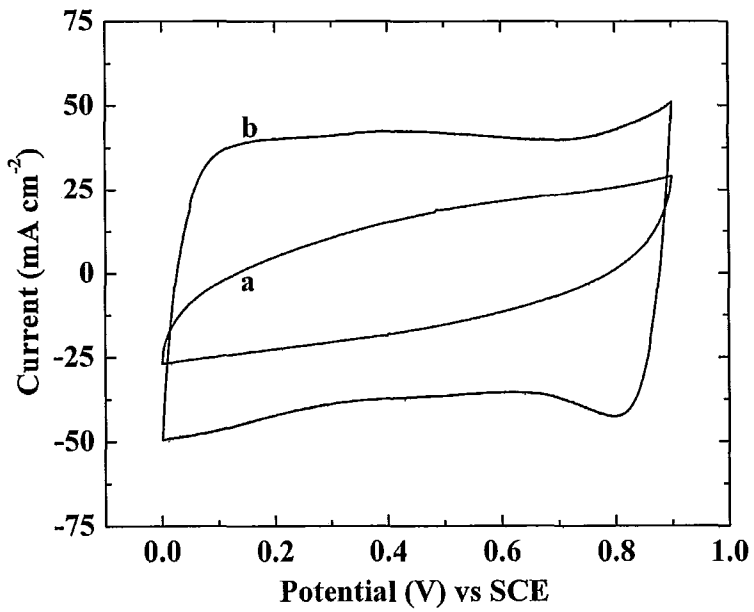

Figure 5-46 CVs at a scan rate of 5 mV s^{-1} for composite electrodes containing (a) undoped manganese dioxide and (b) Ag-doped manganese dioxide with Ag/Mn atomic ratio of 0.07 respectively, prepared at pH 3 and mixed with 20 wt% carbon black using method A.

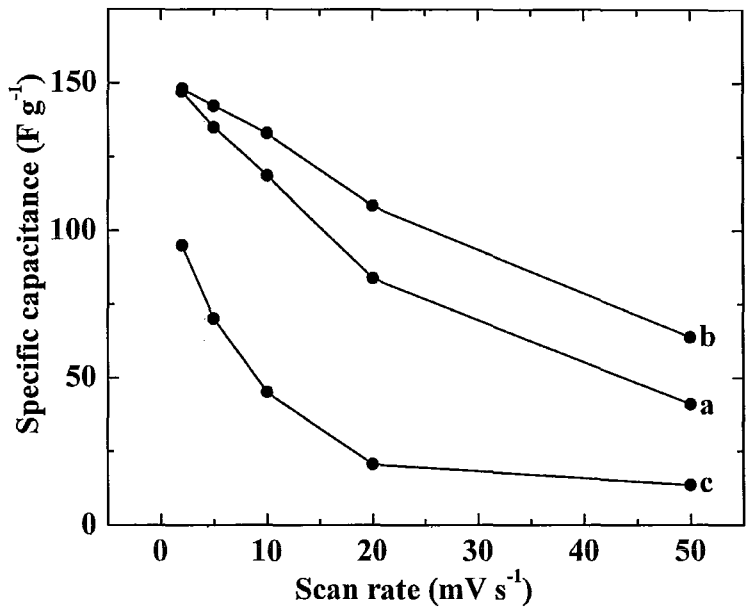

Figure 5-47 SC vs. scan rate for composite electrodes containing Ag-doped manganese dioxide with Ag/Mn atomic ratio of (a) 0.04 (b) 0.07 (c) 0.15 prepared at pH 3 and mixed with 20 wt% of carbon black using methods A.

The results indicate that composite electrodes prepared from Ag-doped manganese dioxide with Ag/Mn atomic ratio of 0.04 and 0.07 showed higher SC (Figure 5-47) then electrodes prepared from undoped manganese dioxide (Figure 5-29 and Figure 5-42). Figure 5-48 shows CVs at different scan rates for electrodes prepared from Ag-doped manganese dioxide with Ag/Mn atomic ratio of 0.07.

It is suggested that the co-precipitation of manganese dioxide and Ag using KBH_4 as a common reducing agent can result in composite materials with improved

conductivity and higher SC. However, the SC of doped manganese dioxide without carbon black was lower than the SC of manganese dioxide-carbon black composite.

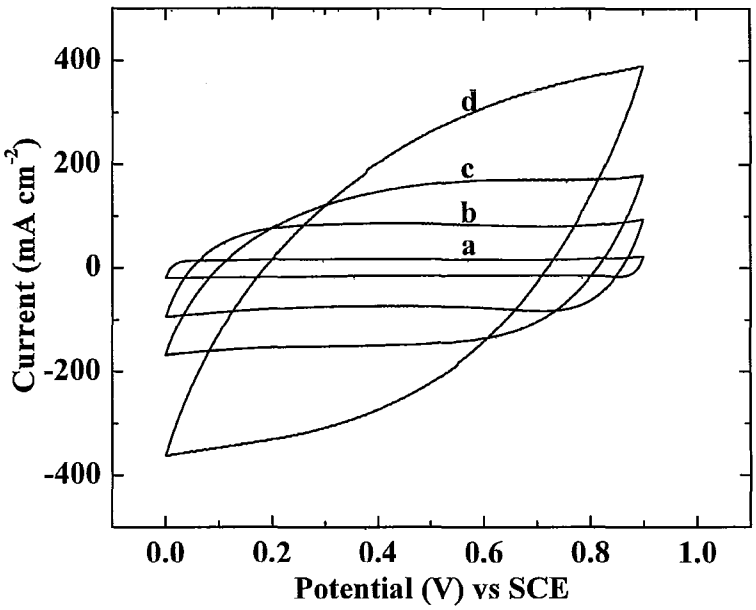

Figure 5-48 CVs at a scan rate of (a) 2 (b) 10 (c) 20 (d) 50 mV s^{-1} for electrodes containing Ag-doped manganese dioxide with Ag/Mn atomic ratio of 0.07.

Figure 5-49 shows complex impedance of the composite electrodes containing Ag-doped manganese dioxide with Ag/Mn ratio of 0.07. The Ag-doped manganese dioxide-carbon black composites showed a resistance of 0.1 Ohm, which is lower than the resistance of undoped manganese dioxide-carbon black composites (Figure 5-43).

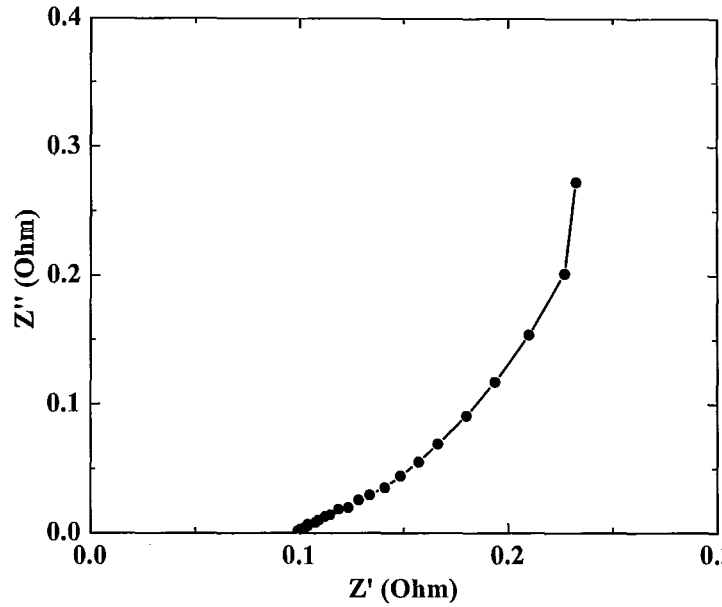

Figure 5-49 Nyquist plot of the impedance for the composite electrodes containing Ag-doped (Ag/Mn atomic ratio of 0.07) manganese dioxide prepared at pH 3 and mixed with 20 wt% of carbon black using method A.

Figure 5-50 shows charge-discharge behaviour of the Ag-doped composite electrodes in the potential range of 0-0.9 V at a current density of 40 mA cm^{-2}. The charge and discharge curves are almost linear, however initial voltage drop was observed in the discharge curve. This can be attributed to electrode resistance, resulting from diffusion limitations in pores.

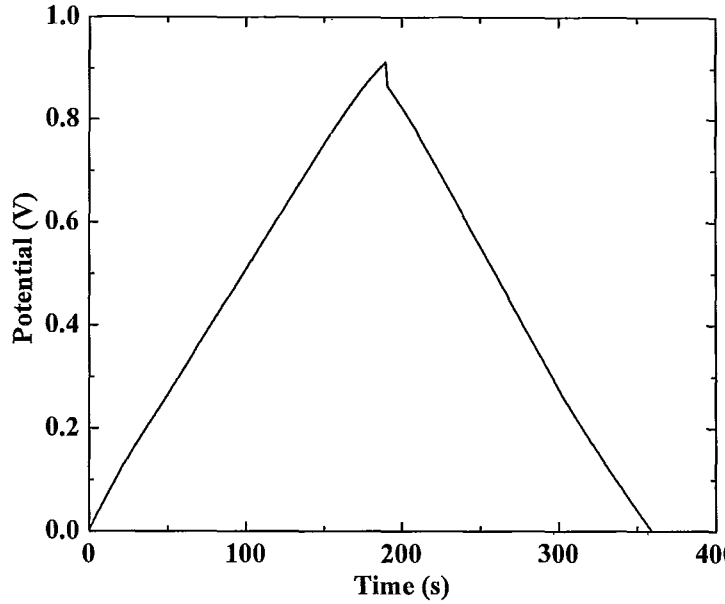

Figure 5-50 Charge-discharge behaviour at a current density of 40 mA cm^{-2} for composite electrodes containing Ag-doped (Ag/Mn atomic ratio of 0.07)manganese dioxide prepared at pH 3 and mixed with 20 wt% of carbon black by method A.

Figure 5-51 shows cycling behaviour of the composite electrodes in the 0.5 M Na_2SO_4 aqueous solution. The electrodes showed initial increase in SC during first 200 cycles. Similar increase in SC was observed[101] in thin films and was attributed to changes in microstructure and oxidation of non-stoichiometric manganese dioxide. However, no loss in SC was observed during the 1000 cycles.

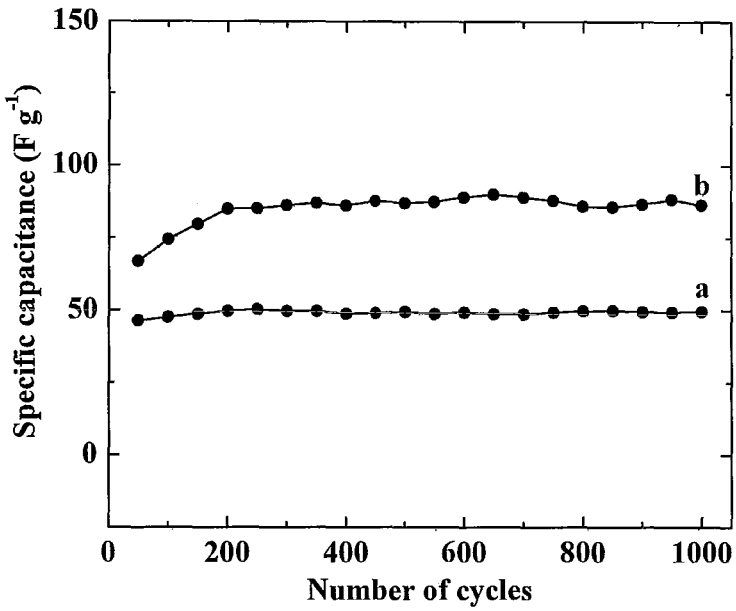

Figure 5-51 Cycling behaviour at a scan rate of 50 mV s^{-1} for composite electrodes containing (a) undoped manganese dioxide and (b) Ag-doped manganese dioxide with Ag/Mn atomic ratio of 0.07 prepared at pH 3 and mixed with 20 wt% carbon black using method A.

It is suggested that the further optimization of electrode composition and microstructure will result in reduced resistance and improved capacitive behavior.

5.3 Comparison of the two methods.

ELD can be utilised to fabricate nanostructured manganese oxide thin film electrodes for supercapacitor application. Thin film electrodes exhibit higher SC, and SC decreases as thickness of the film increases, but still higher than the bulk electrodes. However, thin films have lower active material loading and hence their applications are

limited to lower energy requiring appliances. Thin films can also be used to modify the current collector/active material interface to decrease the resistance and to increase the total capacitance and overall performance of the bulk electrodes. Bulk electrodes have higher active material loading, hence can be utilized for higher energy requiring appliances such as electric vehicle hybrid power systems, pulse power applications, as well as back-up and emergency power supplies.

6. CONCLUSIONS

Nanostructured manganese dioxide films were prepared by cathodic reduction of 0.01 – 0.15 M $KMnO_4$ solutions. It was shown that deposition can be performed in galvanostatic, pulse and reverse pulse deposition regimes. QCM studies showed that deposition rate increased with increasing current density and decreased with increasing $KMnO_4$ concentration. The diffusion-controlled deposition mechanism is based on the reduction of anionic MnO_4^- species at the cathode surface. The deposit microstructure can be varied by variation in deposition conditions. Porous and crack free 1-2 μm films were obtained using galvanostatic or reverse pulse deposition from 0.02 M $KMnO_4$ solutions. It was shown that film porosity is beneficial for charge transfer during deposition and crack prevention during drying. X-ray studies revealed poor crystallinity of as-prepared films. EDS, TGA and DTA studies showed that the composition of the films can be described by formula $K_xMnO_{2+y}(H_2O)_z$. Porous films showed capacitive behavior in the 0.1 M Na_2SO_4 solutions in a potential window of 0 - 1.0 V vs. SCE. The films prepared in the reverse pulse regime showed higher SC compared to films prepared under galvanostatic conditons. The SC decreased with increasing scan rate due to the low conductivity of MnO_2 and diffusion limitations in pores. The highest SC of 279 F g^{-1} was obtained for the 80 μg cm^{-2} films at a scan rate of 2 mV s^{-1}. Obtained films can be considered as possible electrode materials for electrochemical supercapacitors.

A novel chemical precipitation process had been developed to produce manganese oxide nanoparticles. Manganese oxide powders were prepared by chemically

reducing 0.2 M $KMnO_4$ solution with isopropanol. TEM investigations showed that as-prepared powders contained nearly spherical particles with particles size of about 50 nm. Composite electrodes containing nanoparticles of manganese dioxide and carbon black, were fabricated by impregnation of slurries of the manganese dioxide and carbon black into porous nickel foam current collectors. The composite electrodes with total mass loading of 55 mg cm^{-2} showed a capacitive behavior in the 0.1-0.5 M Na_2SO_4 solutions. Testing in the 0.5 M Na_2SO_4 solutions showed higher SC compared to the SC in the 0.1 M Na_2SO_4 solutions. Carbon black improved electrochemical performance of the electrodes by forming a secondary conductivity network within the nickel foam cells. The SC increased with increasing carbon black content in the range of 0-30 wt. %. The highest SC of 128 Fg^{-1} was obtained at a scan rate of 2 mV s^{-1} in the 0.5 M Na_2SO_4 solutions.

KBH_4 has also been utilized as a reducing agent for the precipitation of manganese oxide, Ag and Ag-doped manganese dioxide powders. TEM studies showed that powders prepared at pH 3 contained nanoparticles with particle size of 5-10 nm and nanofibers with diameter of ~5 nm and length of 0.1-0.5 μm. The powders prepared at pH 6 showed significant agglomeration and larger particle size. The composite electrodes showed a capacitive behaviour in the 0.5 M Na_2SO_4 solutions. The difference in particle morphology explains the higher SC observed for powders prepared at pH 3. The capacitive behaviour of the composite electrodes can be improved by mixing of manganese dioxide and carbon black in solutions rather the mixing them as solids. The

conductivity of composite electrodes was further increased by using Ag-doped manganese dioxide powders. The highest SC of 150 F g^{-1} was obtained at a scan rate of 2mV s^{-1} in the 0.5 M Na_2SO_4 solutions. The composite electrodes showed good cycling behavior with no loss in SC during 1000 cycles. Fabricated films and composite electrodes can be considered as possible electrode materials for electrochemical capacitors.

7. REFERENCES

1. Winter, M. & Brodd, R. J. What are batteries, fuel cells, and supercapacitors? *Chemical reviews* **104**, 4245-4269 (2004).

2. Sarangapani, S., Lessner, P., Manoukian, M. & Giner, J. Non-noble electrocatalysts for alkaline fuel cells. *Journal of Power Sources* **29**, 437-442 (1990).

3. Sarangapani, S., Tilak, B. V. & Chen, C. -. Materials for electrochemical capacitors. Theoretical and experimental constraints. *Journal of the Electrochemical Society* **143**, 3791-3799 (1996).

4. Zheng, J. P. & Jow, T. R. New charge storage mechanism for electrochemical capacitors. *Journal of the Electrochemical Society* **142**, L6-L8 (1995).

5. Zheng, J. P., Cygan, P. J. & Jow, T. R. Hydrous ruthenium oxide as an electrode material for electrochemical capacitors. *Journal of the Electrochemical Society* **142**, 2699-703 (1995).

6. H.I. Becker. Low voltage electrolytic capacitors. *U.S., Patent 2 800 616* (1957).

7. R.A. Rightmire. *Electrical energy storage apparatus*. U.S., Patent 3 288 641 (1966).

8. R. Kotz, M. Bartschi, F. Buchi, R. Gallay, and P. Dietrich. *Hy.Power - A fuel cell car boosted with supercapacitors*, 2002).

9. Li, W. &Joos, G. *A power electronic interface for a battery supercapacitor hybrid energy storage system for wind applications* (2008 IEEE Power Electronics Specialists Conference, IEEE, Piscataway, NJ, USA, 2008).

10. Hapler, M. S. & Ellenbogen, J. C. Supercapacitor: A brief overview. *MITRE* (March 2006).

11. Kötz, R. & Carlen, M. Principles and applications of electrochemical capacitors. *Electrochimica Acta* **45**, 2483-2498 (2000).

12. Shukla, A. K., Sampath, S. & Vijayamohanan, K. Electrochemical supercapacitors: energy storage beyond batteries. *Current science* **79**, 1656-61 (2000).

13. B.E. Conway. in *Electrochemical supercapacitors - Scientific fundamentals and technological applications* (Kulwer, New York, 1999).

14. Burke, A. Ultracapacitors: why, how, and where is the technology. *Journal of Power Sources* **91**, 37-50 (2000).

15. Pandolfo, A. G. & Hollenkamp, A. F. Carbon properties and their role in supercapacitors. *Journal of Power Sources* **157**, 11-27 (2006).

16. Simon, P. & Gogotsi, Y. Materials for electrochemical capacitors. *Nature Materials* **7**, 845-854 (2008).

17. Rudge, A., Davey, J., Raistrick, I., Gottesfeld, S. & Ferraris, J. P. Conducting polymers as active materials in electrochemical capacitors. *Journal of Power Sources* **47**, 89-107 (1994).

18. Frackowiak, E., Khomenko, V., Jurewicz, K., Lota, K. & Béguin, F. Supercapacitors based on conducting polymers/nanotubes composites. *Journal of Power Sources* **153**, 413-418 (2006).

19. Jurewicz, K., Delpeux, S., Bertagna, V., Béguin, F. & Frackowiak, E. Supercapacitors from nanotubes/polypyrrole composites. *Chemical Physics Letters* **347**, 36-40 (2001).

20. Arbizzani, C., Mastragostino, M. & Soavi, F. New trends in electrochemical supercapacitors. *Journal of Power Sources* **100**, 164-170 (2001).

21. Laforgue, A. *et al.* Activated carbon/conducting polymer hybrid supercapacitors. *Journal of the Electrochemical Society* **150**, A645-A651 (2003).

22. Wang, X. & Zheng, J. P. The optimal energy density of electrochemical capacitors using two different electrodes. *Journal of the Electrochemical Society* **151**, A1683-A1689 (2004).

23. Pell, W. G. & Conway, B. E. Peculiarities and requirements of asymmetric capacitor devices based on combination of capacitor and battery-type electrodes. *Journal of Power Sources* **136**, 334-345 (2004).

24. Du Pasquier, A., Plitz, I., Menocal, S. & Amatucci, G. A comparative study of Li-ion battery, supercapacitor and nonaqueous asymmetric hybrid devices for automotive applications. *Journal of Power Sources* **115**, 171-178 (2003).

25. Frackowiak, E. Carbon materials for supercapacitor application. *Physical Chemistry Chemical Physics* **9**, 1774-85 (2007).

26. Probstle, H., Wiener, M. & Fricke, J. Carbon Aerogels for Electrochemical Double Layer Capacitors. *Journal of Porous Materials* **10**, 213-222 (2003).

27. Pröbstle, H., Schmitt, C. & Fricke, J. Button cell supercapacitors with monolithic carbon aerogels. *Journal of Power Sources* **105**, 189-194 (2002).

28. Zheng, J. P., Cygan, P. J. & Jow, T. R. Hydrous ruthenium oxide as an electrode material for electrochemical capacitors. *Journal of the Electrochemical Society* **142**, 2699-2703 (1995).

29. Liu, K. & Anderson, M. A. Porous nickel oxide/nickel films for electrochemical capacitors. *Journal of the Electrochemical Society* **143**, 124-130 (1996).

30. Srinivasan, V. & Weidner, J. W. An electrochemical route for making porous nickel oxide electrochemical capacitors. *Journal of the Electrochemical Society* **144**, 210-13 (1997).

31. Nam, K. & Kim, K. A study of the preparation of NiOx electrode via electrochemical route for supercapacitor applications and their charge storage mechanism. *Journal of the Electrochemical Society* **149**, A346-A354 (2002).

32. Jayalakshmi, M. & Balasubramanian, K. Simple Capacitors to Supercapacitors - An Overview. *International Journal of Electrochemical Science* **3**, 1196-1217 (2008).

33. Lin, C., Ritter, J. A. & Popov, B. N. Characterization of sol-gel-derived cobalt oxide xerogels as electrochemical capacitors. *Journal of the Electrochemical Society* **145**, 4097-4103 (1998).

34. Kandalkar, S. G., Gunjakar, J. L. & Lokhande, C. D. Preparation of cobalt oxide thin films and its use in supercapacitor application. *Applied Surface Science* **254**, 5540-5544 (2008).

35. Srinivasan, V. & Weidner, J. W. Capacitance studies of cobalt oxide films formed via electrochemical precipitation. *Journal of Power Sources* **108**, 15-20 (2002).

36. Hill, L. I., Portal, R., Verbaere, A. & Guyomard, D. One-step electrochemical synthesis of -MnO2 and &middot-MnO2 compounds for lithium batteries. *Electrochemical and Solid-State Letters* **4**, A180-A183 (2001).

37. Bai, L. *et al.* Rechargeability of a chemically modified MnO2/Zn battery system at practically favorable power levels. *Journal of the Electrochemical Society* **140**, 884-9 (1993).

38. Das, D., Sen, P. K. & Das, K. Electrodeposited MnO2 as electrocatalyst for carbohydrate oxidation. *Journal of Applied Electrochemistry* **36**, 685-690 (2006).

39. Luo, X., Xu, J., Zhao, W. & Chen, H. Ascorbic acid sensor based on ion-sensitive field-effect transistor modified with MnO2 nanoparticles. *Analytica Chimica Acta* **512**, 57-61 (2004).

40. Djurfors, B., Broughton, J. N., Brett, M. J. & Ivey, D. G. Electrochemical oxidation of Mn/MnO films: formation of an electrochemical capacitor. *Acta Materialia* **53**, 957-965 (2005).

41. Broughton, J. N. & Brett, M. J. Variations in MnO2 electrodeposition for electrochemical capacitors. *Electrochimica Acta* **50**, 4814-4819 (2005).

42. Kyung-Wan Nam & Kwang-Bum Kim. Manganese oxide film electrodes prepared by electrostatic spray deposition for electrochemical capacitors. *Journal of the Electrochemical Society* **153**, 81-8 (2006).

43. Bélanger, D., Brousse, T., Long, J. W. Manganese oxide: Battery materials make the leap to electrochemical capacitors. *The Electrochemical Society Interface*, 49 - 52 (Spring 2008).

44. Jeng-Kuei Chang & Wen-Ta Tsai. Material characterization and electrochemical performance of hydrous manganese oxide electrodes for use in electrochemical pseudocapacitors. *Journal of the Electrochemical Society* **150**, 1333-8 (2003).

45. Djurfors, B., Broughton, J. N., Brett, M. J. & Ivey, D. G. Microstructural characterization of porous manganese thin films for electrochemical supercapacitor applications. *Journal of Materials Science* **38**, 4817-30 (2003).

46. Lee, H. Y. & Goodenough, J. B. Supercapacitor Behavior with KCl Electrolyte. *Journal of Solid State Chemistry* **144**, 220-223 (1999).

47. Wei, J., Nagarajan, N. & Zhitomirsky, I. Manganese oxide films for electrochemical supercapacitors. *Journal of Materials Processing Technology* **186**, 356-361 (2007).

48. Hu, C. & Tsou, T. Capacitive and textural characteristics of hydrous manganese oxide prepared by anodic deposition. *Electrochimica Acta* **47**, 3523-3532 (2002).

49. Hu, C. & Tsou, T. Capacitive and textural characteristics of hydrous manganese oxide prepared by anodic deposition. *Electrochimica Acta* **47**, 3523-3532 (2002).

50. Yi-Shiun Chen, Chi-Chang Hu & Yung-Tai Wu. Capacitive and textural characteristics of manganese oxide prepared by anodic deposition: effects of manganese precursors and oxide thickness. *Journal of Solid State Electrochemistry* **8**, 467-73 (2004).

51. Sharma, R. K., Oh, H., Shul, Y. & Kim, H. Carbon-supported, nano-structured, manganese oxide composite electrode for electrochemical supercapacitor. *Journal of Power Sources* **173**, 1024-1028 (2007).

52. Raymundo-Pinero, E., Khomenko, V., Frackowiak, E. & Beguin, F. Performance of manganese oxide/CNTs composites as electrode materials for electrochemical capacitors. *Journal of the Electrochemical Society* **152**, A229-A235 (2005).

53. Sub-Cem Pang, Anderson, M. A. & Chapman, T. W. Novel electrode materials for thin-film ultracapacitors: comparison of electrochemical properties of sol-gel-derived and electrodeposited manganese dioxide. *Journal of the Electrochemical Society* **147**, 444-50 (2000).

54. Pang, S. & Anderson, M. A. Novel electrode materials for electrochemical capacitors: Part II. Material characterization of sol-gel-derived and electrodeposited manganese dioxide thin films. *Journal of Materials Research* **15**, 2096-2106 (2000).

55. Mastragostino, M., Arbizzani, C. & Soavi, F. Polymer-based supercapacitors. *Journal of Power Sources* **97-98**, 812-815 (2001).

56. Rudge, A., Davey, J., Raistrick, I., Gottesfeld, S. & Ferraris, J. P. Conducting polymers as active materials in electrochemical capacitors. *Journal of Power Sources* **47**, 89-107 (1994).

57. Zheng, J. P. Resistance distribution in electrochemical capacitors with a bipolar structure. *Journal of Power Sources* **137**, 158-162 (2004).

58. Portet, C., Taberna, P. L., Simon, P. & Laberty-Robert, C. Modification of Al current collector surface by sol-gel deposit for carbon-carbon supercapacitor applications. *Electrochimica Acta* **49**, 905-912 (2004).

59. Portet, C., Taberna, P. L., Simon, P. & Flahaut, E. Modification of Al current collector/active material interface for power improvement of electrochemical capacitor electrodes. *Journal of the Electrochemical Society* **153**, A649-A653 (2006).

60. Reddy, R. N. & Reddy, R. G. Sol–gel MnO2 as an electrode material for electrochemical capacitors. *Journal of Power Sources* **124**, 330-337 (2003).

61. Tsang, C., Kim, J. & Manthiram, A. Synthesis of Manganese Oxides by Reduction of KMnO4with KBH4in Aqueous Solutions. *Journal of Solid State Chemistry* **137**, 28-32 (1998).

62. Jeong, Y. U. & Manthiram, A. Nanocrystalline manganese oxides for electrochemical capacitors with neutral electrolytes. *Journal of the Electrochemical Society* **149**, A1419-A1422 (2002).

63. Toupin, M., Brousse, T. & Belanger, D. Influence of microstructure on the charge storage properties of chemically synthesized manganese dioxide. *Chemistry of Materials* **14**, 3946-52 (2002).

64. Jeng-Kuei Chang, Yi-Lun Chen & Wen-Ta Tsai. Effect of heat treatment on material characteristics and pseudo-capacitive properties of manganese oxide prepared by anodic deposition. *Journal of Power Sources* **135**, 344-53 (2004).

65. Chang, J. -. & Tsai, W. -. Effects of temperature and concentration on the structure and specific capacitance of manganese oxide deposited in manganese acetate solution. *Journal of Applied Electrochemistry* **34**, 953-61 (2004).

66. Chi-Chang Hu & Ta-Wang Tsou. Ideal capacitive behavior of hydrous manganese oxide prepared by anodic deposition. *Electrochemistry Communications* **4**, 105-9 (2002).

67. Chen, Y. & Hu, C. Capacitive characteristics of binary manganese-nickel oxides prepared by anodic deposition. *Electrochemical and Solid-State Letters* **6**, A210-A213 (2003).

68. Chen, C. H., Kelder, E. M., Jak, M. J. G. & Schoonman, J. Electrostatic spray deposition of thin layers of cathode materials for lithium battery. *Solid State Ionics* **86-88**, 1301-1306 (1996).

69. Switzer, J. A. Electrochemical synthesis of ceramic films and powders. *American Ceramic Society Bulletin* **66**, 1521-1524 (1987).

70. Chi-Chang Hu & Ta-Wang Tsou. The optimization of specific capacitance of amorphous manganese oxide for electrochemical supercapacitors using experimental strategies. *Journal of Power Sources* **115**, 179-86 (2003).

71. Boccaccini, A. R. & Zhitomirsky, I. Application of electrophoretic and electrolytic deposition techniques in ceramics processing. *Current Opinion in Solid State and Materials Science* **6**, 251-260 (2002).

72. Zhitomirsky, I. Electrophoretic and electrolytic deposition of ceramic coatings on carbon fibers. *Journal of the European Ceramic Society* **18**, 849-856 (1998).

73. Zhitomirsky, I. Cathodic electrodeposition of ceramic and organoceramic materials. Fundamental aspects. *Advances in Colloid and Interface Science* **97**, 279-317 (2002).

74. Therese, G. H. & Kamath, P. V. Electrochemical Synthesis of Metal Oxides and Hydroxides. *Chemistry of Materials* **12**, 1195-1204 (2000).

75. Nagarajan, N., Humadi, H. & Zhitomirsky, I. Cathodic electrodeposition of MnOx films for electrochemical supercapacitors. *Electrochimica Acta* **51**, 3039-3045 (2006).

76. Brousse, T. *et al.* Long-term cycling behavior of asymmetric activated carbon/MnO2 aqueous electrochemical supercapacitor. *Journal of Power Sources* **173**, 633-641 (2007).

77. Khomenko, V., Raymundo-Piñero, E. & Béguin, F. Optimisation of an asymmetric manganese oxide/activated carbon capacitor working at 2 V in aqueous medium. *Journal of Power Sources* **153**, 183-190 (2006).

78. Ye, C., Lin, Z. M. & Hui, S. Z. Electrochemical and capacitance properties of rod-shaped MnO2 for supercapacitor. *Journal of the Electrochemical Society* **152**, A1272-A1278 (2005).

79. Reddy, R. N. & Reddy, R. G. Sol–gel MnO2 as an electrode material for electrochemical capacitors. *Journal of Power Sources* **124**, 330-337 (2003).

80. Yang, Q. M., Ettel, V. A., Babjak, J., Charles, D. K. & Mosoiu, M. A. Pasted Ni(OH)2 electrodes using Ni powders for high-drain-rate, Ni-based batteries. *Journal of the Electrochemical Society* **150**, A543-A550 (2003).

81. Paserin, V., Marcuson, S., Shu, J. & Wilkinson, D. S. CVD Technique for Inco Nickel Foam Production. *Advanced Engineering Materials* **6**, 454-459 (2004).

82. Yan, D. & Cui, W. Preparation and properties of no-binder electrode Ni/MH battery. *Journal of Alloys and Compounds* **293**, 780-783 (1999).

83. Taucher-Mautner, W. & Kordesch, K. Studies of pasted nickel electrodes to improve cylindrical nickel–zinc cells. *Journal of Power Sources* **132**, 275-281 (2004).

84. Yu, Y., Chen, C., Shui, J. & Xie, S. Nickel-foam-supported reticular CoO-Li2O composite anode materials for lithium ion batteries. *Angewandte Chemie - International Edition* **44**, 7085-7089 (2005).

85. Deakin, M. R. & Buttry, D. A. Electrochemical applications of the quartz crystal microbalance. *Analytical Chemistry* **61**, 1147A-1154A (1989).

86. Pourbaix, M. in *Atlas of electrochemical equilibria in aqueous solutions,* (Pergamon Press, Oxford; New York, 1966).

87. Tang, L. Concentration dependence of diffusion and migration of chloride ions: Part 2. Experimental evaluations. *Cement and Concrete Research* **29**, 1469-1474 (1999).

88. Nestle, N. F. E. I. & Kimmich, R. Concentration-dependent diffusion coefficients and sorption isotherms. Application to ion exchange progresses as an example. *Journal of physical chemistry* **100**, 12569-12573 (1996).

89. Nakamura, T. & Wang, Z. Simulations of crack propagation in porous materials. *Transactions of the ASME. Journal of Applied Mechanics* **68**, 242-51 (2001).

90. Deng, Z. *et al.* Reinforcement by crack-tip blunting in porous ceramics. *Journal of the European Ceramic Society* **24**, 2055-2059 (2004).

91. Moon, J., Awano, M., Takagi, H. & Fujishiro, Y. Synthesis of nanocrystalline manganese oxide powders: Influence of hydrogen peroxide on particle characteristics. *Journal of Materials Research* **14**, 4594-4601 (1999).

92. Prasad, K. R. & Miura, N. Potentiodynamically deposited nanostructured manganese dioxide as electrode material for electrochemical redox supercapacitors. *Journal of Power Sources* **135**, 354-360 (2004).

93. Nakayama, M., Tanaka, A., Sato, Y., Tonosaki, T. & Ogura, K. Electrodeposition of manganese and molybdenum mixed oxide thin films and their charge storage properties. *Langmuir* **21**, 5907-5913 (2005).

94. Ma, Y., Luo, J. & Suib, S. L. Syntheses of Birnessites Using Alcohols as Reducing Reagents: Effects of Synthesis Parameters on the Formation of Birnessites. *Chemistry of Materials* **11**, 1972-1979 (1999).

95. Watanabe, T., Zhou, H. & Honma, I. Cathode properties of nanocrystalline manganese oxide synthesized through soft solution processing. *Journal of the Electrochemical Society* **152**, A1568-A1573 (2005).

96. Ching, S., Petrovay, D. J., Jorgensen, M. L. & Suib, S. L. Sol–Gel Synthesis of Layered Birnessite-Type Manganese Oxides. *Inorganic chemistry* **36**, 883-890 (1997).

97. Wei, J. & Zhitomirsky, I. Electrosynthesis of manganese oxide films. *Surface Engineering* **24**, 40-46 (2008).

98. Kim, H. & Popov, B. N. A Mathematical Model of Oxide/Carbon Composite Electrode for Supercapacitors. *Journal of the Electrochemical Society* **150**, A1153-A1160 (2003).

99. Wu, X. M. *et al.* Silver-doped lithium manganese oxide thin films prepared by solution deposition. *Materials Letters* **60**, 2497-2500 (2006).

100. Ahn, H., Sung, Y., Kim, W. B. & Seong, T. Crystalline Ag nanocluster-incorporated RuO2 as an electrode material for thin-film micropseudocapacitors. *Electrochemical and Solid-State Letters* **11**, A112-A115 (2008).

101. Nagarajan, N., Cheong, M. & Zhitomirsky, I. Electrochemical capacitance of MnOx films. *Materials Chemistry and Physics* **103**, 47-53 (2007).